The method of fundamental solutions for computing interior transmission eigenvalues

Lukas Julian Pieronek

IAS Series
Band / Volume 44
ISBN 978-3-95806-504-8

Mitglied der Helmholtz-Gemeinschaft

JÜLICH
Forschungszentrum

Schriften des Forschungszentrums Jülich
IAS Series Band / Volume 44

Forschungszentrum Jülich GmbH
Institute for Advanced Simulation (IAS)
Jülich Supercomputing Centre (JSC)

The method of fundamental solutions for computing interior transmission eigenvalues

Lukas Julian Pieronek

Schriften des Forschungszentrums Jülich
IAS Series

Band / Volume 44

ISSN 1868-8489

ISBN 978-3-95806-504-8

Bibliografische Information der Deutschen Nationalbibliothek.
Die Deutsche Nationalbibliothek verzeichnet diese Publikation in der Deutschen Nationalbibliografie; detaillierte Bibliografische Daten sind im Internet über http://dnb.d-nb.de abrufbar.

Herausgeber und Vertrieb: Forschungszentrum Jülich GmbH
Zentralbibliothek, Verlag
52425 Jülich
Tel.: +49 2461 61-5368
Fax: +49 2461 61-6103
zb-publikation@fz-juelich.de
www.fz-juelich.de/zb

Umschlaggestaltung: Grafische Medien, Forschungszentrum Jülich GmbH

Druck: Grafische Medien, Forschungszentrum Jülich GmbH

Copyright: Forschungszentrum Jülich 2020

Schriften des Forschungszentrums Jülich
IAS Series, Band / Volume 44

DE 634 (Diss. BTU Cottbus-Senftenberg, 2020)

ISSN 1868-8489
ISBN 978-3-95806-504-8

Vollständig frei verfügbar über das Publikationsportal des Forschungszentrums Jülich (JuSER) unter www.fz-juelich.de/zb/openaccess.

This is an Open Access publication distributed under the terms of the Creative Commons Attribution License 4.0, which permits unrestricted use, distribution, and reproduction in any medium, provided the original work is properly cited.

Abstract

This thesis deals with a novel approach for analyzing and computing interior transmission eigenvalues of (piecewise) homogeneous media in two dimensions. It is based on approximating boundary data of respective eigenfunctions by the method of fundamental solutions. However, since a straightforward implementation would solely exploit ill-conditioned matrices and thus evoke spurious results, a stabilization scheme is incorporated. The combined method is then studied with a distinction between isotropic and anisotropic materials, and complemented by novel approximation theory each. Numerical validations complete the investigations for different wave type scenarios.

Acknowledgements

First and foremost, I would like to thank my advisor, Dr. Andreas Kleefeld, for guiding me through my research during the last years. I really enjoyed discussing with him when new ideas or techniques did not work out as they were supposed to be. He generally supported my academic career and networking in the community which is of enduring value to me.

I likewise acknowledge the encouragement, patience and safe haven provided by my family and friends. Throughout, but especially at the final stages of this thesis, they helped me to keep the focus pleasantly.

Special thanks go to Professor Andreas Kirsch from whose expertise as one of the pioneers in inverse scattering I could frequently learn when meeting him on conferences, summer schools or being even invited to one of his seminars. Also some technical improvements within this thesis were initiated by his careful eye.

Moreover, I want to thank Janosch Preuß and Christof Päßler for many inspiring conversations on the topic and for proofreading earlier versions of this thesis, respectively.

Finally, I am grateful for the financial support and good working environment provided by the 'Mathematics and Education' group headed by Professor Johannes Grotendorst during my doctoral studies at the Jülich Supercomputing Center.

Table of contents

Chapter 1

Motivation and scope of this thesis

Interior transmission eigenvalues (ITEs) are complex-valued quantities which originally arose in the study of inverse scattering problems, see [58, 35]. Here, the general task is to characterize the interior of some hidden object through its scattering behavior with incident waves. While a full reconstruction is computationally expensive, non-linear and ill-posed, see [25], detecting only the support of the scatterer can be considered in an easier linear fashion, see [59]. However, those sampling methods then suffer from the fact that wave numbers of magnitude equal to ITEs, whose discrete spectrum is scatterer-specific, need to be excluded to avoid the possibility of non-trivial waves with evanescent and thus deficient scattering response, see [28]. Because of this restrictive phenomenon, it is desired to compute ITEs with high accuracy yet at preferably low numerical costs, see [26].

On the other hand, ITEs do also contain information about governing material parameters from an isospectral perspective, see [25, 42, 18]. For instance, fixing the support of the scatterer, it can be shown that for homogeneous media the smallest real-valued ITE is strictly monotone with respect to some propagation constant, cf. Section 4.2, while for spherically symmetric inhomogeneous media the entire spectrum even encodes corresponding profiles completely, see [28]. Those relations can especially be used in non-destructive testing, see [19, 48]. ITEs apparently exhibit both a deteriorating and descriptive nature in practice which merit to be investigated further.

Mathematically, ITEs are non-linear eigenvalues of a modeling forward operator, the interior transmission problem (ITP), which is given for several types of waves altogether by a coupled, non-self-adjoint and second-order PDE system. In the easiest case of acoustic

scattering it reads

$$\begin{aligned} \Delta v + k^2 v &= 0 \quad \text{in } D \\ \Delta w + nk^2 w &= 0 \quad \text{in } D \\ v &= w \quad \text{on } \partial D \\ \partial_\nu v &= \partial_\nu w \quad \text{on } \partial D\,. \end{aligned}$$

where n denotes the refractive index as governing material parameter and D is the global support of $n-1$, defining the underlying sonic scatterer. Corresponding ITEs are then determined as wave numbers k for which non-trivial eigenfunction pairs (v,w) exist. Although a profound theoretical analysis has been established for their theory over the years, there are still many open questions, see [33]. Complementing numerical studies might yield new or even deeper insights for ITEs at that point. Regarding their direct computation, a non-standard eigenproblem needs to be solved for whose discretization mostly mesh-based methods like finite element or boundary element methods are currently used due to their robustness and broad applicability, see [92, 62, 24, 26, 29, 102, 54, 53, 43]. But also more sophisticated techniques have been developed in the course of ITE research such as aforementioned sampling methods, see [24], or the inside-outside duality method, see [83, 61, 85]. However, neither of them achieves satisfactory accuracy for common test scatterers compared to the workload required which suggests the investigation of simpler approaches, see [26].

For the listed purposes, the method of fundamental solutions (MFS) will be representatively studied in 2D. It is a mesh-free boundary collocation method which was originally proposed in [69] to approximate functions subject to fulfilling a certain PDE only by linear combinations of corresponding singularity-translated fundamental solutions. Hence we must limit the ITP to homogeneous media (or piecewise homogeneous media with a moderate number of components) which is actually not that far from ITE calculations for arbitrary inhomogeneous materials thanks to the aforementioned monotonicity relations. Facilitating thus non-local trial functions with the potential of exponential convergence rates, the still cautious use of the MFS nowadays comes from the observation that its straightforward implementation is generally ill-conditioned, see [8]. However, efficient numerical remedies have been developed simultaneously one of which has been proposed by [13] in the special context of eigenproblems with excellent results using the method of particular solutions. In combination with the related MFS, to be called *modified MFS* then, it will be our inspirational basis for upcoming ITE calculations and novel approximation theory. Taking also into account that computing resources, including standards for higher precision arithmetics,

have been growing tremendously in the last decades and continue so, this finally motivates to revive formerly-affected methods.

The overall structure of this thesis is as follows: We continue with an overview of mathematical concepts in Chapter 2 which is necessary for our subsequent theoretical analysis of ITEs and introduce in Chapter 3 the modified MFS as our representative numerical method of investigation. Since the ITP is generally distinguished by whether the associated scattering material is isotropic or not with respect to penetrable waves, we discuss the modified MFS for both cases separately in Chapter 4 and 5, respectively. Chapter 6 then extends our computational framework to further ITP models, including a prospect for 3D applications, and Chapter 7 finally summarizes the main results of this work. Altogether, it is based on [66–68, 86] where the author of this thesis was also corresponding author and which were published during his doctoral studies.

Chapter 2

Mathematical preliminaries

The following sections of this chapter are designed to provide a compact recap on mathematical tools relevant for the theoretical scope of this thesis that would otherwise be spread over several textbooks. Concerning later proofs we may readily refer back to selected results that we are going to discuss here. Apart from the terminology to be introduced, differential calculus, complex analysis and the language of PDEs are the least required knowledge that will be built on.

2.1 Basic notation

For having a common starting ground and setting notations, we spend especially this section to shortly overview some vector and matrix algebra. Except for in combination with Bessel or Hankel functions, see [1], we follow the convention to use lower indices for components of multidimensional objects or functions, whereas superscripts in parenthesis refer to sequence labels and are thus clearly distinguishable from power exponents. Regarding the variety of possible product-type operations then, we need to keep two cases apart on the basis of index summation: Those where two factors might be of different size but have compatible adjacent dimensions, e.g. matrix-vector multiplication, and on the other hand there are scalar products which are defined for objects from the same set.

Concerning the first kind, we skip any product symbol and confine to matrix-vector and matrix-matrix multiplications. Embedding vectors according to $\mathbb{C}^d \simeq \mathbb{C}^{d\times 1}$, we define

$$(MV)_{i,j} = \sum_{p=1}^{d} M_{i,p} V_{p,j} \ ,$$

where $M \in \mathbb{C}^{c\times d}$ and $V \in \mathbb{C}^{d\times e}$. We state two important matrix decompositions that will be crucial for the numerical core of this thesis: for any full-rank matrix $M \in \mathbb{C}^{c\times d}$ with $c \geq d$ there is a unique QR factorization

$$M = QR\,,$$

where $Q \in \mathbb{C}^{c\times d}$ is unitary and $R \in \mathbb{C}^{d\times d}$ is upper triangular with positive diagonal elements, see [91]. The QR decomposition can be used to find an orthonormal basis for the range of M. Besides, the singular value decomposition divides

$$M = U\Sigma V \tag{2.1}$$

such that $U \in \mathbb{C}^{c\times c}$ and $V \in \mathbb{C}^{d\times d}$ are unitary and $\Sigma \in \mathbb{C}^{c\times d}$ is non-negative diagonal, see [91]. The positive diagonal entries $0 < \sigma_{min} = \sigma^{(1)} \leq \cdots \leq \sigma^{(e)}$ with $e \leq d$ are called singular values and encode the matrix' singularity if $\sigma_{min} \approx 0$, its spectral norm by $\sigma^{(e)}$, and finally the relative condition number which can be expressed by $\sigma^{(e)}/\sigma_{min}$ and thus serves as worst-case measure for numerical error propagation from general matrix manipulations.

For elements from the same argument class $V, W \in \mathbb{C}^{d\times e}$, representing again vectors or matrices dependent on whether e is equal to 1 or not, respectively, a commutative bilinear form can additionally be defined. It runs over all indices tuple-wise and will be signified by the dot symbol "$\cdot$", i.e.

$$V \cdot W = \sum_{i=1}^{d}\sum_{j=1}^{e} V_{i,j}W_{i,j} = \mathrm{tr}(VW^{\top})\,. \tag{2.2}$$

Here, $\mathrm{tr}(\bullet)$ abbreviates the trace operator for quadratic matrices with universal place holder $\bullet$ also used in different argument contexts later, and $\top$ denotes matrix transposition. In the further course of complex-valued calculus, taking real and imaginary parts will be abbreviated by $\mathrm{Re}(\bullet)$ and $\mathrm{Im}(\bullet)$, respectively, complex conjugation is expressed by overbars, i denotes the imaginary unit and $\arg(\bullet)$ outputs the complex argument. In order to turn (2.2) into a positive definite scalar product then, one of the arguments (without loss of generality the second) needs to be conjugated. Hence we set $|V| := |V|_2 := \sqrt{V \cdot \overline{V}}$ as well as $|V|_1 := \sum_{i=1}^{d}\sum_{j=1}^{e} |V_{i,j}|$. While norms for finite dimensional vector spaces, emphasized with single bars, are equivalent and thus only a matter of convenience, successful structural insights for problems in infinite dimensions, such as in function spaces, depend strongly on the selected topology. Especially Section 2.3 aims at giving an interconnected overview

of related concepts. Before, we recall some well-known basics about eigenvalues as being literally the focus of this thesis.

2.2 Linear and non-linear eigenvalue problems

Eigenvalues k are characteristic numbers which solve the system

$$M(k)\alpha = 0 \tag{2.3}$$

for some eigenvector $\alpha \in V\backslash\{0\}$, where $M(\kappa) : V \to V$ is a linear operator on a normed vector space V for each $\kappa \in \mathbb{C}$, see [14]. By convention, κ denotes a variable eigenvalue parameter while k the exact solution. Obviously, eigenvalues are interesting both from a technical point of view since they reduce certain operator-actions into scalar manipulations, but also from a modeling perspective as their spectrum can reflect resonance states. It might consist of duplicates of identical k with linear independent eigenvectors α whose span is referred to as the eigenspace and its dimension as geometric multiplicity.

Most commonly, eigenproblems arise linearly in κ, e.g. $M(\kappa) = A - \kappa I$, with the identity map I, which is occasionally dropped symbolically, and some spectral endomorphism $A : V \to V$. If V is finite dimensional with $\dim V = m$, it is well-known that the overall count of eigenvalues corresponding to A including geometric multiplicity is at most m. For compact self-adjoint operators A equality holds according to the Hilbert-Schmidt theorem for $m = \infty$ and there exists a complete orthonormal basis of eigenvectors, see [5]. With the concept of algebraic multiplicity then, i.e. the stagnating dimension of the kernel for $(A - kI)^r$ as $r \to \infty$, it can be shown for $m < \infty$ that V again decomposes into the direct sum of associated generalized eigenspaces. A corresponding decomposition for the case $m = \infty$ is generally not possible and requires more individual structures of the spectral operator involved. However, many other results from the finite dimensional setting such as the rank–nullity theorem can still be extended in the functional analytic context of Fredholm operators which abstract eigenvalue analysis is often built on.

Luckily, linear and non-linear eigenproblems are sometimes not that different from each other. This comes from the observation that if M is a polynomial in κ, (2.3) can be transformed into linear block form. For instance, if $M(\kappa) = A_0 + \kappa A_1 + \kappa^2 A_2$ is quadratic, we can easily verify that $k \neq 0$ is a nonlinear eigenvalue of M with eigenvector $\alpha \in V$ if and

only if

$$\left(\begin{pmatrix} A_0^{-1}A_1 & I \\ -A_0^{-1}A_2 & 0 \end{pmatrix} + \frac{1}{k}\begin{pmatrix} I & 0 \\ 0 & I \end{pmatrix}\right)\begin{pmatrix} \alpha \\ kA_0^{-1}A_2\alpha \end{pmatrix} = 0\,, \tag{2.4}$$

provided $A_0 : V \to V$ is invertible. An analogue substitution pattern applies to higher order polynomials. For general non-linear eigenproblems, linearization is only possible modulo truncation errors which then needs to be controlled individually.

2.3 Functions, distributions and shared operations

One of the prior concerns when investigating boundary value problems faces the question in which sense appearing partial derivatives or assigned boundary data for a given bounded domain $D \subset \mathbb{R}^d$ should be understood. Their meaning is therefore closely connected to setting a specific target space to which potential solutions are prescribed to belong. As this thesis focuses on the computation of certain PDE-based eigenvalues via approximation of corresponding eigenfunctions, we automatically have to deal with more than one class of elements. We now list systematically the mathematical foundations necessary for the setup of the ITP and its analysis from the next chapters. Upcoming definitions are taken from [76] if not stated otherwise and are compressed or adapted to the content we need.

First we introduce classical $C^l(D)$-spaces, $l \in \mathbb{N}_0$, which consist of all functions $f : D \to \mathbb{C}$ whose derivatives (as pointwise difference quotient limits) $\partial^\alpha f$ up to order l exist and are continuous. Here, we have used the multi-index power notation abbreviating $\partial^\alpha f = \partial_1^{\alpha_1} \dots \partial_d^{\alpha_d}$ with $\alpha_i \in \mathbb{N}_0$ for $1 \leq i \leq d$ such that $|\alpha|_1 \leq l$. Besides, we set $\nabla f(x) = \big(\partial_1 f(x), \dots, \partial_d f(x)\big)$ for the total differential at $x = (x_1, \dots, x_d)^\top \in D$. If all $\partial^\alpha f$ are continuous up to the boundary (denoted by $C^l(\overline{D})$) and the highest order derivatives fulfill additionally that

$$\sup_{\substack{x,y \in D, \\ x \neq y}} \frac{|\partial^\alpha f(x) - \partial^\alpha f(y)|}{|x-y|^\gamma} < \infty$$

for some $0 < \gamma \leq 1$, then we denote the corresponding set of Hölder-continuous functions as $C^{l,\gamma}(D)$. In particular, if $l = 0$ and $\gamma = 1$, its elements are more commonly known as Lipschitz functions. At best, $f \in C^l(D)$ for all l which is referred to as being infinitely smooth and ephasized by $C^\infty(D)$. Overcoming potential regularity difficulties near the boundary then, one can either reintroduce $C^\infty(\overline{D})$ in previous analogy or constrain to functions that have

compact support within D. For the latter we define the space of test functions

$$\mathscr{D}(D) := \left\{ f \in C^\infty(D) : \ \mathrm{supp} f \subset D \right\}$$

and note that they can be trivially extended to all of $\mathbb{R}^d$ by zero while obviously preserving global smoothness. One of the main motivations for their consideration stems from the attempt to assign a calculus of differentiation also to those objects which, as control quantities in some idealized model problems for example, are not sufficiently regular for the classical definition, or are not even defined locally in terms of some Lebesgue-measurable function such as Schwartz distributions. The delta-distribution δ_x for $x \in D$ is one famous instance and acts like a point evaluation on any test function, i.e.

$$\delta_x(\varphi) := \varphi(x) \ .$$

When endowing $\mathscr{D}(D)$ with the topology of uniform convergence on compact subsets of D, distributions appear as sequentially-continuous functionals in the dual space $\mathscr{D}(D)^*$. Their differentiation then enters upon its effect on test functions and is defined as $\partial^\alpha : \mathscr{D}(D)^* \to \mathscr{D}(D)^*$ for $f \in \mathscr{D}(D)^*$ and $\varphi \in \mathscr{D}(D)$ by

$$\partial^\alpha f(\varphi) := (-1)^{|\alpha|_1} f(\partial^\alpha \varphi) \ .$$

Identifying by abuse of notation any locally Lebesgue-integrable function f with its naturally induced functional in $\mathscr{D}(D)^*$, i.e. $\varphi \mapsto \int_D f(x)\varphi(x)\,\mathrm{d}x$ (giving indeed a one-to-one correspondence according to the fundamental theorem of variational calculus), we point out that distributional derivatives go hand in hand with the classical formula of integration by parts. Using the duality trick similarly, many other operations for functions can be rigorously generalized to certain subclasses of distributions, see Chapter 1 of [49]. Those include, for example, multiplication with smooth functions, convolution defined pointwise by

$$(f * g)(x) := \int_{\mathbb{R}^d} f(x-y)g(y)\,\mathrm{d}y \tag{2.5}$$

and extendible to pairs $f, g \in \mathscr{D}(\mathbb{R}^d)^*$ one of which has compact support (in the sense that test functions being supported outside that closed range are evaluated to zero), and the Fourier transform

$$\mathscr{F} f(\xi) := \int_{\mathbb{R}^d} f(x) \mathrm{e}^{\mathrm{i}x\cdot\xi}\,\mathrm{d}x$$

which is likewise feasible for distributions of compact support, but additionally for so-called tempered distributions $\mathscr{S}(\mathbb{R}^d)^*$ as its invariant class, see [76]. In combination, they yield back the formula $\mathscr{F}(f*g) = \mathscr{F}f\mathscr{F}g$ conform to the function setting, see Theorem 1.7.6 of [49].

Coming back to functions from a generalized distributional perspective via the aforementioned embedding, we denote by $L^p(D)$ for $1 \leq p \leq \infty$ the Banach space of Lebesgue-measurable functions f such that

$$\|f\|_{L^p(D)}^p := \int_D |f(x)|^p \,\mathrm{d}x < \infty$$

for $p < \infty$ whereas the borderline case $p = \infty$ emerges as $\|f\|_{L^\infty(D)} := \operatorname{ess\,sup}_D |f| < \infty$. Local integrability or boundedness with respect to all compact subsets of D can then be expressed by $L^p_{loc}(D)$, respectively. To enable a symmetric interplay with other elements, we confine to the Hilbert space setting $p = 2$ in the following which is endowed with the scalar product

$$(f,g)_{L^2(D)} := \int_D f(x)\overline{g}(x) \,\mathrm{d}x \,.$$

According to the Cauchy-Schwarz inequality we can bound

$$(f,g)_{L^2(D)} \leq \|f\|_{L^2(D)}\|g\|_{L^2(D)} \,. \tag{2.6}$$

If l is some non-negative integer, we introduce similarly Sobolev spaces of corresponding order by

$$H^l(D) := \{f \in L^2(D) : \ \partial^\alpha f \in L^2(D) \ \forall |\alpha|_1 \leq l\}$$

whose norm $\|\bullet\|_{H^l(D)} := (\bullet,\bullet)_{H^l(D)}$ is induced by

$$(f,g)_{H^l(D)} := \sum_{|\alpha|_1 \leq l} (\partial^\alpha f, \partial^\alpha g)_{L^2(D)} \,.$$

Being actually understood as distributional derivatives therein, the regularity assignment $\partial^\alpha f \in L^2(D)$ within $H^l(D)$ then claims the existence of a unique square-integrable function which is called weak derivative with overloaded notation $\partial^\alpha f$. Since the Fourier transform acts unitary on $L^2(\mathbb{R}^d)$ via Plancherel's identity

$$\int_{\mathbb{R}^d} f(x)\overline{g}(x) \,\mathrm{d}x = \frac{1}{(2\pi)^d} \int_{\mathbb{R}^d} \mathscr{F}f(\xi)\overline{\mathscr{F}g}(\xi) \,\mathrm{d}\xi \tag{2.7}$$

and generally turns differentiation into multiplication, i.e. $\mathscr{F}\partial_i f(\xi) = \mathrm{i}\xi_i \mathscr{F} f(\xi)$ for $1 \leq i \leq d$, there is the equivalent characterization

$$H^l(D) = \{f_{|D} : \ f \in \mathscr{S}(\mathbb{R}^d)^*, \ \int_{\mathbb{R}^d} (1+|\xi|^2)^l |\mathscr{F} f(\xi)|^2 \,\mathrm{d}\xi < \infty\} \ .$$

as long as there exists a continuous extension operator $E : H^l(D) \to H^l(\mathbb{R}^d)$. Apparently, both definitions of $H^l(D)$ share some reformulation in terms of L^2-controlled integrands but the advantage of the latter is that it readily applies to all $l \in \mathbb{R}$. With that it can be shown that, additional to $H^l(D)^* \simeq H^l(D)$ in terms of $(\bullet,\bullet)_{H^l(D)}$ according to the Riesz representation theorem, there exists an alternative isometric realization of $H^l(D)^*$ which is induced by the $(\bullet,\bullet)_{L^2(D)}$-based duality product

$$\langle f, g \rangle_{\widetilde{H}^{-l}(D), H^l(D)} := \frac{1}{(2\pi)^d} \int_{\mathbb{R}^d} \mathscr{F} f(\xi) \mathscr{F} g(-\xi) \,\mathrm{d}\xi \ . \tag{2.8}$$

The above integral resembles Plancherel's identity without conjugation using

$$\widetilde{H}^l(D) := \{f \in H^l(\mathbb{R}^d) : \ \mathrm{supp} f \subset \overline{D}\} \ .$$

In particular, (2.8) is independent of the extension of g and justifies why taking negative exponents of Sobolev spaces is associated with passing to their duals, see [17].

The facts listed so far for spaces defined on domains D can be largely adapted to ∂D as long as it is sufficiently smooth which we want to specify now. Generally, since manifolds are locally representable as the graph of a scalar function, smoothness of the boundary is reflected by the regularity of that function. For realizing a surface measure $\mathrm{d}s$ on manifolds in a differential manner, it is reasonable to request that D is at least a bounded Lipschitz domain due to Rademacher's theorem which thus also offers the determination of outer normal vectors $\nu \in \mathbb{S}^{d-1} := \{x \in \mathbb{R}^d : |x| = 1\}$ almost everywhere along ∂D. Hence, equivalent definitions of integrability and $H^l(\partial D)$ for $l \geq 0$ arise via a partition-of-unity pullback to the Euclidean reference frame in $\mathbb{R}^{d-1}$ with $d > 1$ and for $l < 0$ by duality again. In the special case when the boundary is homeomorph to the $(d-1)$-dimensional torus, Fourier calculus and in particular Sobolev spaces can even be treated in a corresponding periodic manner for which Plancherel's identity (2.7) then reduces to

$$\|f\|^2_{L^2([0,2\pi)^{d-1})} = \frac{1}{(2\pi)^{d-1}} \sum_{\xi \in \mathbb{Z}^{d-1}} |\mathscr{F} f(\xi)|^2 \tag{2.9}$$

and likewise

$$\|f\|^2_{H^l([0,2\pi)^{d-1})} = \frac{1}{(2\pi)^{d-1}} \sum_{\xi\in\mathbb{Z}^{d-1}} |\mathscr{F}f(\xi)|^2(1+|\xi|^2)^l \,, \tag{2.10}$$

where the Fourier coefficients are now given by

$$\mathscr{F}f(\xi) := \int_{[0,2\pi)^{d-1}} f(x)\mathrm{e}^{\mathrm{i}x\cdot\xi}\,\mathrm{d}x \,, \tag{2.11}$$

see [45]. At last, the overall connection of boundary and interior part of admissible functions is summarized by the celebrated trace theorem: For a $C^{l-1,1}$-domain D there is a unique continuous and right-invertible trace operator

$$\tau : H^s(D) \to H^{s-\frac{1}{2}}(\partial D)$$

such that $\tau(f) = f_{|\partial D}$ for all $f \in C^\infty(\overline{D})$, provided $1/2 < s \le l$. Hence we sometimes write $f_{|\partial D}$ or just f instead of $\tau(f)$ also for Sobolev functions f. Choosing $2 \le s \le l$, the results even extend to $\tau : H^s(D) \to H^{s-\frac{1}{2}}(\partial D) \times H^{s-\frac{3}{2}}(\partial D)$, where now $\tau(f) = (f_{|\partial D}, (\partial_\nu f)_{|\partial D})$, see Appendix 2 of [79]. The trace operator kernels can be characterized by

$$H^l_0(D) := \overline{\mathscr{D}(D)} \,,$$

with the closure taken in the $H^s(D)$-norm which thus extend the assignment of zero Dirichlet data to Sobolev functions. If $s \le 1/2$, the operator norm of τ blows up, but restricting to functions which respond to some differential operator in divergence form more regular than corresponding weak derivatives would a priori suggest, duality again yields a proper definition of traces based on variants of Green's second identity such as

$$\int_D f(x)\Delta g(x) - g(x)\Delta f(x)\,\mathrm{d}x = \int_{\partial D} f(s)\partial_\nu g(s) - g(s)\partial_\nu f(s)\,\mathrm{d}s \,, \tag{2.12}$$

which is originally valid for smooth functions and likewise for $f, g \in H^2(D)$ by density arguments from the next paragraph. Exploiting right-invertibility of the trace operator with $s = 2$ to ensure existence of some lifting function $g \in H^2(D)$ such that $\|g\|_{H^2(D)} \le C\big(\|g\|_{H^{\frac{3}{2}}(\partial D)} + \|\partial_\nu g\|_{H^{\frac{1}{2}}(\partial D)}\big)$ given $g_{|\partial D}$ and $\partial_\nu g_{|\partial D}$, we then see with (2.6) that

$$\|\partial_\nu f\|_{H^{-\frac{3}{2}}(\partial D)} := \sup_{\substack{\partial_\nu g_{|\partial D}=0,\\ \|g\|_{H^{\frac{3}{2}}(\partial D)}=1}} \int_D \Delta f(x)g(x) - f(x)\Delta g(x)\,\mathrm{d}x \leq C\big(\|f\|_{L^2(D)} + \|\Delta f\|_{L^2(D)}\big) \tag{2.13}$$

and

$$\|f\|_{H^{-\frac{1}{2}}(\partial D)} := \sup_{\substack{g_{|\partial D}=0,\\ \|\partial_\nu g\|_{H^{\frac{1}{2}}(\partial D)}=1}} \int_D f(x)\Delta g(x) - \Delta f(x)g(x)\,\mathrm{d}x \leq C\big(\|f\|_{L^2(D)} + \|\Delta f\|_{L^2(D)}\big) \tag{2.14}$$

are well-defined provided $f, \Delta f \in L^2(D)$ and D is a $C^{1,1}$ domain, see [29].

In order to close the gap within our overall function-distribution excursion, we want to point out that Sobolev spaces with their weak derivatives are in fact not far from being classically differentiable. The famous Sobolev embeddings show that under affine conditions on $l, d, s, \gamma \geq 0$ and for bounded Lipschitz domains $D \subset \mathbb{R}^d$ it holds that $H^s(D) \subset C^{l,\gamma}(D)$, whereas density results such as $\mathscr{D}(\mathbb{R}^d)_{|D} \subset H^l(D)$ always persist without restrictions, see [37]. For our analysis, the transitions between Sobolev spaces themselves with different exponents will be of major importance because the inclusions $H^s(D) \subset H^l(D)$ are always compact for $l < s$ and unbounded D. This implies that any weakly convergent sequence $\{f^{(m)}\}_{m\in\mathbb{N}} \subset H^s(D)$, signified by

$$f^{(m)} \rightharpoonup f \quad \text{in } H^s(D)$$

and which embodies $\big(\widetilde{f}, f^{(m)}\big)_{H^s(D)} \to \big(\widetilde{f}, f\big)_{H^s(D)}$ for all $\widetilde{f} \in H^s(D)$ (or with respect to (2.8) and $\widetilde{f} \in \widetilde{H}^{-s}(D)$), converges then strongly in $H^l(D)$, i.e.

$$f^{(m)} \to f \quad \text{in } H^l(D)$$

or equivalently $\big\|f^{(m)} - f\big\|_{H^l(D)} \to 0$. The case $l = s$ still exhibits weak compactness and ensures for any bounded sequence $\{f^{(m)}\}_{m\in\mathbb{N}} \subset H^l(D)$ a subsequence that we will not explicitly relabel such that $f^{(m)} \rightharpoonup f$ in $H^l(D)$. As for strong convergence, we want to recall that weak limits are unique, but the associated sequence norm is only weakly lower semi-continuous when $m \to \infty$. The methodology of weak convergence is thus very convenient

for passing from bounded approximate solutions of a given linear and non-trivial problem to some desired limit as long as the latter can be shown to be non-trivial.

At last, we want to mention that all the listed results stated for scalar functions or distributions until here can be adopted to the vector-valued case by interpreting the corresponding definitions component-wise. The augmented ranges are then, for instance, expressed via $H^l(D,\mathbb{C}^r)$, i.e. $f \in H^l(D,\mathbb{C}^r)$ implies $f_i \in H^l(D,\mathbb{C})$ for all $1 \leq i \leq r$, and to keep consistent to the old notation, we set $H^l(\mathbb{C}^d) := H^l(\mathbb{C}^d,\mathbb{C})$ if $r = 1$. Depending on whether the output of product-based operations or definitions have to become a scalar or vector when $r > 1$, the ambiguous multiplication so far need to be adjusted according to Section 2.1. With all these conventions at hand, we are now ready to address more PDE-related aspects towards the ITP.

2.4 Elliptic PDEs and fundamental solutions

In Chapter 1 we have already encountered the acoustic ITP as a representative from a more general family of modeling systems in focus of this thesis. They have in common that their distributional forms, i.e. the PDEs for the pairs v and w separately, are linear eigenproblems with eigenvalue parameter κ given by

$$\Delta_T + \kappa^2 I \,. \tag{2.15}$$

Here, I denotes the identity in some definite function space to be specified and Δ_T is some linear, second order differential operator in divergence form, i.e.

$$\Delta_T u(x) = \operatorname{div}\big(T(\nabla u(x))\big) \tag{2.16}$$

associated with the tensor-based map $T : \mathbb{C}^{r\times d} \to \mathbb{C}^{r\times d}$, where $u : D \to \mathbb{C}^r$ and the outer divergence $\operatorname{div}(\bullet)$ is taken row-wise. As convention, we always skip the trivial specification of T in the Laplace case $\Delta u = \operatorname{div}(\nabla u)$. The operators Δ_T are generally assumed to share the characteristics of strong ellipticity according to our constitutive ITP assumptions later: Δ_T is said to be strongly elliptic on D, see [76], if it holds for some uniform positive constant $c > 0$ that

$$(\eta\xi^\top)\cdot\Big(T(\eta\xi^\top)\Big) \geq c|\xi|^2|\eta|^2 \qquad \text{for all } x \in D,\ \xi \in \mathbb{R}^d \text{ and } \eta \in \mathbb{C}^r \,. \tag{2.17}$$

In the context of scalar PDEs, the addition “strong” is usually dropped because (2.17) actually states that T is uniformly positive definite with respect to certain rank-one matrices which are as such unambiguous for $r = 1$.

One benefit of strongly elliptic operators is that once $\Delta_T u$ exists in some relatively weak sense, regularity theory for proper spaces like in $H^l(D,\mathbb{C}^r)$ ensures that u is as good as the smoothness of PDE coefficients, the boundary itself and the traces of u allow. An accompanying a priori estimate for second order systems is therefore typically of the form

$$\|u\|_{H^{l+2}(D,\mathbb{C}^r)} \leq C\left(\|\Delta_T u\|_{H^l(D,\mathbb{C}^r)} + \|\mathscr{B}u\|_{H^{l+\frac{3}{2}}(\partial D,\mathbb{C}^r)} + \|u\|_{L^2(D,\mathbb{C}^r)}\right), \tag{2.18}$$

see [76], or, since $\kappa^2 u$ accounts as a compact perturbation in $H^l(D)$ for any $u \in H^{l+2}(D)$,

$$\|u\|_{H^{l+2}(D,\mathbb{C}^r)} \leq C\left(\|(\Delta_T + \kappa^2 I)u\|_{H^l(D,\mathbb{C}^r)} + \|\mathscr{B}u\|_{H^{l+\frac{3}{2}}(\partial D,\mathbb{C}^r)} + \|u\|_{L^2(D,\mathbb{C}^r)}\right), \tag{2.19}$$

where $C > 0$ is a constant and D is a bounded $C^{l+1,1}$-domain. Further, the last summand on the right-hand side of (2.18) and (2.19) can even be dropped if u is unique as a solution subject to the boundary data provided, e.g. $\mathscr{B}u = \tau u$ in the Dirichlet case. Alternatively, also other boundary control terms with corresponding norms can be used such as the co-normal derivative $\mathscr{B}u(x) = T(\nabla u(x))\nu \in H^{l+\frac{1}{2}}(\partial D,\mathbb{C}^r)$ from the Neumann problem whose solutions can at most be determined modulo the addition of constants, making $\|u\|_{L^2(D,\mathbb{C}^r)}$ in the a priori estimates then unavoidable. The complementing question of existence of solutions to strongly elliptic system subject to fulfilling given boundary data is generally linked to the applicability of the Fredholm alternative. While for vanishing Dirichlet data this is sufficiently assured by (2.17), cf. [76], more complex scenarios, including higher order differential operators, are completed in virtue of elliptic boundary value problems via complementing conditions, see [3, 2].

In free space or exterior domains, boundary data at infinity generally do not make sense as before and are replaced, for instance, by certain radiation conditions for $r := |x| \to \infty$ to obtain well-posedness. In this case, existence of solutions can often be handled explicitly in terms of fundamental solutions exhibiting the prescribed decay properties and which thus form the most important distribution class for our ITP analysis: Given $\Delta_T + \kappa^2 I$, $\Phi_{T,\kappa}$ is a fundamental solution (system), see [81, 51], if it is a distributional solution to

$$(\Delta_T + \kappa^2 I)\Phi_{T,\kappa} = -\delta_0 .$$

Existence of $\Phi_{T,\kappa}$ itself is guaranteed by the Malgrange–Ehrenpreis theorem for constant-coefficients-PDEs and depending on the symmetry of Δ_T it can often be expressed as a radial basis function in $C^\infty(\mathbb{C}\backslash(-\infty,0],\mathbb{C}^r)$. For example, in the case $d = 2,\ r = 1$ and $\Delta_T = \Delta$, it is well-known, see [96, 72], that a valid choice is $\Phi_\kappa = \mathrm{i}H_0^{(1)}(\kappa|\bullet|)/4$, where we have also

skipped the tensor index and with $H_0^{(1)}$ being the first Hankel function of order zero, see [1]. On the one hand, fundamental solutions cannot be globally smooth functions up to the underlying PDE order due to their singular right-hand-side inhomogeneity per definition. On the other hand, it is this subtlety which enables the aforementioned direct construction of particular solutions u to $(\Delta_T + \kappa^2 I)u = f$ via $\Phi_{T,\kappa} * f$ whenever $f \in \mathscr{D}(\mathbb{R}^d, \mathbb{C}^r)^*$ is compactly supported. It should be mentioned that for $r > 1$ the corresponding fundamental solution $\Phi_{T,\kappa}$ is matrix-valued, so $\Phi_{T,\kappa} * f$ might not be commutative as it is in the scalar case. However, similar to (2.18), it holds that if $f \in \widetilde{H}^l(D, \mathbb{C}^r)$ for some bounded set D and $l \in \mathbb{R}$, then $\Phi_{T,\kappa} * f \in H^{l+2}_{loc}(\mathbb{R}^d, \mathbb{C}^r)$, see Theorem 10.3.1 in [50].

While the latter generates inhomogeneous solutions of $(\Delta_T + \kappa^2 I)$ with right-hand side given by f, the outcome is totally different if the convolution involved is performed on some $(d-1)$-dimensional closed contour Γ. We will write for $f \in L^2(\Gamma, \mathbb{C}^r)$

$$x \mapsto (\Phi_{T,\kappa} *_{|\Gamma} f)(x) := \int_\Gamma \Phi_{T,\kappa}(x - s) f(s) \, \mathrm{d}s \tag{2.20}$$

and call (2.20) single layer potential, which now solves $(\Delta_T + \kappa^2 I)(\Phi_{T,k} *_{|\Gamma} f) = 0$ classically in $\Gamma^c = \mathbb{R}^d \backslash \Gamma$ and appears mostly in potential theory with the choice $\Gamma = \partial D$ to study corresponding homogeneous boundary value problems on D. However, this also comes along with certain jump conditions across the shared boundary that are harder to handle numerically than for the choice $\Gamma = \partial\Omega$ with $\Omega \supset \overline{D}$ being some open and bounded superset. In this way singularities from $\Phi_{T,\kappa}$ are indeed shifted away from $\overline{D}$ so that $\Phi_{T,k} *_{|\Gamma} f$ keeps smooth across ∂D for all $f \in L^2(\Gamma, \mathbb{C}^r)$. With the freedom of locating Γ and choosing proper coefficient functions f then, we will try to approximate eigenfunctions of the ITP and give thus rise to the MFS described in the next chapter.

Chapter 3

The method of fundamental solutions

The MFS is our special representative of boundary approximation methods that we will analyze in detail for ITE computations in two dimensions. In this chapter we are going to introduce the standard version, discuss its natural failures in the context of eigenproblems and present a successful improvement.

3.1 About PDE discretization techniques

Given the task of approximating solutions to a given boundary value problem which will be an intermediate step of our eigenvalue detection procedure to be presented, there are many ways to do so. Usually, they have in common that two families of functions (or distributions) are involved: on the one hand there is the set of trial functions, which are to generate approximate eigenfunctions and should therefore be chosen as a dense set in the prescribed target space of the sought solution. On the other hand there are the test elements, which serve to measure some residual quantity to be minimized by approximate eigenfunctions.

Among the most famous and approved methods is the finite element Galerkin method for which both sets coincide. Its span is normally generated by easily-constructible functions like local polynomials that are supported on few adjacent cells of an auxiliary and preferably fine mesh covering the domain of interest. This quite general but costly formulation makes this approach applicable for a wide range of numerical PDE applications, especially for the treatment of inhomogeneous coefficients. Although the relatively high number of degrees of freedom involved rarely affects the method's stability in practice due to sparsity of resulting discretization matrices, it does influence the convergence rate through the global smoothness incompatibility of finite elements being mostly either non-trivially analytic or identically zero within each mesh cell. As a consequence, the achievable accuracy of the method's

outcome is primarily limited through the discretization complexity to algebraic error decay, even for regular PDEs or smooth domain samples, see [80].

While finite element methods, as a subclass of Ritz methods, aim to optimize conditions which are supported on the interior domain such as PDEs via localized trial functions and thus exhibit correct boundary data already by construction, Trefftz methods go the other way round and consider superpositions of particular global PDE-solutions instead whose boundary misfits need to be controlled then in the ordinary terms of collocation, least-squares or Galerkin projections, see [95]. The advantages of the latter approach are two-fold: First, it reduces the residual quantity from the interior to the lower-dimensional boundary of the domain which usually results in less unknowns for the approximation procedure. Second, the corresponding trial functions can be infinitely smooth and are therefore expected to reach optimal convergence rates as for general spectral problems, see [94]. According to conservation of mysery though, the price one typically has to pay is that the discretization matrices generated by convenient trial elements become dense and severely ill-conditioned. In our particular case of radial basis functions there is even an uncertainty principle, see [89], which states that both the attainable error and the condition number for the approximation procedure cannot be kept small simultaneously. To cope with critical round-off error amplifications from ill-conditioning then, one could apply regularization techniques, see [60], or elaborate the choice of a more efficient trial function basis via some additional pre-process, see [40]. Since we will be interested in solving eigenproblems which are associated with explicitly filtering degenerate systems, we will make use of the latter remedy for the MFS later.

3.2 The standard method of fundamental solutions

The MFS, also called charge simulation method [57], is a Trefftz method which goes back to Kupradze and Aleksidze at the beginning of the 1960s. It was designed to find approximate solutions to well-posed boundary value problems, see [69], and is a boundary-type collocation method with translated fundamental solutions as trial functions varied in their characteristic delta-distribution-singularity outside the domain of interest. As such it can be interpreted as a discretization of (2.20) according to the following basic setup:
Assume we want to find a numerical solution u to a constant-coefficient-PDE (or to a system for $r > 1$) of the form $\Delta_T u + \kappa^2 u = 0$ for some non-degenerate and fixed $\kappa \in \mathbb{C}$ on a bounded, simply connected domain $D \subset \mathbb{R}^2$ such that $\mathscr{B}u = f$. Here, f is a given (vector) function on ∂D which is piecewise smooth to admit reasonable point evaluations. According to collocation, a classical MFS approximation with $rm \in \mathbb{N}$ degrees of freedom is based on

a least-squares optimization for matching boundary data which requires m representative collocation points, labeled relative to their total count according to

$$\left\{x^{(1/m)},\ldots,x^{(m/m)}\right\}\subset\partial D\,,$$

and $n\geq m$ PDE-fulfilling trial functions derived from corresponding fundamental solutions via

$$x\mapsto\varphi_{T,\kappa}^{(j/n)}(x):=\Phi_{T,\kappa}\left(x-s^{(j/n)}\right)\in\mathbb{C}^{r\times r}\,. \tag{3.1}$$

Here, $\left\{s^{(1/n)},\ldots,s^{(n/n)}\right\}\subset\overline{D}^{\mathsf{c}}$ are n distinct so-called sources or charge points, in association with the delta peaks from $\Phi_{T,\kappa}$ whose efficient locations are worth some discussion as being still a partially open problem nowadays, see [6]: The main idea behind their introduction as specified so far is on the one hand the easy generation of linear independent trial functions $\varphi_{T,\kappa}^{(j/n)}(x)$ just by varying $s^{(j/n)}$, and on the other hand to avoid artificial singularities within the domain of interest that would otherwise be inherited from any resulting approximate solution. Being thus justified as auxiliary instances for the solution procedure than intrinsic to the boundary value problem itself, $\left\{s^{(1/n)},\ldots,s^{(n/n)}\right\}$ can either be interpreted as n further degrees of freedom in the non-linear process of minimizing the boundary collocation defect, see [38], or, as we will do thanks to many concrete guidelines, cf. [6, 10, 57], they are to be preselected manually for each m. For the latter one usually fixes some Jordan curve Γ as admissible distribution range independent of m so that $\Gamma=\partial\Omega$ as well as $\overline{D}\subset\Omega$ holds, see Figure 3.1. It is thus ensured that $\Gamma\cap\partial D=\emptyset$, in particular $\varphi_{T,\kappa}^{(j/n)}\in C^{\infty}(\overline{D},\mathbb{C}^{r})$, and that any linear combination of our singularity-free trial functions indeed resembles the Riemann-sum-version of (2.20), see Lemma 6. The latter is the starting point of numerous discretization techniques for boundary integral equations such as the boundary element method, see [63, 62] in the ITP context. Although looking similar, a clear advantage and difference of the MFS is that it is mesh-free and avoids numerical evaluation of singular integrals. Moreover, the fact that MFS convergence rates even slow down when Γ approaches ∂D, see [10, 93, 74], finally hints that independent studies are required.

To continue with the MFS based on the above assumptions, at each approximation step m we specify $n=m$ sources for (3.1)

$$\left\{s^{(1/m)},\ldots,s^{(m/m)}\right\}\subset\Gamma$$

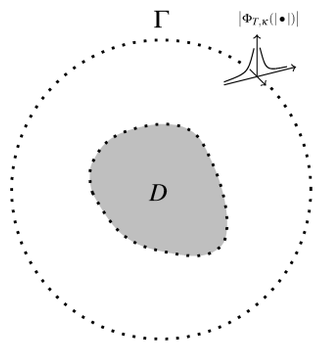

Fig. 3.1 Exemplary MFS configuration for some $D \subset \mathbb{R}^2$ with sampled collocation points $x^{(i/m)} \in \partial D$ and sources $s^{(j/n)} \in \Gamma$ along the circular boundary of Ω.

and aim to solve the linear system of equations

$$\sum_{j=1}^{m} \mathscr{B}\varphi_{T,\kappa}^{(j/m)}\left(x^{(i/m)}\right)\alpha^{(j/m)} = f\left(x^{(i/m)}\right) , \qquad 1 \le i \le m , \tag{3.2}$$

where $\alpha := \left(\alpha^{(1/m)}, \ldots, \alpha^{(1/m)}\right)^\top \in \mathbb{C}^{mr}$ lists the coefficients (or coefficient vectors) to be determined for our numerical solution

$$u^{(m)}(x) := \sum_{j=1}^{m} \varphi_{T,\kappa}^{(j/m)}(x)\alpha^{(j/m)} . \tag{3.3}$$

Accordingly, the (block) coefficient matrix for (3.2) with Dirichlet boundary data reads

$$B_T(\kappa) := \begin{pmatrix} \varphi_{T,\kappa}^{(1/m)}\left(x^{(1/m)}\right) & \cdots & \varphi_{T,\kappa}^{(m/m)}\left(x^{(1/m)}\right) \\ \vdots & \ddots & \vdots \\ \varphi_{T,\kappa}^{(1/m)}\left(x^{(m/m)}\right) & \cdots & \varphi_{T,\kappa}^{(m/m)}\left(x^{(m/m)}\right) \end{pmatrix} , \tag{3.4}$$

while for Neumann problems it becomes

$$T(\nabla B_T(\kappa))\nu := \begin{pmatrix} T\left(\nabla\varphi_{T,\kappa}^{(1/m)}\left(x^{(1/m)}\right)\right)\nu & \cdots & T\left(\nabla\varphi_{T,\kappa}^{(m/m)}\left(x^{(1/m)}\right)\right)\nu \\ \vdots & \ddots & \vdots \\ T\left(\nabla\varphi_{T,\kappa}^{(1/m)}\left(x^{(m/m)}\right)\right)\nu & \cdots & T\left(\nabla\varphi_{T,\kappa}^{(m/m)}\left(x^{(m/m)}\right)\right)\nu \end{pmatrix} , \tag{3.5}$$

where $B_T(\kappa), T(\nabla B_T(\kappa))\nu \in \mathbb{C}^{mr\times mr}$ are designed in the style of (2.3). In the Laplace case, we may skip the trivial tensor index again and simply write $B(\kappa)$ or $\nabla B(\kappa)\nu$, respectively. Some selected analysis results for MFS applications with $f \neq 0$ can be found in [17, 10]. The special case of eigenproblems, i.e. $f = 0$ and degenerate κ, is usually a bit trickier since the trivial solution $\alpha = 0$ turns out to spoil the computation procedure which will therefore be discussed in more detail in the next section.

3.3 The standard method of fundamental solutions applied to eigenproblems

Having derived the implementation for the standard MFS in the last section, we want to focus now on how to compute eigenvalues with it. We confine first to the scalar Dirichlet eigenproblem ($r = 1$) for the sake of simple presentation since the adaption to the ITP case will be quite straightforward once we have set an accompanying approximation theory. We call $k > 0$ a Dirichlet eigenvalue for the Laplace operator (which has a purely real spectrum as being self-adjoint) if there exists a non-trivial solution u to

$$\Delta u + k^2 u = 0 \quad \text{in } D \tag{3.6}$$

$$u = 0 \quad \text{on } \partial D\,. \tag{3.7}$$

Our MFS matrix from (3.4) then formally becomes in analogy to (2.3)

$$\begin{pmatrix} H_0^{(1)}\big(\kappa\big|x^{(1/m)} - s^{(1/m)}\big|\big) & \dots & H_0^{(1)}\big(\kappa\big|x^{(1/m)} - s^{(m/m)}\big|\big) \\ \vdots & \ddots & \vdots \\ H_0^{(1)}\big(\kappa\big|x^{(m/m)} - s^{(1/m)}\big|\big) & \dots & H_0^{(1)}\big(\kappa\big|x^{(m/m)} - s^{(m/m)}\big|\big) \end{pmatrix} \begin{pmatrix} \alpha^{(1/m)} \\ \vdots \\ \alpha^{(m/m)} \end{pmatrix} = \begin{pmatrix} 0 \\ \vdots \\ 0 \end{pmatrix}, \tag{3.8}$$

where the trial functions (3.1) are already expressed by $\Phi_\kappa = \mathrm{i}H_0^{(1)}(\kappa|\bullet|)/4$ modulo pre-factors and which are holomorphic with respect to κ in the branch $\mathbb{C}\backslash(-\infty, 0]$. Note that although the original eigenproblem (3.6) is linear in κ^2, the resulting MFS system turns non-linear. The total $2m$ computational points are without further specification $\{x^{(1/m)}, \dots, x^{(m/m)}\} \subset \partial D$ and $\{s^{(1/m)}, \dots, s^{(m/m)}\} \subset \Gamma$ for now. We are interested in finding those $\kappa = \kappa^{(m)}$ in (3.8) such that (3.6) is solved approximately for some non-trivial MFS candidate $u^{(m)}$ according to (3.3). Approximately means here that we cannot expect in general for all tuples of source and collocation points $u^{(m)}$ to vanish identically along all $x^{(i/m)}$, but we can at least hope that these boundary misfit samples become altogether close

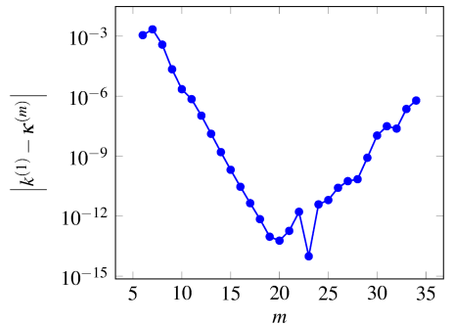

Fig. 3.2 Declining error behavior for the nearest eigenvalue output $\kappa^{(m)}$ of Beyn's algorithm approximating the first Dirichlet eigenvalue $k^{(1)}$ of the unit disc.

to zero for $\kappa^{(m)}$ near exact eigenvalues, or in other words that the right hand side of (3.8) can be made small compared to the coefficient norm of $\alpha \in \mathbb{C}^m$.

An elegant way to compute those non-linear eigenvalues κ for which the quadratic matrix $B(\kappa)$ in (3.8) becomes numerically singular is given by Beyn's algorithm, see [14]. It is based on a generalization of the residue theorem applied to matrix-valued functions that are holomorphic in each component. In this way Beyn's algorithm is capable of finding all degenerating κ of $B(\kappa)$, or equivalently approximate eigenvalue candidates for (3.6) including multiplicities, within a prescribed search region $R \subset \mathbb{C}$. Implemented similar as in Section 3.1 of [67], we aim to measure the absolute deviation of the nearest output $\kappa^{(m)}$ of Beyn's algorithm from the smallest eigenvalue $k^{(1)}$ of the unit disc $D = B_1(0)$ for different m. For this comparison, we note that $k^{(1)} \leq k^{(2)} \leq \dots$ can easily be computed analytically: separation of variables in polar coordinates $(r, \varphi) \in (0,1) \times [0, 2\pi)$ leads to the eigenfunction expansion, see [30],

$$u(r,\varphi) = a^{(0)} J_0(kr) + \sum_{p=1}^{\infty} J_p(kr)\left(a^{(p)}\cos(p\varphi) + b^{(p)}\sin(p\varphi)\right) , \tag{3.9}$$

where J_p denotes the p-th Bessel function of the first kind, see [1], and $a^{(0)}, a^{(p)}, b^{(p)} \in \mathbb{C}$ with $p \in \mathbb{N}$ are the unknown coefficients. The boundary condition in (3.6) then becomes $u(1,\varphi) = 0$ for all $0 \leq \varphi < 2\pi$ and orthogonality of the trigonometric factors yields $J_p(k) = 0$ whenever $a^{(p)} \neq 0$ or $b^{(p)} \neq 0$. Thus, the Dirichlet spectrum for the unit disc coincides with the roots of J_p whose smallest is found to be $k^{(1)} = 2.404825557695772\dots$ for $p = 0$. Figure 3.2 shows that for moderate m the error of $\kappa^{(m)}$ first decays very fast to a minimum above machine precision. Afterwards, it suddenly tends to deteriorate (except for one outlier) at

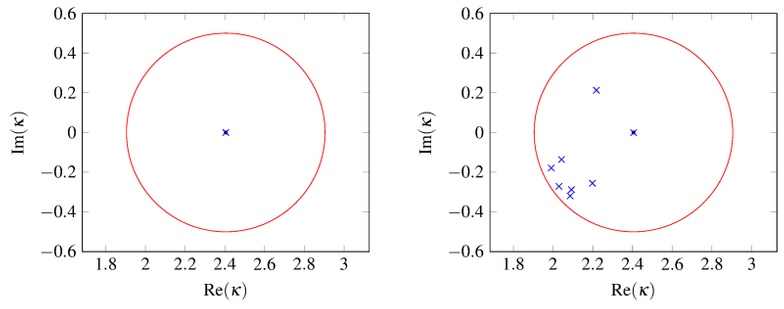

Fig. 3.3 Spurious output from Beyn's algorithm for $m = 20$ (left) and $m = 35$ (right) within $B_{0.5}\left(k^{(1)}\right) \subset \mathbb{C}$ as eigenvalue search region .

$m = 23$ and any further increase of collocation points only spoils the approximation process. What is going wrong?

A direct look at the output of Beyn's algorithm in Figure 3.3 reveals that with the addition of more and more collocation points the total number of numerical eigenvalue candidates grows within any localized region R of the complex plane. Knowing all $k^{(\ell)}$ due to our independent root calculations via Bessel functions, we can conclude that spurious eigenvalues arise if m is critically large. To understand their origin heuristically, we go back to (2.20) which is our associated boundary integral of convolution type that we think to be discretized by the MFS. Because of $\partial D \cap \Gamma \neq \emptyset$, $\Phi_\kappa *_{|\Gamma} f$ contains effectively a smooth kernel with respect to ∂D and can thus be interpreted, after restriction, as the $L^2(\partial D)$-outcome of a compact operator acting on coefficient functions $f \in L^2(\Gamma)$. In this spirit the associated MFS boundary matrix $B(\kappa)$ is to reflect properties of general compact operators for sufficiently large m one of which is the accumulation of singular values around zero, see [25]. In other words, for every κ there exists a sequence of coefficient functions $\left\{f^{(m)}\right\} \subset L^2(\Gamma)$ which are without restriction scaled to unit norm such that $\left\|\Phi_\kappa *_{|\Gamma} f^{(m)}\right\|_{L^2(\partial D)} \to 0$. By discretization, we then also expect the smallest singular values of $B(\kappa)$ to approach zero for $m \to \infty$ for all κ, turning it thus numerically singular everywhere. Beyn's algorithm would finally detect both the desired approximations for exact eigenvalues $k^{(\ell)}$ with their naturally evanescent boundary defects as well as samples of indistinguishably spurious eigenvalues arising from the underlying, ill-posed eigenproblem formulation by compact operators.

3.4 The modified method of fundamental solutions for handling eigenproblems

It seems that the MFS in its standard form is not well-suited for the treatment of eigenproblems and we seek for an extension that remedies the aforementioned pollution problem. In short, eigenvalue differentiation based on trace information of approximate eigenfunction candidates has proven to be ill-posed, hence taking additionally their interior behavior into account might turn out beneficial. With that in mind, the main difference between spurious and real Dirichlet eigenvalues will emerge, from a trial function perspective, in the norm ratio of boundary to interior which is either bounded from below or goes down to zero for eigenfunctions, respectively. More precisely, the asserted bound associated with spurious eigenvalues comes heuristically from (2.19) and the fact that MFS trial functions $\widetilde{u}$ perfectly fulfill the PDE condition from the eigenproblem by definition. Since κ is non-degenerate when being spurious, (2.19) reduces to

$$\frac{1}{C_{\kappa,D}} \leq \frac{\|\widetilde{u}\|_{H^{l+\frac{3}{2}}(\partial D)}}{\|\widetilde{u}\|_{H^{l+2}(D)}} ,$$

where the left-hand side depends only on κ and D. With a more elaborate derivation for self-adjoint operators, see [70, 10] for the Laplacian treatment, one can get rid of higher order fractional Sobolev norms to deal exclusively with more practical L^2-norms and the κ-dependent lower bound can even be specified as

$$\frac{1}{C_D} \min_{\ell \in \mathbb{N}} \frac{\left|\kappa - k^{(\ell)}\right|}{\left|k^{(\ell)}\right|} \leq \frac{\|\widetilde{u}\|_{L^2(\partial D)}}{\|\widetilde{u}\|_{L^2(D)}} \tag{3.10}$$

with some pure domain constant $C_D > 0$ now. In particular, note that the right-hand side can only vanish if κ approaches some $k^{(\ell)}$. In this way a clear eigenvalue filter is indicated in terms of computable quantities that combine to avoid the accumulation problem around zero seen in the last section. Inequality (3.10) will play a model role for our ITE analysis as it directly relates the boundary misfit of PDE-fulfilling trial functions with the deviation from any nearby eigenvalue k. It also shows that the main failure of the standard MFS originates from the undesired approximation of the zero function both on ∂D and in D whenever spurious eigenvalues are detected. What the MFS community usually does in the context of eigenproblems, see for instance [7], is to incorporate one inner indicator point $\widehat{x} \in D$ on which the eigenfunction u is assumed not to vanish. By a scaling argument one can then

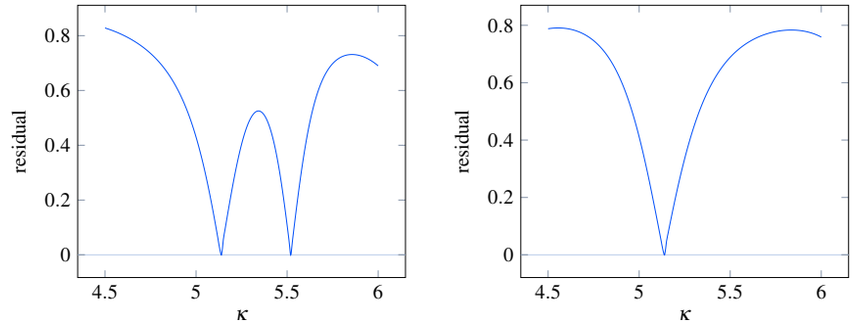

Fig. 3.4 Comparison of residuals with respect to optimal α from (3.11), evaluated at different interior points $\widehat{x}$ within the unit disc D for $m = 20$ source and collocation points each: On the left we choose $\widehat{x} = (0.8, 0)^\top$ whereas on the right we take $\widehat{x}_* = \left(k^{(1)}/k^{(3)}, 0\right)^\top$. The latter obviously misses the dip around $k^{(3)}$ since any of its eigenfunctions fulfills $u^{(3)}(\widehat{x}_*) = 0$ according to (3.9) and thus fails to fulfill the normalization constraint within the least-squares procedure.

demand $u(\widehat{x}) = 1$ so that the overdetermined system to be solved now reads

$$\begin{pmatrix} H_0^{(1)}\left(\kappa\left|x^{(1/m)} - s^{(1/m)}\right|\right) & \dots & H_0^{(1)}\left(\kappa\left|x^{(1/m)} - s^{(m/m)}\right|\right) \\ \vdots & \ddots & \vdots \\ H_0^{(1)}\left(\kappa\left|x^{(m/m)} - s^{(1/m)}\right|\right) & \dots & H_0^{(1)}\left(\kappa\left|x^{(m/m)} - s^{(m/m)}\right|\right) \\ H_0^{(1)}\left(\kappa\left|\widehat{x} - s^{(1/m)}\right|\right) & \dots & H_0^{(1)}\left(\kappa\left|\widehat{x} - s^{(m/m)}\right|\right) \end{pmatrix} \begin{pmatrix} \alpha^{(1/m)} \\ \vdots \\ \alpha^{(m/m)} \end{pmatrix} = \begin{pmatrix} 0 \\ \vdots \\ 0 \\ 1 \end{pmatrix}, \tag{3.11}$$

which is to be understood in a least-squares sense. Although mostly working well in practice, problems still arise if $\widehat{x}$ is accidentally chosen as a root of an exact eigenfunction. Figure 3.4 confirms that corresponding eigenvalues would not even be detected any more when solving (3.11) and therefore lead to incomplete results. Also, we want to recall that it is actually the full $L^2(D)$-norm instead of only a single point evaluation which controls the eigenvalue approximation via the denominator in (3.10). Reflecting this consistently will become crucial in the non-self-adjoint ITP case, see Theorem 1.

From this point of view it becomes desirable to attach more than one representative inner point to the MFS boundary matrices B to better align the norm discrepancy as well as lower the chance of hitting inadmissible zero-level-contours. Obtained via scaling before, the individual yet unknown inner structure of any eigenfunction now hinders some direct normalization assignment on the right-hand side of (3.11) for more than one interior point $\widehat{x}$. Luckily, Betcke and Trefethen proposed in [13] another elegant way to still implement

this idea which they presented within the framework of the method of particular solutions, a related boundary collocation technique. It is based on a gimmick of the *QR* factorization and therefore also applicable to the MFS case which we will describe in the following:

First, we select $\widehat{m} \in \mathbb{N}$ interior points $\left\{\widehat{x}^{(1/\widehat{m})}, \ldots, \widehat{x}^{(\widehat{m}/\widehat{m})}\right\}$ which are to exhaust the domain D with two possible strategies. Namely, their locations and total number can be chosen either dynamically proportional to m as explicit degrees of freedom within the MFS routine, or sufficiently large and fixed in the sense of unchanged quadrature points to better resemble the $L^2(D)$-norm of superposed trial functions within (3.10) at each step m. Hence, we wish to choose $\left\{\widehat{x}^{(1/\widehat{m})}, \ldots, \widehat{x}^{(\widehat{m}/\widehat{m})}\right\}$ sufficiently dense to hit non-zero niveau lines for every $\kappa \in \mathbb{C}$. Then, the MFS matrix (3.8) shall again be extended by the information of trial functions at those interior points which defines

$$\widehat{I}(\kappa) = \begin{pmatrix} H_0^{(1)}\left(\kappa\left|\widehat{x}^{(1/\widehat{m})} - s^{(1/m)}\right|\right) & \ldots & H_0^{(1)}\left(\kappa\left|\widehat{x}^{(1/\widehat{m})} - s^{(m/m)}\right|\right) \\ \vdots & \ddots & \vdots \\ H_0^{(1)}\left(\kappa\left|\widehat{x}^{(\widehat{m}/\widehat{m})} - s^{(1/m)}\right|\right) & \ldots & H_0^{(1)}\left(\kappa\left|\widehat{x}^{(\widehat{m}/\widehat{m})} - s^{(m/m)}\right|\right) \end{pmatrix} \in \mathbb{C}^{\widehat{m}\times m} \, .$$

Concatenating both, we arrive at the so-called modified MFS matrix

$$M(\kappa) = \begin{pmatrix} B(\kappa) \\ \widehat{I}(\kappa) \end{pmatrix} = \begin{pmatrix} H_0^{(1)}\left(\kappa\left|x^{(1/m)} - s^{(1/m)}\right|\right) & \ldots & H_0^{(1)}\left(\kappa\left|x^{(1/m)} - s^{(m/m)}\right|\right) \\ \vdots & \ddots & \vdots \\ H_0^{(1)}\left(\kappa\left|x^{(m/m)} - s^{(1/m)}\right|\right) & \ldots & H_0^{(1)}\left(\kappa\left|x^{(m/m)} - s^{(m/m)}\right|\right) \\ H_0^{(1)}\left(\kappa\left|\widehat{x}^{(1/\widehat{m})} - s^{(1/m)}\right|\right) & \ldots & H_0^{(1)}\left(\kappa\left|\widehat{x}^{(1/\widehat{m})} - s^{(m/m)}\right|\right) \\ \vdots & \ddots & \vdots \\ H_0^{(1)}\left(\kappa\left|\widehat{x}^{(\widehat{m}/\widehat{m})} - s^{(1/m)}\right|\right) & \ldots & H_0^{(1)}\left(\kappa\left|\widehat{x}^{(\widehat{m}/\widehat{m})} - s^{(m/m)}\right|\right) \end{pmatrix} , \tag{3.12}$$

which we are still left to turn into a filter against spurious eigenvalues similar to (3.11). However, if $\widehat{m} > 1$, the lifting '1'-assignment from the last row would have to be formally replaced by an entire unit vector with unknown orientation. Therefore, instead of imposing a concrete normalization condition on the right-hand side, the idea is now to already normalize $M(\kappa)$ properly. This can be easily realized by a *QR* decomposition of the modified MFS matrix whose unitary factor can then again be divided into a boundary and interior part according to

$$M(\kappa) = Q(\kappa)R(\kappa) = \begin{pmatrix} Q_B(\kappa) \\ Q_I(\kappa) \end{pmatrix} R(\kappa) \, ,$$

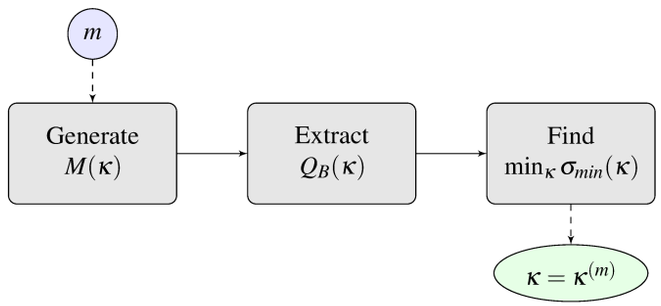

Fig. 3.5 Numerical steps within the modified MFS algorithm with input m and approximate eigenvalue output $\kappa^{(m)}$.

where $R(\kappa), Q_B(\kappa) \in \mathbb{C}^{m\times m}$ and $Q_I(\kappa) \in \mathbb{C}^{\widehat{m}\times m}$. The crucial observation now is that the ranges of $M(\kappa)$ and $Q(\kappa)$ are the same since $R(\kappa)$ is invertible by rank conservation, in particular the ranges of $Q_B(\kappa)$ and $B(\kappa)$ coincide. So we may replace the standard MFS matrix $B(\kappa)$ in (3.8) by $Q_B(\kappa)$ without changing the non-trivial solvability of that system. Being thus mathematically equivalent, only the latter reformulation embodies the demanded pollution filter though: assume there is $\kappa \in \mathbb{C}$ and $\beta \in \mathbb{C}^m$ with $|\beta| = 1$ such that $Q_B(\kappa)$ is approximately singular, i.e. $|Q_B(\kappa)\beta| \approx 0$. Since orthogonalization corresponds to a change of basis, we can find a linear combination of MFS trial functions, denoted by $u^{(m)}$ with actual coefficient vector $\alpha = R(\kappa)^{-1}\beta$, whose sampled boundary misfit is given by

$$\begin{pmatrix} u^{(m)}\left(x^{(1/m)}\right) \\ \vdots \\ u^{(m)}\left(x^{(m/m)}\right) \end{pmatrix} = B(\kappa)\alpha = Q_B(\kappa)\beta \ .$$

The benefit of working with $Q_B(\kappa)$ instead of $B(\kappa)$ now is that having confined to a fixed vector length $|\beta| = 1$ gives us direct control over $u^{(m)}$'s interior contribution via

$$\begin{aligned} 1 = |Q(\kappa)\beta|^2 &= |Q_B(\kappa)\beta|^2 + |Q_I(\kappa)\beta|^2 \\ &= \sum_{i=1}^{m} \left|u^{(m)}\left(x^{(i/m)}\right)\right|^2 + \sum_{i=1}^{\widehat{m}} \left|u^{(m)}\left(\widehat{x}^{(i/\widehat{m})}\right)\right|^2 \\ &\approx \sum_{i=1}^{\widehat{m}} \left|u^{(m)}\left(\widehat{x}^{(i/\widehat{m})}\right)\right|^2 . \end{aligned} \tag{3.13}$$

For the first equality we used explicitly that Q is unitary which links the transformed coefficient norm of β in a norm-preserving way to the boundary plus interior collocation

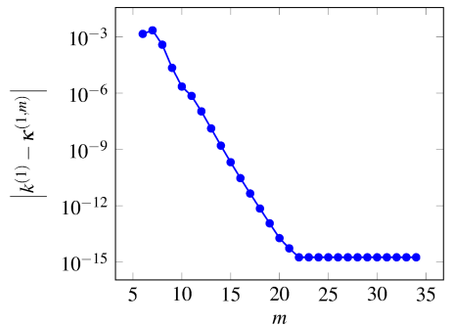

Fig. 3.6 Geometric error decay reaching machine precision for the modified MFS computing $\kappa^{(1,m)}$ as approximation for the first Dirichlet eigenvalue $k^{(1)}$ of the unit disc.

contribution of its associated trial function $u^{(m)}$. This is what we thought of before by shifting the normalization condition from the right-hand side of (3.11) into the final system matrix $Q(\kappa)$. The last estimate then formalizes why spurious eigenvalues are not detected any more by approximate solutions of $|Q_B(\kappa)\beta| \approx 0$ which we are left to turn into a concrete minimization procedure for κ: the closer it is to a real eigenvalue, the more the interior (boundary) part of optimal trial functions should approach unity (zero) in norms. Thus the trivial solution $u^{(m)} = 0$ cannot be generated any more numerically. Hence, we choose the minimal singular value $\sigma_{min}(\kappa)$ of $Q_B(\kappa)$ as a measure for how small the boundary misfit can be made at best for fixed κ. The objective of interest for the non-linear eigenproblem based on the MFS then becomes

$$\kappa \mapsto \sigma_{min}(\kappa) = \min_{\beta \in \mathbb{C}^m, |\beta|=1} |Q_B(\kappa)\beta| \ .$$

The entire algorithm for establishing and minimizing $\kappa \mapsto \sigma_{min}(\kappa)$, cf. Figure 3.5, will be referred to as *modified MFS* in the spirit of [13] and we call those $\kappa = \kappa^{(m)}$, giving sufficiently small values $\sigma_{min}\big(\kappa^{(m)}\big)$ or its roots, approximate eigenvalues. As before, their superscript indicates the degrees of freedom within the boundary collocation process and we can optionally add a further one as the eigenvalue's (or the eigenfunction's) order label $\kappa^{(\ell,m)}$ according to (3.10), i.e.

$$\min_{j\in\mathbb{N}} \frac{\left|\kappa^{(\ell,m)} - k^{(j)}\right|}{\left|k^{(j)}\right|} = \frac{\left|\kappa^{(\ell,m)} - k^{(\ell)}\right|}{\left|k^{(\ell)}\right|} \le C_D \frac{\left\|u^{(\ell,m)}\right\|_{L^2(\partial D)}}{\left\|u^{(\ell,m)}\right\|_{L^2(D)}} \approx C_D \frac{\sqrt{\widehat{m}|D|}\left|Q_B\big(\kappa^{(\ell,m)}\big)\beta\right|}{\sqrt{m|\partial D|}\left|Q_I\big(\kappa^{(\ell,m)}\big)\beta\right|} \ .$$

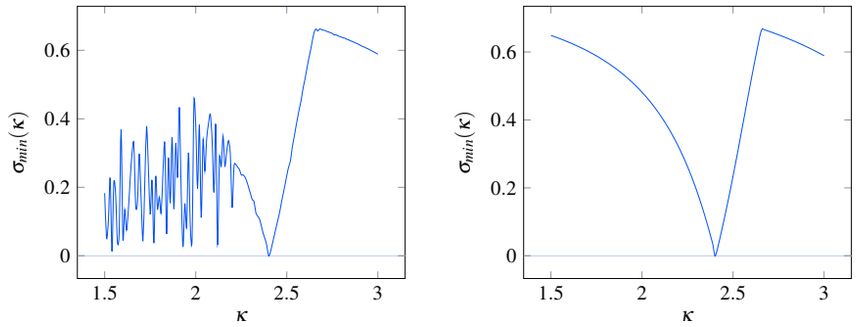

Fig. 3.7 Effect of single precision (left) and double precision (right) arithmetics on the modified MFS illustrated exemplarily for the unit disc D with $m = 25$ collocation and source points each.

Here, $|D|$ and $|\partial D|$ denote the measure within the Riemann-sum-versions of corresponding L^2-norms, respectively. Basically, these informal identifications justify the modified MFS when disregarding discretization errors for m and $\widehat{m}$ large. Figure 3.6 shows an extract of the convergence history for our canonical example $D = B_1(0)$ and $k^{(1)}$ which proves great success of the proposed method.

Unlike the choice and discretization of Γ, varying $\widehat{m}$ and corresponding point locations do not show any significant impact on the final modified MFS outcome, so we can readily fix some random distribution for $\widehat{m} = 10$, for instance. Concerning the computation of $\kappa^{(m)}$ at last, we note that Beyn's algorithm does not apply any more because the unitary part $Q(\kappa)$ of any matrix-valued function can only be holomorphic component-wise if it is constant. This can be seen by applying Cauchy's integral formula column-wise in combination with the triangle inequality for integrals. Nevertheless, $\kappa^{(m)}$ can still be computed efficiently by standard yet derivative-free minimization techniques from non-linear optimization such as the Nelder-Mead simplex method, see [98]. Altogether, due to its convincing results and close consistency with (3.10), we investigate the modified MFS as the method of choice for the approximation of ITEs in the remaining scope of this thesis .

A last word should be noted about conditioning, however. Although having introduced some kind of regularization for the MFS in the context of eigenproblems through the QR-extension compared to (3.8), this does not imply that its implementation in finite arithmetics will yield unconditionally good ITE results. The problem is that the robustness of the remedying orthogonalization depends on the condition number of the underlying modified MFS matrix, see [55]. The latter was seen to grow with the collocation number until it becomes severely ill-conditioned, in particular no stable algorithm around could compensate

a corresponding loss of accuracy upon a critical threshold for m. At least the determination of singular values as second numerical ingredient within the modified MFS is perfectly conditioned, cf. [90]. Altogether, our ITP algorithm will be expected beneficial especially for quite regular scatterers whose boundary can be approximately represented by a moderate number of collocation points already. Otherwise, higher precision arithmetics will be needed whose error propagation effects for single and double precision standards are exemplarily displayed in Figure 3.7, respectively. A detailed analysis for exact ITE convergence rates will be provided in Section 4.3.3 to have a measure at hand which decay to achieve at best in practice.

Chapter 4

Computing interior transmission eigenvalues of isotropic and homogeneous media

The two-dimensional acoustic ITP for isotropic and homogeneous media serves as our model problem for ITE analysis and will therefore be discussed most elaborately. In this chapter we recall different aspects of this particular eigenproblem and develop novel theory for ITE approximations in the spirit of the modified MFS from Section 3.4 for which we then provide numerical results as well as an accompanying convergence analysis. Since most of these findings have already been addressed in [67], whose proof techniques were improved in [68], we will occasionally recycle passages from both without explicit citation details.

4.1 Mathematical framework

The ITP arises as a special case of the more general transmission problem. Modeling for instance acoustics in ideal fluids, i.e. isotropic media with vanishing shear modulus $\mu \to 0$ in (6.1), sound propagation obeys a reduced elastic wave equation of Helmholtz type for the hydrostatic pressure $p = -\mathrm{tr}(\sigma)/2$, see [39]: Assume we are given the spatial part $\widetilde{v}\colon \mathbb{R}^2 \to \mathbb{C}$ of some time-harmonic wave $p(x,t) = \mathrm{e}^{-\mathrm{i}\omega t}\widetilde{v}(x)$ which travels at frequency $\omega > 0$ along a fixed plane in 3D. We think of the latter as $\mathbb{R}^2$ for simplicity. When at some point within there is a transition of different media, let us say between a uniform background material and some inhomogeneity whose support is mathematically represented by a simply connected, bounded domain $D \subset \mathbb{R}^2$ (to be understood as cross-sections of some planar-symmetric object in 3D accordingly), scattering effects occur as superposition of local reflections and

refracted transmission. The resulting total wave $\widetilde{w}:\mathbb{R}^2\to\mathbb{C}$ is then characterized by the aforementioned PDE, see [25],

$$\Delta\widetilde{w}+\kappa^2\widetilde{n}\widetilde{w}=0\quad\text{in }\mathbb{R}^2\,. \tag{4.1}$$

Here, $\widetilde{n}:\mathbb{R}^2\to\mathbb{R}_{>0}$ denotes the global dispersion-free index of refraction which could also be complex-valued when including absorption effects, but measures for our purposes just the ratio of wave speeds with respect to propagation in the background medium. Hence $\widetilde{n}_{|D^c}=1$ and the scatterer D itself, that we assume to be (piecewise) homogeneous throughout this thesis, is distinguished from its exterior by $n:=\widetilde{n}_{|D}=\text{const}\neq 1$. We further encounter the wave number κ of upcoming main interest and $\widetilde{w}=\widetilde{v}-\widetilde{u}$ that is interpreted as the perturbation of $\widetilde{v}$, solving the Helmholtz equation entirely with respect to κ in absence of the interfering scatterer, by some scattered wave $\widetilde{u}$ to be determined. Finally, in order to model the intuition of $\widetilde{u}$ being outgoing as excited by D, the 2D Sommerfeld radiation condition

$$\lim_{r\to\infty}\sqrt{r}\,(\partial_r\widetilde{u}-\mathrm{i}\kappa\widetilde{u})=0\,, \tag{4.2}$$

is imposed which is understood uniformly in the angular direction of the argument. It is then well known that the direct scattering problem of finding $\widetilde{w}\in H^1_{loc}(\mathbb{R}^2)$ for (4.1) such that $\widetilde{u}$ is radiating in the sense of (4.2) given $\widetilde{v}$ is uniquely solvable, see [28].

We are particularly interested in the possibility when $\widetilde{w}_{|D^c}=\widetilde{v}_{|D^c}$.This implicates $\widetilde{u}\in H^2_0(D)$ by a bootstrap argument and embodies the phenomenon that D becomes invisible for the pair $(\widetilde{v},\widetilde{w})$, i.e. there is no exterior-wave difference between the scatterer being present or not. A necessary condition for this to happen would be the solvability of the ITP: Determine $k\in\mathbb{C}\backslash\{0\}$ and $v,w\in L^2(D)$ such that $u:=v-w\in H^2_0(D)$ is non-trivial and which solve

$$\begin{aligned}\Delta v+k^2v&=0\quad\text{in }D\\ \Delta w+nk^2w&=0\quad\text{in }D\\ v&=w\quad\text{on }\partial D\\ \partial_\nu v&=\partial_\nu w\quad\text{on }\partial D\end{aligned} \tag{4.3}$$

in a distributional sense. Note we may recover

$$v=\frac{\Delta u+nk^2u}{(1-n)k^2}\qquad\text{and}\qquad w=\frac{\Delta u+k^2u}{(1-n)k^2} \tag{4.4}$$

which are well-defined and conclude that u is the actual unknown to be determined via the polynomial-type eigenproblem

$$(\Delta + nk^2)(\Delta + k^2)u = 0\,. \tag{4.5}$$

The intuitive attempt of interpreting (4.3) as a coupled second order system in the usual $H^1(D)$-manner would result in a non-compact perturbation of a coercive operator and thus inhibit the application of Fredholm theory, see [25]. In particular, the ITP is non-elliptic and ITEs k are naturally relaxed to fulfill the PDE requirements for some eigenfunction pair (v,w) in a distributional sense. Note that their existence, however, does generally not imply w to be extendible to all of $\mathbb{R}^2$ as exterior Helmholtz solution $\widetilde{w}$ which then spoils our former interpretation of being a non-scattering incident field for (4.1). Indeed, in [16] the authors even showed that regions D with rectangular corners always scatter despite the existence of infinitely many ITEs.

Apart from their elaborate interpretation, the study of ITEs itself is also highly non-standard as already indicated by the subtle choice of eigenfunction spaces. It is further strengthened by the fact that the spectral operator to (4.5) after substitution in linear form according to (2.4) is non-self-adjoint and thus allows for complex-valued eigenvalues, too. When to be distinguished, real-valued ITEs will be denoted by $k_{\mathbb{R}}$. We devote the next section to provide an overview over mathematical properties of ITEs.

4.2 State-of-the-art facts about interior transmission eigenvalues

There are many things that are already known about ITEs for general isotropic media as will be listed below, but also a lot of questions that are still open. It is the huge mathematical variety of the refractive index n, especially for generally inhomogeneous media, that restricts certain results. While regularity assumptions on n can often be weakened up to $L^\infty(D)$ via the Fredholm approach, its differentiation within $\overline{D}$ from unity being the distinguished exterior index makes more trouble as already indicated by (4.4). A feasible constraint is often found by imposing $\mathrm{Re}(n)-1$ to be uniformly bounded away from zero with no sign change. One of the first successful relaxation attempts was then the inclusion of material voids in the scatterer, i.e. open subsets of D on which n is identically one, but showed that already a different functional framework is necessary, see [23]. Some recent developments concerning $n \geq \mathrm{const} > 0$ being infinitely smooth can be found in [87] using semi-classical analysis. The case of $n-1$ changing sign more unconditionally is rather unexplored as well as the analysis

of absorbing media, see [33], whose refractive index admits a complex-valued dispersion relation of the form $n(x) = n_1(x) + \mathrm{i}n_2(x)/k$ with its non-trivial imaginary parts damping former time-harmonic waves. Yet it is known for the latter that if $n_1 > 0$ and either $n_2 > 0$ or $n_2 < 0$ in some open subregion of D, real-valued ITEs do not exist, cf. Theorem 3.3 of [25].

The history of studying ITEs started in the 1980s and focused primarily on proving existence and discreteness to estimate the practical consequences of their critical nature within sampling methods from inverse scattering, see [36] for an early survey. Showing that the spectrum is at most countable without finite accumulation points could be shown relatively straightforward via Fredholm theory, see [31]. Further, the algebraic multiplicity is finite each and corresponding generalized eigenspaces form a complete set in $L^2(D)$ as found out recently, cf. [15]. Unlike showing discreteness, it took about two decades to prove for the first time that infinitely many real-valued eigenvalues in the case $\inf_D n > 1$ or $\sup_D n < 1$ do exist, cf. [27, 82]. A corresponding result covering the complex-valued spectrum is still open except for in combination with selected scatterers such as the unit disc which then enables the construction of explicit solutions, see [34]. However, all ITEs k are known to fulfill $\mathrm{Re}(k) > \mathrm{Im}(k)$ for $n > 0$, see [21], and are limited to lie in an arbitrary small strip modulo finitely many exceptions about the real axis, see [97].

Over the time, also the focus as direct sources of information for D has attracted the analysis of ITEs. Similar to the famous paper "Can one hear the shape of a drum?", see [56], but confining to variable indices of refraction with fixed support D in the ITP context, a corresponding positive answer could be obtained so far for the inverse spectral problem of spherically stratified media, see [25]. As the whole complex spectrum must be taken into account then, this again shows that imaginary structures of ITEs are important to understand. The same might also hold true for shape optimizations with respect to eigenvalues that are minimal subject to scatterers of fixed area and constant n. Here, numerical studies of Kleefeld, see [64], show that $k^{(1)}$, defined as the complex-valued ITE of smallest magnitude, attains a relative minimum for the unit disc among other sampled scatterers with the same area. The smallest real-valued ITE $k_{\mathbb{R}}^{(1)} = k_{\mathbb{R}}^{(1)}(n,D)$ is even more characteristic because it determines $n = \text{const}$ uniquely for fixed D as long as $n > 1$ or $n < 1$ is known in advance, see [28]. Besides, $k_{\mathbb{R}}^{(1)}$ obeys a monotonicity principle for ITEs of inhomogeneous media in terms of homogeneous ones: Given three scatterers $D_* \subset D \subset D^*$, it holds for $1 < n_* := \inf_D n$ with $n^* := \sup_D n$ that

$$k_{\mathbb{R}}^{(1)}(n^*,D^*) \leq k_{\mathbb{R}}^{(1)}(n,D) \leq k_{\mathbb{R}}^{(1)}(n_*,D_*)\ , \tag{4.6}$$

whereas for $n^* < 1$ the corresponding inequality reads

$$k_{\mathbb{R}}^{(1)}(n_*, D^*) \leq k_{\mathbb{R}}^{(1)}(n, D) \leq k_{\mathbb{R}}^{(1)}(n^*, D_*) \, . \tag{4.7}$$

Therefore, knowing the spectrum of the ITP with constant index of refraction can help locating eigenvalues in the variable coefficient case.

4.3 Boundary approximation theory for interior transmission eigenvalues

In this section we present a novel approximation framework for the computation of ITEs in the isotropic and homogeneous case. It formalizes the concept of the modified MFS from Section 3.4 for the ITP in Sobolev spaces as precursor for numerical implementations afterwards.

4.3.1 A general trial function ansatz

As we have already seen in Chapter 3, there is a direct connection between eigenvalue and eigenfunction approximations in the case of self-adjoint eigenproblems. Our aim is a corresponding result for ITEs which, however, requires a different derivation since decomposition properties like the existence of an orthonormal eigenfunction basis are not provided for non-self-adjoint operators any more, see [41]. Therefore, we first consider quite general Trefftz-like trial functions for approximating v and w in (4.3), respectively, and exploit concrete properties of fundamental solutions in the next subsection. Since $0 < n \neq 1$ is constant, the ITP is turned into a coupled system of Helmholtz equations which can in particular be treated with an MFS ansatz. In order to allow for convenient conversions from interior to boundary data of trial functions via trace theorems, cf. (2.13) and (2.14), we assume D to be of class $C^{1,1}$ if not stated otherwise but focus on the effects of domain regularity towards eigenvalue approximations in the numerical part later.

We start our analysis with setting a relaxed trial function space of Trefftz kind for approximate solutions of (4.3) by

$$U := \bigcup_{0 \leq \arg(\kappa) < \frac{\pi}{4}} U(\kappa) \, ,$$

where for variable $\kappa \in \mathbb{C}\backslash\{0\}$ and fixed index of refraction $n > 0$

$$U(\kappa) := \left\{ (\widetilde{v}, \widetilde{w}) \in C^\infty(\overline{D}) \times C^\infty(\overline{D}) : \ \Delta\widetilde{v} + \kappa^2 \widetilde{v} = 0 \ , \ \Delta\widetilde{w} + n\kappa^2 \widetilde{w} = 0 \right\} .$$

The reduced regime for κ emerges from the aforementioned fact that all ITEs k fulfill $\mathrm{Re}(k) > \mathrm{Im}(k)$ in combination with the simple observation that $k, -k, \overline{k}, -\overline{k}$, are ITEs at once one of which lies in the first quadrant of the complex plane. Consistent with the MFS, any candidate pair $(\widetilde{v}, \widetilde{w})$ in $U(\kappa)$ is sufficiently smooth to enable collocation procedures, fulfills the required PDE conditions in the interior and it is the remaining choice of the wave number which determines in how far boundary data match the ITP. As for the Dirichlet eigenproblem (3.6), boundary errors of trial functions should only be considered small if the scale-invariant ratio of corresponding trace and interior norm is so. Both existence and location bounds for some exact Laplace eigenvalue could then be deduced via inequality (3.10) and thus established the strategy for the modified MFS in the self-adjoint case. For the ITP we need to divide a corresponding result into two consecutive steps and show first how ITEs can be detected within an indefinite process. The main idea is again that the normalized boundary data are bounded from below by the wave-number-dependent constant $1/C_\kappa > 0$ according to the a priori estimate

$$\|\widetilde{v}\|_{L^2(D)} + \|\widetilde{w}\|_{L^2(D)} \leq C_\kappa \left(\|\widetilde{f}\|_{H^{\frac{3}{2}}(\partial D)} + \|\widetilde{g}\|_{H^{\frac{1}{2}}(\partial D)} \right) ,$$

when solving

$$\begin{aligned} \Delta\widetilde{v} + \kappa^2 \widetilde{v} = 0 \quad & \text{in } D \\ \Delta\widetilde{w} + n\kappa^2 \widetilde{w} = 0 \quad & \text{in } D \\ \widetilde{v} - \widetilde{w} = \widetilde{f} \quad & \text{on } \partial D \\ \partial_\nu(\widetilde{v} - \widetilde{w}) = \widetilde{g} \quad & \text{on } \partial D \end{aligned}$$

for $\kappa \neq k$, see [25]. The latter system reflects actual trial function states from U for which we then investigate $\kappa \to k$.

Theorem 1. *Assume that the sequence* $\left\{ \left(v^{(m)}, w^{(m)}, \kappa^{(m)} \right) \right\}_{m \in \mathbb{N}} \subset U \times \mathbb{C}$ *fulfills for some constant* $1 \leq C < \infty$ *the following conditions:*

(i) eigenvalue convergence: $\kappa^{(m)} \to k \neq 0$ *such that* $0 \leq \arg(k) < \frac{\pi}{4}$,

(ii) uniform interior bound: $\frac{1}{C} \leq \left(\left\| v^{(m)} \right\|^2_{L^2(D)} + \left\| w^{(m)} \right\|^2_{L^2(D)} \right) \leq C$ *for m large enough,*

(iii) vanishing boundary misfit: $\left(\left\|v^{(m)}-w^{(m)}\right\|_{H^{\frac{3}{2}}(\partial D)}+\left\|\partial_\nu\left(v^{(m)}-w^{(m)}\right)\right\|_{H^{\frac{1}{2}}(\partial D)}\right)\to 0$ *when* $m\to\infty$.

Then, the limit k *from* (i) *is an ITE and a subsequence of* $\left\{\left(v^{(m)},w^{(m)}\right)\right\}_{m\in\mathbb{N}}$ *converges weakly in* $L^2(D)\times L^2(D)$ *to some eigenfunction pair* (v,w).

Proof. By rescaling $\left\{\left(v^{(m)},w^{(m)}\right)\right\}_{m\in\mathbb{N}}$, if necessary, we can assume without loss of generality that $C=1$ and aim to apply weak compactness in order to construct a solution candidate that will then indeed meet all the required ITE criteria. By assumption (ii) we know modulo the extraction of a subsequence that $v^{(m)}\rightharpoonup v$ and $w^{(m)}\rightharpoonup w$ in $L^2(D)$ which implies with (i) that $(v,w)\in L^2(D)\times L^2(D)$ fulfills the interior conditions of the ITP according to

$$\begin{aligned}\int_D v(\Delta\varphi+k^2\varphi)\,\mathrm{d}x&=\lim_{m\to\infty}\int_D v^{(m)}\left(\Delta\varphi+\left(\kappa^{(m)}\right)^2\varphi\right)\mathrm{d}x\\&=\lim_{m\to\infty}\int_D\left(\Delta v^{(m)}+\left(\kappa^{(m)}\right)^2 v^{(m)}\right)\varphi\,\mathrm{d}x=0\end{aligned}$$

for any test function $\varphi\in\mathscr{D}(D)$. Analogue calculus applies to w. In order to prove that $(v-w)$ has the correct ITP boundary data, it suffices to show that the differences $\left(v^{(m)}-w^{(m)}\right)$ are bounded in $H^2(D)$ and thus a subsequence is weakly convergent. This would then imply by continuity of the trace operator $\tau:H^2(D)\to H^{\frac{3}{2}}(\partial D)$ and (iii) that

$$0=\lim_{m\to\infty}\left(v^{(m)}-w^{(m)},f\right)_{H^{\frac{3}{2}}(\partial D)}=\lim_{m\to\infty}\left(\tau\left(v^{(m)}-w^{(m)}\right),f\right)_{H^{\frac{3}{2}}(\partial D)}=\left(\tau(v-w),f\right)_{H^{\frac{3}{2}}(\partial D)}$$

for all $f\in H^{\frac{3}{2}}(\partial D)$, i.e. $\tau(v-w)=0$, with a similar calculation for the normal derivative. For deducing the uniform $H^2(D)$-bound with respect to m, we note that $\left(v^{(m)}-w^{(m)}\right)$ solves the inhomogeneous Helmholtz equation

$$\Delta\left(v^{(m)}-w^{(m)}\right)+\left(\kappa^{(m)}\right)^2\left(v^{(m)}-w^{(m)}\right)=(1-n)w^{(m)}\quad\text{in } D\,,$$

so elliptic estimates like (2.18) tell us that

$$\left\|v^{(m)}-w^{(m)}\right\|_{H^2(D)}\le C\left(\left\|v^{(m)}-w^{(m)}\right\|_{H^{\frac{3}{2}}(\partial D)}+\left\|v^{(m)}\right\|_{L^2(D)}+\left\|w^{(m)}\right\|_{L^2(D)}\right)\,.$$

It remains to show that (v,w) is non-trivial. For this we recall that the embedding $H^2(D)\hookrightarrow L^2(D)$ is compact which implies $\left(v^{(m)}-w^{(m)}\right)\to(v-w)$ strongly in $L^2(D)$. Apparently, $(v,w)\neq 0$ if $\|v-w\|_{L^2(D)}>0$ so we will assume contrarily that $\left(v^{(m)}-w^{(m)}\right)\to 0$

in $L^2(D)$. Then, on the one hand, the bounded sequence

$$a_m := \int_D w^{(m)} \overline{v}^{(m)} \, \mathrm{d}x$$

may be singled out to converge to some $a \in \mathbb{C}$ from which we know by (ii) with $C = 1$ that

$$\frac{1}{2} \geq |a| \geq \mathrm{Re}(a) = \lim_{m\to\infty} \frac{\left\|v^{(m)}\right\|^2_{L^2(D)} + \left\|w^{(m)}\right\|^2_{L^2(D)} - \left\|v^{(m)} - w^{(m)}\right\|^2_{L^2(D)}}{2} \geq \frac{1}{2} \, ,$$

i.e. $a = 1/2$. Since $0 \leq \arg(k) < \pi/4$ and $n \neq 1$, we may also conclude

$$\left|\mathrm{Re}\big(a(nk^2 - \overline{k}^2)\big)\right| > 0 \, . \tag{4.8}$$

On the other hand, right-invertibility of the trace operator in combination with assumption (iii) ensures the existence of boundary-compatible lifting functions $\theta^{(m)} \in H^2(D)$ for all $m \in \mathbb{N}$ such that $\theta^{(m)}_{|\partial D} = \big(v^{(m)} - w^{(m)}\big)_{|\partial D}$, $\partial_\nu \theta^{(m)}_{|\partial D} = \partial_\nu \big(v^{(m)} - w^{(m)}\big)_{|\partial D}$ and $\left\|\theta^{(m)}\right\|_{H^2(D)} \to 0$. Green's second identity (2.12) then yields

$$\begin{aligned}
\left|\mathrm{Re}\big(a(nk^2 - \overline{k}^2)\big)\right| &= \lim_{m\to\infty} \left| \mathrm{Re} \left(\int_D n\big(\kappa^{(m)}\big)^2 w^{(m)} \overline{v}^{(m)} - w^{(m)} \big(\overline{\kappa}^{(m)}\big)^2 \overline{v}^{(m)} \, \mathrm{d}x \right) \right| \\
&= \lim_{m\to\infty} \left| \mathrm{Re} \left(\int_D \overline{v}^{(m)} \Delta w^{(m)} - w^{(m)} \Delta \overline{v}^{(m)} \, \mathrm{d}x \right) \right| \\
&= \lim_{m\to\infty} \left| \mathrm{Re} \left(\int_{\partial D} \overline{v}^{(m)} \partial_\nu w^{(m)} - w^{(m)} \partial_\nu \overline{v}^{(m)} \, \mathrm{d}s \right) \right| \\
&= \lim_{m\to\infty} \left| \mathrm{Re} \left(\int_{\partial D} \big(\overline{v}^{(m)} - \overline{w}^{(m)}\big) \partial_\nu w^{(m)} - w^{(m)} \partial_\nu \big(\overline{v}^{(m)} - \overline{w}^{(m)}\big) \, \mathrm{d}s \right) \right| \\
&= \lim_{m\to\infty} \left| \mathrm{Re} \left(\int_D \overline{\theta}^{(m)} \Delta w^{(m)} - w^{(m)} \Delta \overline{\theta}^{(m)} \, \mathrm{d}x \right) \right| \\
&\leq \lim_{m\to\infty} C \left\|\theta^{(m)}\right\|_{H^2(D)} \left\|w^{(m)}\right\|_{L^2(D)} \\
&= 0 \, ,
\end{aligned}$$

which is a contradiction to (4.8). □

Note that the previous convergence result can only hold modulo subsequences in general since no information about ITE multiplicites are used, implying possibly different eigenfunction limits. Next, we derive an a posteriori estimate similar to (3.10) which allows to bound eigenvalue deviations, cf. assumption (i) above, at each approximation step m in terms of boundary errors, cf. assumption (iii), for any weakly convergent sequence $\big(v^{(m)}, w^{(m)}\big)$ in

$L^2(D)\times L^2(D)$. It will also facilitate to establish convergence rates for concrete minimizing sequences when $m\to\infty$, cf. Theorem 17.

Lemma 2. *Let k be an ITE with eigenfunction pair $(v,w)\in L^2(D)\times L^2(D)$ and assume that $(\widetilde{v},\widetilde{w})\in U(\kappa)$. If*

$$\frac{\left|\int_D v\widetilde{v}-nw\widetilde{w}\,\mathrm{d}x\right|}{\|\widetilde{v}\|_{L^2(D)}+\|\widetilde{w}\|_{L^2(D)}}\geq\widetilde{\varepsilon}>0\,, \tag{4.9}$$

then there exists a constant $\widetilde{C}>0$ which depends only on the boundary data of (v,w) such that for admissible $(\widetilde{v},\widetilde{w})$ it holds that

$$|k^2-\kappa^2|\leq\frac{\widetilde{C}}{\widetilde{\varepsilon}}\frac{\sqrt{\|\widetilde{v}-\widetilde{w}\|^2_{H^{\frac{3}{2}}(\partial D)}+\|\partial_\nu(\widetilde{v}-\widetilde{w})\|^2_{H^{\frac{1}{2}}(\partial D)}}}{\|\widetilde{v}\|_{L^2(D)}+\|\widetilde{w}\|_{L^2(D)}}\,. \tag{4.10}$$

Proof. Since $v-w\in H_0^2(D)$, we may infer with (2.12) that

$$\int_D(v-w)\Delta\widetilde{v}-\widetilde{v}\Delta(v-w)\,\mathrm{d}x=0$$

and in particular

$$\int_D v\Delta\widetilde{v}-\widetilde{v}\Delta v\,\mathrm{d}x=\int_D w\Delta\widetilde{v}-\widetilde{v}\Delta w\,\mathrm{d}x\,.$$

Simple manipulations show that

$$\begin{aligned}
&(k^2-\kappa^2)\int_D\widetilde{v}v-n\widetilde{w}w\,\mathrm{d}x\\
&=(k^2-\kappa^2)\int_D\widetilde{v}v\,\mathrm{d}x-(k^2-\kappa^2)\int_D n\widetilde{w}w\,\mathrm{d}x\\
&=\int_D v\Delta\widetilde{v}-\widetilde{v}\Delta v\,\mathrm{d}x-\int_D w\Delta\widetilde{w}-\widetilde{w}\Delta w\,\mathrm{d}x\\
&=\int_D w\Delta\widetilde{v}-\widetilde{v}\Delta w\,\mathrm{d}x-\int_D w\Delta\widetilde{w}-\widetilde{w}\Delta w\,\mathrm{d}x\\
&=\int_D w\Delta(\widetilde{v}-\widetilde{w})-(\widetilde{v}-\widetilde{w})\Delta w\,\mathrm{d}x
\end{aligned}$$

or equivalently, in rearranged form

$$|k^2-\kappa^2|\leq\frac{1}{\widetilde{\varepsilon}}\frac{\left|\int_D w\Delta(\widetilde{v}-\widetilde{w})-(\widetilde{v}-\widetilde{w})\Delta w\,\mathrm{d}x\right|}{\|\widetilde{v}\|_{L^2(D)}+\|\widetilde{w}\|_{L^2(D)}}\,.$$

We can take an auxiliary lifting function $\theta \in H^2(D)$ thanks to right-invertibility of the trace operator which fulfills $\theta_{|\partial D} = (\widetilde{v}-\widetilde{w})_{|\partial D}$ and $\partial_\nu \theta_{|\partial D} = 0$. Exploiting (2.13) and (2.14) gives

$$\begin{aligned}
&\left| \int_D w\Delta(\widetilde{v}-\widetilde{w}) - (\widetilde{v}-\widetilde{w})\Delta w \,\mathrm{d}x \right| \\
\leq &\left| \int_D w\Delta(\widetilde{v}-\widetilde{w}-\theta) - (\widetilde{v}-\widetilde{w}-\theta)\Delta w \,\mathrm{d}x \right| + \left| \int_D w\Delta\theta - \theta\Delta w \,\mathrm{d}x \right| \\
\leq &\|\partial_\nu(\widetilde{v}-\widetilde{w}-\theta)\|_{H^{\frac{1}{2}}(\partial D)} \|w\|_{H^{-\frac{1}{2}}(\partial D)} + \|\theta\|_{H^{\frac{3}{2}}(\partial D)} \|\partial_\nu w\|_{H^{-\frac{3}{2}}(\partial D)} \\
\leq &\|\partial_\nu(\widetilde{v}-\widetilde{w})\|_{H^{\frac{1}{2}}(\partial D)} \|w\|_{H^{-\frac{1}{2}}(\partial D)} + \|\widetilde{v}-\widetilde{w}\|_{H^{\frac{3}{2}}(\partial D)} \|\partial_\nu w\|_{H^{-\frac{3}{2}}(\partial D)} \\
\leq &\widetilde{C} \sqrt{\|\widetilde{v}-\widetilde{w}\|^2_{H^{\frac{3}{2}}(\partial D)} + \|\partial_\nu(\widetilde{v}-\widetilde{w})\|^2_{H^{\frac{1}{2}}(\partial D)}} \,,
\end{aligned}$$

where we have set

$$\widetilde{C} := \sqrt{\|w\|^2_{H^{-\frac{1}{2}}(\partial D)} + \|\partial_\nu w\|^2_{H^{-\frac{3}{2}}(\partial D)}} < \infty \,.$$

□

The previous two results then complement in the following way.

Corollary 3. *Let conditions (i)–(iii) of Theorem 1 hold for $\left\{ \left(v^{(m)}, w^{(m)}, \kappa^{(m)}\right) \right\}_{m\in\mathbb{N}} \subset U \times \mathbb{C}$ which detects some ITE k. Assume that each eigenfunction pair (v,w) from the eigenspace of k fulfills*

$$\int_D v^2 - nw^2 \,\mathrm{d}x \neq 0 \tag{4.11}$$

(or alternatively $\|v\|^2_{L^2(D)} - n\|w\|^2_{L^2(D)} \neq 0$ if $k = k_{\mathbb{R}}$). Then there is a constant $C > 0$ which depends only on the data of corresponding (v,w) such that

$$\left| k^2 - \left(\kappa^{(m)}\right)^2 \right| \leq C \frac{\sqrt{\left\|v^{(m)} - w^{(m)}\right\|^2_{H^{\frac{3}{2}}(\partial D)} + \left\|\partial_\nu\left(v^{(m)} - w^{(m)}\right)\right\|^2_{H^{\frac{1}{2}}(\partial D)}}}{\left\|v^{(m)}\right\|_{L^2(D)} + \left\|w^{(m)}\right\|_{L^2(D)}} \,. \tag{4.12}$$

Proof. Since ITEs are isolated points, we restrict to the case that either $\kappa^{(m)} = k$, or $\kappa^{(m)}$ fails to be any other ITE. Assume then contrarily that there is a subsequence of

$\left\{\left(v^{(m)}, w^{(m)}, \kappa^{(m)}\right)\right\}_{m\in\mathbb{N}}$, which we do not relabel in the following and which satisfies

$$\left|k^2 - \left(\kappa^{(m)}\right)^2\right| \geq C^{(m)} \frac{\sqrt{\left\|v^{(m)} - w^{(m)}\right\|^2_{H^{\frac{3}{2}}(\partial D)} + \left\|\partial_\nu\left(v^{(m)} - w^{(m)}\right)\right\|^2_{H^{\frac{1}{2}}(\partial D)}}}{\left\|v^{(m)}\right\|_{L^2(D)} + \left\|w^{(m)}\right\|_{L^2(D)}}$$

with $C^{(m)} \nearrow \infty$. According to Theorem 1, a further subsequence of $\left\{\left(v^{(m)}, w^{(m)}\right)\right\}_{m\in\mathbb{N}}$ converges weakly to some eigenfunction pair (v,w) in $L^2(D)\times L^2(D)$ that satisfies (4.11). In particular, due to the lower bound from assumption (ii) therein, we conclude

$$\frac{\left|\int_D v v^{(m)} - n w w^{(m)}\,\mathrm{d}x\right|}{\|v^{(m)}\|_{L^2(D)} + \|w^{(m)}\|_{L^2(D)}} \geq \widetilde{\varepsilon} > 0$$

for m large enough. Hence, Lemma 2 recovers $C^{(m)} \leq \widetilde{C}/\widetilde{\varepsilon}$ to be bounded for those m, which then contradicts our initial blow-up assumption. □

Corollary 3 is still limited for fully justifying (4.12) due to (4.11) which depends on the unknown exact eigenfunction pairs (v,w). The next theorem therefore shows that at least for $k^{(1)}_{\mathbb{R}}$ and sufficiently large refractive indices n the real-valued-ITE version of the critical integral term does not vanish.

Theorem 4. *Let $k = k^{(1)}_{\mathbb{R}}(n,D)$ be the smallest real-valued ITE for the scatterer D with refractive index n. If $n>1$ is large or $0<n<1$ is small enough, we have the eigenfunction relations*

$$\|v\|^2_{L^2(D)} - n\|w\|^2_{L^2(D)} < 0 \qquad \textit{or} \qquad \|v\|^2_{L^2(D)} - n\|w\|^2_{L^2(D)} > 0\,, \tag{4.13}$$

respectively.

Proof. For the sake of presentation we will assume that $n>1$ since the case $0<n<1$ works structurally similar. Because v and w can be expressed by

$$v = \frac{\Delta u + nk^2 u}{(1-n)k^2} \qquad \text{and} \qquad w = \frac{\Delta u + k^2 u}{(1-n)k^2}$$

according to (4.4), the basic idea for proving (4.13) will be to exploit isometry of the Fourier transform with respect to the single function u to obtain an algebraic quantity which is controlled by n. The fact $u\in H^2_0(D)$ shows that u,v,w extend naturally by zero outside of D so Plancherel's identity (2.7) gives

$$\begin{aligned}\int_D |v|^2 - n|w|^2 \,\mathrm{d}x &= \frac{1}{(2\pi)^2}\int_{\mathbb{R}^2} |\mathscr{F}v|^2 - n|\mathscr{F}w|^2 \,\mathrm{d}\xi \\ &= \frac{1}{(2\pi)^2}\int_{\mathbb{R}^2} \frac{|\mathscr{F}(\Delta u + nk^2 u)|^2 - n|\mathscr{F}(\Delta u + k^2 u)|^2}{(n-1)^2k^4}\,\mathrm{d}\xi \\ &= \frac{1}{(2\pi)^2}\int_{\mathbb{R}^2} \frac{-|\mathscr{F}\Delta u|^2 + nk^4|\mathscr{F}u|^2}{(n-1)k^4}\,\mathrm{d}\xi \\ &= \frac{1}{(2\pi)^2}\int_{\mathbb{R}^2} \frac{-|\xi|^4 + nk^4}{(n-1)k^4}|\mathscr{F}u|^2 \,\mathrm{d}\xi \ .\end{aligned}$$

As will be shown later, we have for $k = k_{\mathbb{R}}^{(1)}(n,D)$ that $nk^4 \to 0$ and likewise $R(n) \to 0$ for $n \to \infty$, where $R(n) := k\sqrt[4]{(2n-1)}$ is the solution of $p(t) := (-t^4 + nk^4)/(n-1)k^4 = -1$ in t. With $B_{R(n)}(0)$ being the disc centered at the origin with radius $R(n)$, we split the integral and exploit monotonicity of p to deduce

$$\begin{aligned}&\int_{B_{R(n)}(0)} \frac{-|\xi|^4 + nk^4}{(n-1)k^4}|\mathscr{F}u|^2 \,\mathrm{d}\xi + \int_{B_{R(n)}(0)^\mathsf{c}} \frac{-|\xi|^4 + nk^4}{(n-1)k^4}|\mathscr{F}u|^2 \,\mathrm{d}\xi \\ &\leq p(0)\int_{B_{R(n)}(0)} |\mathscr{F}u|^2 \,\mathrm{d}\xi + p\big(R(n)\big)\int_{B_{R(n)}(0)^\mathsf{c}} |\mathscr{F}u|^2 \,\mathrm{d}\xi \\ &= \frac{n}{n-1}\|\mathscr{F}u\|^2_{L^2\left(B_{R(n)}(0)\right)} - \left(\|\mathscr{F}u\|^2_{L^2(\mathbb{R}^2)} - \|\mathscr{F}u\|^2_{L^2\left(B_{R(n)}(0)\right)}\right) \\ &\leq \left(\frac{2n-1}{n-1}\right)\|\mathscr{F}u\|^2_{L^2\left(B_{R(n)}(0)\right)} - (2\pi)^2\|u\|^2_{L^2(D)} \ .\end{aligned}$$

The first summand can be made arbitrarily small in terms of growing n according to

$$\begin{aligned}\|\mathscr{F}u\|^2_{L^2\left(B_{R(n)}(0)\right)} &\leq \left(\max|\mathscr{F}u|\right)^2 \pi R(n)^2 \\ &\leq \|u\|^2_{L^1(D)}\pi R(n)^2 \\ &\leq \|u\|^2_{L^2(D)}|D|\pi R(n)^2 \ ,\end{aligned}$$

where $|D|$ denotes the two-dimensional Lebesgue measure of D. Putting everything together, we finally obtain

$$\int_D |v|^2 - n|w|^2 \,\mathrm{d}x = \frac{\|u\|^2_{L^2(D)}}{4\pi}\left(\frac{2n-1}{n-1}|D|R(n)^2 - 4\pi\right) < 0$$

for n large enough due to the decay of $R(n)$.

It remains to show that $n\big(k_{\mathbb{R}}^{(1)}(n,D)\big)^4 \to 0$ as $n \to \infty$. Due to (4.7), the magnitude of $k_{\mathbb{R}}^{(1)}(n,D)$ can be bounded from above by $k_{\mathbb{R}}^{(1)}(n,B)$ for any included disc $B \subset D$ which thus amounts to show the limit assertion for the unit disc as scatterer. In this case, selected ITEs $k \geq k_{\mathbb{R}}^{(1)}(n,B)$ solve

$$\det \begin{pmatrix} J_1(k) & J_1(k\sqrt{n}) \\ kJ_1'(k) & k\sqrt{n}J_1'(k\sqrt{n}) \end{pmatrix} = 0 \,, \tag{4.14}$$

where J_1 is the first Bessel function of order one and the prime indicates differentiation. This relation follows by expanding (v,w) as in (3.9) and applying the ITP boundary data, respectively. Luckily, (4.14) can be restated more compactly as finding roots k of the piecewise continuous function

$$g(\kappa) := f(\kappa) - f(\sqrt{n}\kappa) \,,$$

where

$$f(y) := \frac{yJ_1'(y)}{J_1(y)} \,.$$

Now let $j_1 < j_2$ be the two smallest positive roots of J_1 and choose $n > 1$ large enough to ensure $j_2 < j_1\sqrt{n}$. Then set $k_1 := j_1/\sqrt{n}$ as well as $k_2 := j_2/\sqrt{n}$ and observe that g is singular at those points, but continuous in between. Also, those poles have different signs according to

$$\lim_{\kappa \searrow k_1} g(\kappa) = -\lim_{\kappa \searrow k_1} f(\sqrt{n}\kappa) = -\infty \qquad \text{and} \qquad \lim_{\kappa \nearrow k_2} g(\kappa) = -\lim_{\kappa \nearrow k_2} f(\sqrt{n}\kappa) = \infty \,,$$

which follows from the basic facts that $J_1 < 0$ in the interval (j_1, j_2), $J_1'(j_1) < 0$ but $J_1'(j_2) > 0$ and that both $f(k_1)$, $f(k_2)$ are finite. Therefore, we can make use of the intermediate value theorem which guarantees for sufficiently large n some root k of g fulfilling $k_1 \leq k \leq k_2$, or equivalently the uniform bound $j_1^2 \leq nk^2 \leq j_2^2$ as $n \to \infty$. In particular, $nk^4 \to 0$ which finally proves our lemma. □

Concerning complex-valued ITEs with regard to the previous theorem, we want to show that (4.13) would vanish whenever k has non-trivial imaginary part. Note, however, this does not exclude (4.11) to be non-zero.

Lemma 5. *If (v,w) is an ITP eigenfunction pair with ITE $k \in \mathbb{C}\backslash\mathbb{R}$, then we have that $\|v\|_{L^2(D)}^2 - n\|w\|_{L^2(D)}^2 = 0$.*

Proof. Let $\left\{\left(v^{(m)},w^{(m)}\right)\right\}_{m\in\mathbb{N}} \in U(k)$ be a recovery sequence for (v,w) in the sense that $\left(v^{(m)}-w^{(m)}\right) \to (v-w)$ in $H^2(D)$, cf. Corollary 9 later. In particular, $v^{(m)} \to v$ and $w^{(m)} \to w$ in $L^2(D)$ according to (4.4). Applying Green's formula then, we obtain

$$\begin{aligned}
&\operatorname{Im}(k^2)\int_D |v|^2 - n|w|^2\,\mathrm{d}x\\
&= \lim_{m\to\infty} \operatorname{Im}\left(k^2\int_D v^{(m)}\overline{v}^{(m)} - nw^{(m)}\overline{w}^{(m)}\,\mathrm{d}x\right)\\
&= \lim_{m\to\infty} \operatorname{Im}\left(\int_D \overline{w}^{(m)}\Delta w^{(m)} - \overline{v}^{(m)}\Delta v^{(m)}\,\mathrm{d}x\right)\\
&= \lim_{m\to\infty} \operatorname{Im}\left(\int_D |\nabla v^{(m)}|^2 - |\nabla w^{(m)}|^2\,\mathrm{d}x + \int_{\partial D} \overline{w}^{(m)}\partial_\nu w^{(m)} - \overline{v}^{(m)}\partial_\nu v^{(m)}\,\mathrm{d}s\right)\\
&= \lim_{m\to\infty} \operatorname{Im}\left(\int_{\partial D} \left(\overline{w}^{(m)}-\overline{v}^{(m)}\right)\partial_\nu w^{(m)} + \overline{v}^{(m)}\partial_\nu\left(w^{(m)}-v^{(m)}\right)\mathrm{d}s\right)\\
&= 0
\end{aligned}$$

and the assertion of the lemma follows since $\operatorname{Im}(k^2) \neq 0$ by assumption. □

4.3.2 Approaching the method of fundamental solutions' framework

So far we have considered the very exhaustive approximation space T which fits all feasible scenarios of Trefftz methods for corresponding ITE detections. However, when turning to practical implementations, one is usually only given a limited subset of trial functions which can mostly be generated via convenient degrees of freedom. The question whether this reduced class is still sufficiently dense to make the approximation assumptions within Theorem 1 realizable is then open but necessary to answer, especially for numerical applications. Thanks to the promising results from Chapter 3 we will representatively confine to MFS trial functions in the following: We recall that $\Phi_\kappa = \mathrm{i}H_0^{(1)}(\kappa|\bullet|)/4$ is the radiating fundamental solution for the Helmholtz equation for which we need to assign auxiliary source contours Γ again whose individual effects on ITE approximations will be discussed in the numerical section later. Up to now Γ is assumed to be of class C^2 and to fulfill the constraints $\Gamma = \partial\Omega$ with $\overline{D} \subset \Omega$ as well as the length bound $|\Gamma| < \infty$. We then refine $U_{MFS} \subset U$ given by

$$U_{MFS} := \bigcup_{\substack{m\in\mathbb{N},\\ 0\leq\arg(\kappa)<\frac{\pi}{4}}} U_{MFS}^{(m)}(\kappa)\ ,$$

where for $\kappa \in \mathbb{C}\backslash\{0\}$ and a sequence of source point sets $\left\{s^{(1/m)},\dots,s^{(m/m)}\right\} \in \Gamma$ becoming dense for $m \to \infty$ we set

$$U_{MFS}^{(m)}(\kappa) := \left\{ \left(v^{(m)}, w^{(m)}\right) :\ v^{(m)} = \sum_{j=1}^{m} \Phi_\kappa\left(x - s^{(j/m)}\right)\alpha^{(j/m)}, \right. \\ \left. w^{(m)} = \sum_{j=1}^{m} \Phi_{\sqrt{n}\kappa}\left(x - s^{(j/m)}\right)\beta^{(j/m)},\ \alpha,\beta \in \mathbb{C}^m \right\}. \tag{4.15}$$

Additionally, we introduce the auxiliary spaces

$$U_{MFS}(\kappa) := \left\{ \left(\widetilde{v}, \widetilde{w}\right) :\ \widetilde{v} = \Phi_\kappa *_{|\Gamma} a,\ \widetilde{w} = \Phi_{\sqrt{n}\kappa} *_{|\Gamma} b, (a,b) \in L^2(\Gamma) \times L^2(\Gamma) \right\} ,$$

which allow for continuous superpositions as in (2.20) and will thus simplify a density proof for U_{MFS} with respect to ITP solutions later. Although $U_{MFS}^{(m)}(\kappa) \not\subset U_{MFS}(\kappa)$ for any $m \in \mathbb{N}$, the next lemma states a direct connection.

Lemma 6. *Given any boundary integral solution $u = \Phi_\kappa *_{|\Gamma} a$ to the Helmholtz equation with $a \in L^2(\Gamma)$ and the above assumptions on Γ. Then there exists a sequence of MFS trial functions*

$$u^{(m)}(x) = \sum_{j=1}^{m} \Phi_\kappa\left(x - s^{(j/m)}\right)\alpha^{(j/m)} ,$$

where $\alpha^{(j/m)} \in \mathbb{C}$ for all $1 \le j \le m$ and $\left\{s^{(1/m)},\dots,s^{(m/m)}\right\} \in \Gamma$ are independent sets of source points becoming dense for $m \to \infty$, such that $u^{(m)} \to u$ in $H^l(D)$ for all $l \in \mathbb{N}$. In particular,

$$U_{MFS}(\kappa) \subset \overline{\bigcup_{m\in\mathbb{N}} U_{MFS}^{(m)}(\kappa)} .$$

Proof. For a fixed collection of source points $\left\{s^{(j/m)}\right\}_{1\le j\le m} \subset \Gamma$ we partition Γ into m disjoint connected fractions $\left\{\gamma^{(j/m)}\right\}_{1\le j\le m}$ such that $s^{(j/m)} \in \gamma^{(j/m)}$ for all $1 \le j \le m$. Then define the approximation kernels $\Phi_\kappa^{(m)} : \overline{D} \times \Gamma \to \mathbb{C}$ by

$$\Phi_\kappa^{(m)}(x,s) = \sum_{j=1}^{m} \mathbb{1}_{\gamma^{(j/m)}}(s)\Phi_\kappa(x-s) ,$$

where $\mathbb{1}_{\gamma^{(j/m)}}$ denotes the indicator function on the set $\gamma^{(j/m)}$. Similar to (2.20) we can then define $u^{(m)}$ by convolution

$$x \mapsto \int_\Gamma \Phi_\kappa^{(m)}(x,s)a(s)\,\mathrm{d}s = \sum_{j=1}^{m} \alpha^{(j/m)} \Phi_\kappa\big(x - s^{(j/m)}\big)$$

with the identifications

$$\alpha^{(j/m)} := \int_{\gamma^{(j/m)}} a(s)\,\mathrm{d}s\ .$$

The difference of u and $u^{(m)}$ can therefore be written for any $l \in \mathbb{N}$ as

$$\sup_{x\in\overline{D}} \big|\partial^l\big(u - u^{(m)}\big)\big| \leq \sup_{x\in\overline{D}} \sum_{j=1}^{m} \int_{\gamma^{(j/m)}} \big|\partial^l\big(\Phi_\kappa\big(x - s^{(j/m)}\big) - \Phi_\kappa(x-s)\big)\big||a(s)|\,\mathrm{d}s\ .$$

Since $\big||x - s^{(j/m)}| - |x-s|\big| \leq \big|s - s^{(j/m)}\big|$, $\Phi_\kappa \in C^\infty(\mathbb{R}^2\backslash\{0\})$ in combination with $\Gamma \cap \overline{D} = \emptyset$ implies the existence of an m-independent Lipschitz constant $L_l > 0$ such that

$$|\partial^l\big(\Phi_\kappa\big(x - s^{(j/m)}\big) - \Phi_\kappa(x-s)\big)\big| \leq L_l \big|s - s^{(j/m)}\big|\ .$$

By density of the source points in the limit $m \to \infty$ and $\big|s - s^{(j/m)}\big| \leq \big|\gamma^{(j/m)}\big|$, where the latter denotes the measure of the segment $\gamma^{(j/m)}$, we finally obtain

$$\sup_{x\in\overline{D}} \big|\partial^l\big(u - u^{(m)}\big)\big| \leq \|a\|_{L^2(\Gamma)} \sqrt{|\Gamma|} L_l \sup_{1\leq j\leq m} \big|\gamma^{(j/m)}\big| \to 0\ .$$

The result now follows by applying the definition of $\|\bullet\|_{H^l(D)}$. □

In order to prove density for $U_{MFS}(k)$ in the space of ITP solutions for every ITE k, we will work with the equivalent 4th order reformulation (4.5) in the sequel and derive its own fundamental solution from corresponding Helmholtz kernels. In particular, its form shows that the MFS ansatz for approximating (v,w) separately as in U_{MFS} and for $u = v - w$ as a whole is equivalent.

Lemma 7. *If Φ_κ and $\Phi_{\sqrt{n}\kappa}$ are fundamental solutions to the Helmholtz equation with wave numbers κ and $\sqrt{n}\kappa$, respectively, then the kernel $\Phi_{(\kappa,\sqrt{n}\kappa)} := \big(\Phi_{\sqrt{n}\kappa} - \Phi_\kappa\big)/((1-n)\kappa^2)$ is a fundamental solution for the composed fourth order operator $(\Delta + \kappa^2)(\Delta + n\kappa^2)$.*

Proof. Let $\varphi \in \mathscr{D}(D)$ be an arbitrary test function and set $\Phi^y_{(\kappa,\sqrt{n}\kappa)}(x) := \Phi_{(\kappa,\sqrt{n}\kappa)}(y-x)$ for some fixed $y \in \mathbb{R}^2$ (likewise for Φ^y_κ and $\Phi^y_{\sqrt{n}\kappa}$). Then we can check easily that

$$\begin{aligned}
&\int_D \Phi^y_{(\kappa,\sqrt{n}\kappa)}(\Delta+\kappa^2)(\Delta+n\kappa^2)\varphi\,\mathrm{d}x \\
&= \int_D \frac{\Phi^y_{\sqrt{n}\kappa^2}-\Phi^y_\kappa}{(1-n)\kappa^2}(\Delta+\kappa^2)(\Delta+n\kappa^2)\varphi\,\mathrm{d}x \\
&= \frac{1}{(1-n)\kappa^2}\left(\int_D \Phi^y_{\sqrt{n}\kappa}(\Delta+\kappa^2)(\Delta+n\kappa^2)\varphi\,\mathrm{d}x - \int_D \Phi^y_\kappa(\Delta+\kappa^2)(\Delta+n\kappa^2)\varphi\,\mathrm{d}x\right) \\
&= \frac{\Delta\varphi(y)+\kappa^2\varphi(y)}{(1-n)\kappa^2} - \frac{\Delta\varphi(y)+n\kappa^2\varphi(y)}{(1-n)\kappa^2} \\
&= \varphi(y)\ ,
\end{aligned}$$

which proves the lemma. □

We are now ready to prove the announced density result.

Theorem 8. *Let $u \in H^2(D)$ be any distributional solution to the fourth order equation $(\Delta+\kappa^2)(\Delta+n\kappa^2)u = 0$ with $0 \le \arg(\kappa) < \pi/4$. Then there exists a sequence of elements $\left\{\left(v^{(m)}, w^{(m)}\right)\right\}_{m\in\mathbb{N}} \subset U_{MFS}(\kappa)$ such that $\left(v^{(m)} - w^{(m)}\right) =: u^{(m)} \to u$ in $H^2(D)$. If ∂D is of class $C^{1,1}$, then in particular $\left\|u^{(m)}-u\right\|_{H^{\frac{3}{2}}(\partial D)} \to 0$ and $\left\|\partial_\nu\left(u^{(m)}-u\right)\right\|_{H^{\frac{1}{2}}(\partial D)} \to 0$.*

Proof. Parts of the following proof are inspired by Theorem 2.1 and Theorem 2.2 from [17]: Fix any κ and assume that $\widetilde{u} \in \widetilde{H}^{-2}(D) \simeq H^2(D)^*$ is chosen such that

$$\left\langle \widetilde{u}, \Phi_{(\kappa,\sqrt{n}\kappa)} *_{|\Gamma} a + \Phi_{\sqrt{n}\kappa} *_{|\Gamma} b \right\rangle_{\widetilde{H}^{-2}(D),H^2(D)} = 0 \tag{4.16}$$

for all $(a,b) \in L^2(\Gamma)\times L^2(\Gamma)$. By definition of $\Phi_{(\kappa,\sqrt{n}\kappa)}$ from the previous lemma we see that $\langle \widetilde{u}, v-w\rangle_{\widetilde{H}^{-2}(D),H^2(D)} = 0$ for any $(v,w) \in U_{MFS}(\kappa)$. Therefore, if we can show that the latter implies

$$\langle \widetilde{u}, u\rangle_{\widetilde{H}^{-2}(D),H^2(D)} = 0 \tag{4.17}$$

for every distributional solution $u \in H^2(D)$ of $(\Delta+\kappa^2)(\Delta+n\kappa^2)u = 0$, the Hahn-Banach theorem would yield the desired density claim since no intermediate functional extension would be possible.

We define the auxiliary functions which fulfill after corresponding restrictions $u^* := \Phi_{(\kappa,\sqrt{n}\kappa)} *_{|D} \widetilde{u} \in L^2(D)\cap C^\infty(D^c)$ and $w^* := \Phi_{\sqrt{n}\kappa} *_{|D} \widetilde{u} \in L^2(D)\cap C^\infty(D^c)$. We then obtain via distributional Fourier calculus, cf. (2.8), and using radial symmetry of the kernels $\Phi_{\sqrt{n}\kappa}$

and $\Phi_{(\kappa,\sqrt{n}\kappa)}$

$$\begin{aligned}
0 &= \left\langle \widetilde{u}, \Phi_{(\kappa,\sqrt{n}\kappa)} *_{|\Gamma} a + \Phi_{\sqrt{n}\kappa} *_{|\Gamma} b \right\rangle_{\widetilde{H}^{-2}(D),H^2(D)} \\
&= \frac{1}{(2\pi)^2} \int_{\mathbb{R}^2} \mathscr{F}\widetilde{u}(\xi) \mathscr{F}\left(\Phi_{(\kappa,\sqrt{n}\kappa)} *_{|\Gamma} a\right)(-\xi) + \mathscr{F}\widetilde{u}(\xi) \mathscr{F}\left(\Phi_{\sqrt{n}\kappa} *_{|\Gamma} b\right)(-\xi)\,\mathrm{d}\xi \\
&= \frac{1}{(2\pi)^2} \int_{\mathbb{R}^2} \mathscr{F}\widetilde{u}(\xi) \mathscr{F}\left(\Phi_{(\kappa,\sqrt{n}\kappa)}\right)(-\xi) \mathscr{F}a(-\xi) + \mathscr{F}\widetilde{u}(\xi) \mathscr{F}\left(\Phi_{\sqrt{n}\kappa}\right)(-\xi) \mathscr{F}b(-\xi)\,\mathrm{d}\xi \\
&= \frac{1}{(2\pi)^2} \int_{\mathbb{R}^2} \mathscr{F}\widetilde{u}(\xi) \mathscr{F}\left(\Phi_{(\kappa,\sqrt{n}\kappa)}\right)(\xi) \mathscr{F}a(-\xi) + \mathscr{F}\widetilde{u}(\xi) \mathscr{F}\left(\Phi_{\sqrt{n}\kappa}\right)(\xi) \mathscr{F}b(-\xi)\,\mathrm{d}\xi \\
&= \frac{1}{(2\pi)^2} \int_{\mathbb{R}^2} \mathscr{F}a(-\xi) \mathscr{F}\left(\Phi_{(\kappa,\sqrt{n}\kappa)} *_{|D} \widetilde{u}\right)(\xi) + \mathscr{F}b(-\xi) \mathscr{F}\left(\Phi_{\sqrt{n}\kappa} *_{|D} \widetilde{u}\right)(\xi)\,\mathrm{d}\xi \\
&= \frac{1}{(2\pi)^2} \int_{\mathbb{R}^2} \mathscr{F}a(\xi) \mathscr{F}\left(u^*\right)(-\xi) + \mathscr{F}b(\xi) \mathscr{F}\left(w^*\right)(-\xi)\,\mathrm{d}\xi \\
&= \int_\Gamma a u^* + b w^*\,\mathrm{d}s
\end{aligned}$$

for all $(a,b) \in L^2(\Gamma) \times L^2(\Gamma)$ whose embeddings as singular-supported distributions on $\mathbb{R}^2$ were not explicitly relabeled as such. In particular, we may conclude that $u^*_{|\Gamma} = w^*_{|\Gamma} = 0$. Using the pointwise estimate

$$|\sqrt{r}(\partial_r w^* - \mathrm{i}\sqrt{n}\kappa w^*)(x)| \leq \sqrt{r} \|\partial_r \Phi_{\sqrt{n}\kappa} - \mathrm{i}\sqrt{n}\kappa \Phi_{\sqrt{n}\kappa}\|_{H^2(x-D)} \|\widetilde{u}\|_{\widetilde{H}^{-2}(D)}\,,$$

where $x - D := \{x - y : \ y \in D\}$, in combination with standard recursive differentiation formulas for the pth Hankel function of the first kind as well as the asymptotic expansions

$$H_p^{(1)}(z) = \sqrt{\frac{2}{\pi z}} \mathrm{e}^{\mathrm{i}z - \frac{p\pi}{2} - \frac{\pi}{4}} + \mathscr{O}\left(\frac{1}{z}\right)$$

for $|z| \to \infty$, cf. [1], we deduce that also w^* fulfills the Sommerfeld radiation condition. By uniqueness of radiating exterior Helmholtz solutions on C^2-domains for $\mathrm{Im}(\kappa) \geq 0$, see [72, 32], and $(\Delta + n\kappa^2)w^* = \widetilde{u}$ in the sense of distributions, we may conclude that $w^* = 0$ outside of Ω (recall $\Gamma = \partial\Omega$). Due to analyticity, w^* even vanishes identically in $\overline{D}^{\mathrm{c}}$ as exterior Helmholtz solution. We want to similarly prove in the following that $u^* \in H^2_0(D)$ for justifying its role as alternative distributional test function later:

Using the definition of $\Phi_{(\kappa,\sqrt{n}\kappa)}$, direct calculations confirm the distributional relations

$$\begin{aligned}
(\Delta + \kappa^2)u^* &= w^* = (\Delta + \kappa^2)(\Phi_\kappa *_{|D} w^*)\,, \\
(\Delta + n\kappa^2)u^* &= \Phi_\kappa *_{|D} \widetilde{u} = (\Delta + n\kappa^2)(\Phi_\kappa *_{|D} w^*)\,.
\end{aligned}$$

This combines to $0 = ((\Delta + n\kappa^2) - (\Delta + \kappa^2))(u^* - \Phi_\kappa *|_D w^*) = (n-1)(u^* - \Phi_\kappa *|_D w^*)$ and implies the additional representation $u^* = \Phi_\kappa *|_D w^*$. The same uniqueness and analyticity reasoning as for w^* now yields $u^* = 0$ in $\overline{D}^c$ again and, by a regularity bootstrap argument due to $w^* \in L^2(D)$, we then conclude $u^* \in H_0^2(D)$. Therefore we can find a sequence of test functions $\left\{\varphi^{*(m)}\right\}_{m\in\mathbb{N}} \subset \mathscr{D}(D)$ such that $\varphi^{*(m)} \to u^*$ in $H^2(D)$. Taking then any distributional solution $u \in H^2(D)$ of $(\Delta + \kappa^2)(\Delta + n\kappa^2)u = 0$ as in (4.17) and another approximation sequence $\left\{\varphi^{(p)}\right\}_{p\in\mathbb{N}} \subset \mathscr{D}(\mathbb{R}^2)$ with $\varphi^{(p)} \to u$ in $H^2(D)$, we may finally compute, using $(\Delta + n\kappa^2)(\Delta + \kappa^2)u^* = \widetilde{u}$ in the sense of distributions,

$$\begin{aligned}
\langle \widetilde{u}, u \rangle_{\widetilde{H}^{-2}(D),H^2(D)} &= \lim_{p\to\infty} \langle \widetilde{u}, \varphi^{(p)} \rangle_{H^{-2}(\mathbb{R}^2),H^2(\mathbb{R}^2)} \\
&= \lim_{p\to\infty} \left\langle (\Delta + n\kappa^2)(\Delta + \kappa^2)u^*, \varphi^{(p)} \right\rangle_{H^{-2}(\mathbb{R}^2),H^2(\mathbb{R}^2)} \\
&= \left\langle (\Delta + n\kappa^2)(\Delta + \kappa^2)u^*, u \right\rangle_{\widetilde{H}^{-2}(D),H^2(D)} \\
&= \lim_{m\to\infty} \int_D (\Delta + \kappa^2)\varphi^{*(m)}(\Delta + n\kappa^2)u \,\mathrm{d}x \\
&= 0 \,.
\end{aligned}$$

Since u was an arbitrary homogeneous solution and thus $\widetilde{u}$, the desired density result for the interior domain is thereby proven. Appling the trace theorem extends the approximation result to the boundary of D in corresponding norms. □

Putting everything together, for any ITE k and its eigenfunctions we can prove existence of approximation sequences $\left\{\left(v^{(m)}, w^{(m)}, \kappa^{(m)}\right)\right\}_{m\in\mathbb{N}} \subset U_{MFS} \times \mathbb{C}$.

Corollary 9. *Let k be any ITE with $0 \leq \arg(k) < \pi/4$. Then there exist MFS trial functions $\left\{\left(v^{(m)}, w^{(m)}, \kappa^{(m)}\right)\right\}_{m\in\mathbb{N}} \in U_{MFS} \times \mathbb{C}$ such that (i)–(iii) from Theorem 1 are satisfied.*

Proof. Choosing $\kappa^{(m)} = k$ for all $m \in \mathbb{N}$, the assertion follows by combining Theorem 8 and Lemma 6 with (4.4) and (4.5). □

Note that in general one cannot waive any additional structure of fundamental solutions generating U_{MFS} like the radiating property yet still keeping the previous density results for any admissible Γ. For example, working only with the singular imaginary part of Φ_κ, i.e. with $Y_0(\kappa|\bullet|)$, where Y_0 is the Bessel function of the second kind of order zero, see [1], $D = B_1(0)$ and $\Gamma = \partial B_R(0)$ such that $R > 1$ is a root of Y_0 show that corresponding trial function (3.1) and thus linear combinations of such vanish at the origin. Consequently, one would not be able to approximate Helmholtz functions for $\kappa = 1$ which are non-zero at the origin any more. From this perspective, the radiation condition (4.2) is also a useful auxiliary feature to ensure unconditional MFS approximations in the end.

4.3.3 Convergence rate analysis

Subsection 4.3.2 has representatively reduced the trial functions of interest to $U_{MFS} \subset U$ which has proven to be sufficiently dense for ITE approximations. However, it is not clear whether MFS sequences as in Corollary 9 converge fast and are numerically attractive at all. In the context of Laplace eigenvalues from Chapter 3, Figure 3.6 indicated for D as unit disc that geometric convergence can be achieved when calculating the smallest Dirichlet eigenvalue via the modified MFS. Generally, one expects the decay to depend on the regularity of solutions to be approximated. Since we can rather control the scattering domain D than its spectrum of eigenfunctions, the next lemma states a regularity connection between both in the context of the ITP.

Lemma 10. *Let ∂D be of class C^l with $l \geq 2$ and (v,w) be a solution to* (4.3) *for some ITE k. Then $v,w \in H^{l-2}(D)$.*

Proof. The result follows by applying regularity theory for elliptic operators of general order, see for example Theorem 9.8 in [2], to (4.5). □

In the sequel we aim at establishing MFS convergence rates for ITE errors controlled by the collocation number m as well as the smoothness order l of the scatterer D. Our analysis will be based on (4.12) whose right-hand side will be bounded by proper approximate eigenfunctions $\left(v^{(m)}, w^{(m)}\right) \in U_{MFS}$ and source points distributed on $\Gamma = \partial B_R(0)$ for technical reasons. Although the actual MFS objective is the difference $v^{(m)} - w^{(m)}$ for which zero target data are given along the boundary by the ITP, we decouple the problem by approximating v and w separately in the interior as Helmholtz solutions. This is motivated by satisfying additionally assumption (ii) from Theorem 1 and the fact that there exists already profound literature on the MFS for solving Helmholtz-type equations. However, they either do not deal with Φ_κ, see [75, 93], for which we refer to our warning after Corollary 9, or they state L^2-boundary estimates with control constants C depending implicitly on the function to be approximated, see [10], which is too restrictive in our case, cf. Theorem 1 (iii) and (4.20) below. Still, we will apply their techniques, especially from the Laplace case in [17]. We start with the following independent result about generalized harmonic polynomials for the Helmholtz equation with real-valued wave numbers $k > 0$ from Vekua theory, see [77, 78].

Theorem 11. *Let D be a bounded Lipschitz domain, star-shaped with respect to a ball and assume that the origin is contained in D. Let the exterior angle of D be bounded from below by $\lambda\pi$ with $\lambda \leq 1$ and assume that $u \in H^l(D)$ with $l \geq 0$ solves the homogeneous Helmholtz equation with wave number $\kappa > 0$. Then for each $\widetilde{m} \in \mathbb{N}$ there are Fourier-Bessel functions*

$\widetilde{u}^{(\widetilde{m})}$ of the form

$$\widetilde{u}^{(\widetilde{m})}(r,\varphi) = a^{(0/\widetilde{m})} J_0(\kappa r) + \sum_{\widetilde{p}=1}^{\widetilde{m}} J_{\widetilde{p}}(\kappa r)\big(a^{(\widetilde{p}/\widetilde{m})}\cos(\widetilde{p}\varphi) + b^{(\widetilde{p}/\widetilde{m})}\sin(\widetilde{p}\varphi)\big) \tag{4.18}$$

such that for all $0 \leq j \leq l$ and a constant $C > 0$ which is independent of u it holds

$$\big\|u - \widetilde{u}^{(\widetilde{m})}\big\|_{H^j(D)} \leq C\left(\frac{\ln(\widetilde{m})}{\widetilde{m}}\right)^{\lambda(l-j)} \|u\|_{H^l(D)} \,. \tag{4.19}$$

Note that for general C^1-domains D, any $\lambda < 1$ is feasible while $\lambda = 1$ implies convexity. In either case, we can bound approximation errors between Helmholtz solutions u and MFS trial functions $u^{(m)} = u^{(m,\widetilde{m})}$ from (3.3) by

$$\big\|u - u^{(m)}\big\|_{H^j(D)} \leq \big\|u - \widetilde{u}^{(\widetilde{m})}\big\|_{H^j(D)} + \big\|\widetilde{u}^{(\widetilde{m})} - u^{(m)}\big\|_{H^j(D)} \,. \tag{4.20}$$

The first summand is then bounded by (4.19) so only convergence for the second term needs to be analyzed. The advantage of changing the MFS target function dynamically within the triangle inequality above is that $\widetilde{u}^{(\widetilde{m})}$ is always an entire function unlike u itself and therefore arguments are not restricted to D any more just like for U_{MFS} which in turn offers a more global investigation. For this, we still need a couple of auxiliary results to encapsulate some technical ingredients.

Lemma 12. *For $p, \widetilde{p} \in \mathbb{N}$ and $0 \leq \theta \leq 2\pi$ fixed it holds that*

$$\int_0^{2\pi} \cos(p(\varphi-\theta))\sin(\widetilde{p}\theta)\,\mathrm{d}\theta = \begin{cases} \pi\sin(p\varphi)\,, & \text{for } p = \widetilde{p} \\ 0\,, & \text{else} \end{cases}$$

$$\int_0^{2\pi} \cos(p(\varphi-\theta))\cos(\widetilde{p}\theta)\,\mathrm{d}\theta = \begin{cases} \pi\cos(p\varphi)\,, & \text{for } p = \widetilde{p} \neq 0 \\ 2\pi\,, & \text{for } p = \widetilde{p} = 0 \\ 0\,, & \text{else}\,. \end{cases}$$

Proof. If $p \neq \widetilde{p} \neq 0$, we may compute for the first identity via integration by parts with identical boundary terms due to periodicity of the integrands

$$\begin{aligned} \int_0^{2\pi} \cos(p(\varphi-\theta))\sin(\widetilde{p}\theta)\,\mathrm{d}\theta &= \frac{p}{\widetilde{p}}\int_0^{2\pi} \sin(p(\varphi-\theta))\cos(\widetilde{p}\theta)\,\mathrm{d}\theta \\ &= \left(\frac{p}{\widetilde{p}}\right)^2 \int_0^{2\pi} \cos(p(\varphi-\theta))\sin(\widetilde{p}\theta)\,\mathrm{d}\theta \end{aligned}$$

and else

$$\begin{aligned}\int_0^{2\pi} \cos(p(\varphi-\theta))\sin(\widetilde{p}\theta)\,\mathrm{d}\theta &= \frac{\widetilde{p}}{p}\int_0^{2\pi} \sin(p(\varphi-\theta))\cos(\widetilde{p}\theta)\,\mathrm{d}\theta \\ &= \left(\frac{\widetilde{p}}{p}\right)^2 \int_0^{2\pi} \cos(p(\varphi-\theta))\sin(\widetilde{p}\theta)\,\mathrm{d}\theta\ ,\end{aligned}$$

which shows in either case that the integral must vanish. Recalling for $p=\widetilde{p}$ the trigonometric addition formula $\sin(\alpha)-\sin(\beta)=2\cos\left((\alpha+\beta)/2\right)\sin\left((\alpha-\beta)/2\right)$, we obtain with $\alpha = p\varphi$ and $\beta = p(\theta-2\varphi)$

$$\int_0^{2\pi} \cos(p(\varphi-\theta))\sin(p\theta)\,\mathrm{d}\theta = \frac{1}{2}\int_0^{2\pi} \sin(p\theta)-\sin(p(\theta-2\varphi))\,\mathrm{d}\theta = \pi\sin(p\varphi)\ .$$

Using $\cos(\alpha)+\cos(\beta)=2\cos\left((\alpha+\beta)/2\right)\cos\left((\alpha-\beta)/2\right)$ for $p=\widetilde{p}\neq 0$, the second identity follows similarly. □

The next lemma expresses (4.18) in terms of Φ_κ and thus builds the first bridge to the MFS framework.

Lemma 13. *With the notation from Theorem 11, we have that*

$$\begin{aligned}\widetilde{u}^{(\widetilde{m})}(r,\varphi) = &\frac{a^{(0/\widetilde{m})}}{2\pi H_0^{(1)}(\kappa R)}\int_0^{2\pi} H_0^{(1)}\left(\kappa\left|re^{\mathrm{i}\varphi}-Re^{\mathrm{i}\theta}\right|\right)\mathrm{d}\theta \\ &+\sum_{\widetilde{p}=1}^{\widetilde{m}} \frac{a^{(\widetilde{p}/\widetilde{m})}}{2\pi H_{\widetilde{p}}^{(1)}(\kappa R)}\int_0^{2\pi} H_0^{(1)}\left(\kappa\left|re^{\mathrm{i}\varphi}-Re^{\mathrm{i}\theta}\right|\right)\cos(\widetilde{p}\theta)\,\mathrm{d}\theta \\ &+\sum_{\widetilde{p}=1}^{\widetilde{m}} \frac{b^{(\widetilde{p}/\widetilde{m})}}{2\pi H_{\widetilde{p}}^{(1)}(\kappa R)}\int_0^{2\pi} H_0^{(1)}\left(\kappa\left|re^{\mathrm{i}\varphi}-Re^{\mathrm{i}\theta}\right|\right)\sin(\widetilde{p}\theta)\,\mathrm{d}\theta\ .\end{aligned} \tag{4.21}$$

Here, $D\subset B_R(0)$ and its source points are similarly represented in polar coordinates by (R,θ).

Proof. According to Graf's addition formula, see Equation 9.1.79 in [1], differences within arguments of the first Hankel function can be expanded as

$$H_0^{(1)}\left(\kappa\left|re^{\mathrm{i}\varphi}-Re^{\mathrm{i}\theta}\right|\right) = H_0^{(1)}(\kappa R)J_0(\kappa r)+2\sum_{p=1}^{\infty} H_p^{(1)}(\kappa R)J_p(\kappa r)\cos(p(\varphi-\theta))\ .$$

We see that the first Bessel function of order $\widetilde{p}$ appears both in (4.18) and above, so it can be extracted from the latter by exploiting the orthogonality relations of trigonometric functions

stated in Lemma 12. We obtain for the p-th cosine term

$$\begin{aligned}
&\int_0^{2\pi} H_0^{(1)}\big(\kappa\big|re^{i\varphi}-Re^{i\theta}\big|\big)\cos(\widetilde{p}\theta)\,d\theta\\
&=\int_0^{2\pi}\left(H_0^{(1)}(\kappa R)J_0(\kappa r)+2\sum_{p=1}^{\infty}H_p^{(1)}(\kappa R)J_p(\kappa r)\cos(p(\varphi-\theta))\right)\cos(\widetilde{p}\theta)\,d\theta \qquad (4.22)\\
&=2\pi H_{\widetilde{p}}^{(1)}(\kappa R)J_{\widetilde{p}}(\kappa r)\cos(\widetilde{p}\varphi)
\end{aligned}$$

and analogue for the sine-dependent summands

$$\begin{aligned}
&\int_0^{2\pi} H_0^{(1)}\big(\kappa\big|re^{i\varphi}-Re^{i\theta}\big|\big)\sin(\widetilde{p}\theta)\,d\theta\\
&=\int_0^{2\pi}\left(H_0^{(1)}(\kappa R)J_0(\kappa r)+2\sum_{p=1}^{\infty}H_p^{(1)}(\kappa R)J_p(\kappa r)\cos(p(\varphi-\theta))\right)\sin(\widetilde{p}\theta)\,d\theta \qquad (4.23)\\
&=2\pi H_{\widetilde{p}}^{(1)}(\kappa R)J_{\widetilde{p}}(\kappa r)\sin(\widetilde{p}\varphi)\ .
\end{aligned}$$

The lemma follows by substituting the above Bessel function identities into (4.18), noting that $H_{\widetilde{p}}^{(1)}(\kappa R)\neq 0$ for all $\kappa,R\in\mathbb{R}$ and $\widetilde{p}\in\mathbb{N}$, see Remark 1 of [10] . □

Similar as in Lemma 6, (4.21) reflects a continuous convolution-type superposition which we need to discretize in order to obtain a valid MFS candidate $u^{(m,\widetilde{m})}$. For instance, the trapezoidal rule would give for m equiangular source points $\left\{Re^{2\pi i\frac{j}{m}}\right\}$, rewritten in the complex plane for $1\leq j\leq m$,

$$\begin{aligned}
u^{(m,\widetilde{m})}(r,\varphi)=&\frac{a^{(0/\widetilde{m})}}{mH_0^{(1)}(\kappa R)}\sum_{j=1}^{m}H_0^{(1)}\left(\kappa\left|re^{i\varphi}-Re^{2\pi i\frac{j}{m}}\right|\right)\\
&+\sum_{\widetilde{p}=1}^{\widetilde{m}}\frac{a^{(\widetilde{p}/\widetilde{m})}}{mH_{\widetilde{p}}^{(1)}(\kappa R)}\sum_{j=1}^{m}H_0^{(1)}\left(\kappa\left|re^{i\varphi}-Re^{2\pi i\frac{j}{m}}\right|\right)\cos\left(2\pi\frac{j}{m}\widetilde{p}\right)\\
&+\sum_{\widetilde{p}=1}^{\widetilde{m}}\frac{b^{(\widetilde{p}/\widetilde{m})}}{mH_{\widetilde{p}}^{(1)}(\kappa R)}\sum_{j=1}^{m}H_0^{(1)}\left(\kappa\left|re^{i\varphi}-Re^{2\pi i\frac{j}{m}}\right|\right)\sin\left(2\pi\frac{j}{m}\widetilde{p}\right)\ .
\end{aligned}$$

We are interested in bounding the defect of $u^{(m,\widetilde{m})}$ and $\widetilde{u}^{(\widetilde{m})}$ for which we freeze the radius $r=\text{const}<R$ in the sequel to switch temporarily to the one-dimensional setting. Hence we

define

$$
\begin{aligned}
e_{a,r}^{(m,\widetilde{p}/\widetilde{m})}(\varphi) :=& \frac{1}{2\pi H_{\widetilde{p}}^{(1)}(\kappa R)} \left(\frac{2\pi}{m} \sum_{j=1}^{m} H_0^{(1)}\left(\kappa \left| r\mathrm{e}^{\mathrm{i}\varphi} - R\mathrm{e}^{2\pi \mathrm{i}\frac{j}{m}} \right|\right) \cos\left(2\pi \frac{j}{m}\widetilde{p}\right) \right. \\
& \left. - \int_0^{2\pi} H_0^{(1)}\left(\kappa \left| r\mathrm{e}^{\mathrm{i}\varphi} - R\mathrm{e}^{\mathrm{i}\theta} \right|\right) \cos(\widetilde{p}\theta)\,\mathrm{d}\theta \right), \qquad 0 \le \widetilde{p} \le \widetilde{m}\,, \\
e_{b,r}^{(m,\widetilde{p}/\widetilde{m})}(r,\varphi) :=& \frac{1}{2\pi H_{\widetilde{p}}^{(1)}(\kappa R)} \left(\frac{2\pi}{m} \sum_{j=1}^{m} H_0^{(1)}\left(\kappa \left| r\mathrm{e}^{\mathrm{i}\varphi} - R\mathrm{e}^{2\pi \mathrm{i}\frac{j}{m}} \right|\right) \sin\left(2\pi \frac{j}{m}\widetilde{p}\right) \right. \\
& \left. - \int_0^{2\pi} H_0^{(1)}\left(\kappa \left| r\mathrm{e}^{\mathrm{i}\varphi} - R\mathrm{e}^{\mathrm{i}\theta} \right|\right) \sin(\widetilde{p}\theta)\,\mathrm{d}\theta \right), \qquad 1 \le \widetilde{p} \le \widetilde{m}\,,
\end{aligned}
$$

which implies

$$
u^{(m,\widetilde{m})}(r,\bullet) - \widetilde{u}^{(\widetilde{m})}(r,\bullet) = a^{(0/\widetilde{m})} e_{a,r}^{(m,0/\widetilde{m})} + \sum_{\widetilde{p}=1}^{\widetilde{m}} a^{(\widetilde{p}/\widetilde{m})} e_{a,r}^{(m,\widetilde{p}/\widetilde{m})} + b^{(\widetilde{p}/\widetilde{m})} e_{b,r}^{(m,\widetilde{p}/\widetilde{m})}\,. \tag{4.24}
$$

Since both $e_{a,r}^{(m,\widetilde{p}/\widetilde{m})}$ and $e_{b,r}^{(m,\widetilde{p}/\widetilde{m})}$ are linear combinations of 2π-periodic functions each, we can study their errors in terms of circular harmonics. Fourier expansion with respect to a sine and cosine basis yields

$$
\begin{aligned}
e_{a,r}^{(m,\widetilde{p}/\widetilde{m})}(\varphi) &= \frac{\mathscr{F}_{\cos} e_{a,r}^{(m,\widetilde{p}/\widetilde{m})}(0)}{2} + \sum_{\widetilde{l}=1}^{\infty} \mathscr{F}_{\cos} e_{a,r}^{(m,\widetilde{p}/\widetilde{m})}(\widetilde{l}) \cos(\widetilde{l}\varphi) + \mathscr{F}_{\sin} e_{a}^{(m,\widetilde{p}/\widetilde{m})}(\widetilde{l}) \sin(\widetilde{l}\varphi)\,, \\
e_{b,r}^{(m,\widetilde{p}/\widetilde{m})}(\varphi) &= \frac{\mathscr{F}_{\cos} e_{b}^{(m,\widetilde{p}/\widetilde{m})}(0)}{2} + \sum_{\widetilde{l}=1}^{\infty} \mathscr{F}_{\cos} e_{b,r}^{(m,\widetilde{p}/\widetilde{m})}(\widetilde{l}) \cos(\widetilde{l}\varphi) + \mathscr{F}_{\sin} e_{b,r}^{(m,\widetilde{p}/\widetilde{m})}(\widetilde{l}) \sin(\widetilde{l}\varphi)\,,
\end{aligned} \tag{4.25}
$$

where $\mathscr{F}_{\cos}, \mathscr{F}_{\sin}$ are adapted from (2.11) and given for $e \in L^2([0,2\pi))$ by

$$
\begin{aligned}
\mathscr{F}_{\cos} e(\widetilde{l}) &= \frac{1}{\pi} \int_0^{2\pi} e(\varphi) \cos(\widetilde{l}\varphi)\,\mathrm{d}\varphi\,, \\
\mathscr{F}_{\sin} e(\widetilde{l}) &= \frac{1}{\pi} \int_0^{2\pi} e(\varphi) \sin(\widetilde{l}\varphi)\,\mathrm{d}\varphi\,,
\end{aligned}
$$

with $0 \le \widetilde{l} < \infty$. Hence we obtain for $0 \le \widetilde{p} \le \widetilde{m}$ with (4.22) after changing the order of integration

$$
\begin{aligned}
&\mathscr{F}_{\cos} e_{a,r}^{(m,\widetilde{p}/\widetilde{m})}(\widetilde{l}) \\
=&\frac{1}{\pi}\int_0^{2\pi} e_{a,r}^{(m,\widetilde{p}/\widetilde{m})}(\varphi)\cos(\widetilde{l}\varphi)\,\mathrm{d}\varphi \\
=&\frac{1}{2\pi^2 H_{\widetilde{p}}^{(1)}(\kappa R)}\int_0^{2\pi}\left(\frac{2\pi}{m}\sum_{j=1}^{m} H_0^{(1)}\left(\kappa\left|r\mathrm{e}^{\mathrm{i}\varphi}-R\mathrm{e}^{2\pi\mathrm{i}\frac{j}{m}}\right|\right)\cos\left(2\pi\frac{j}{m}\widetilde{p}\right)\right. \\
&\left.-\int_0^{2\pi} H_0^{(1)}\left(\kappa\left|r\mathrm{e}^{\mathrm{i}\varphi}-R\mathrm{e}^{\mathrm{i}\theta}\right|\right)\cos(\widetilde{p}\theta)\,\mathrm{d}\theta\right)\cos(\widetilde{l}\varphi)\,\mathrm{d}\varphi \\
=&\frac{1}{2\pi^2 H_{\widetilde{p}}^{(1)}(\kappa R)}\left(\frac{2\pi}{m}\sum_{j=1}^{m}\left(\int_0^{2\pi} H_0^{(1)}\left(\kappa\left|r\mathrm{e}^{\mathrm{i}\varphi}-R\mathrm{e}^{2\pi\mathrm{i}\frac{j}{m}}\right|\right)\cos(\widetilde{l}\varphi)\,\mathrm{d}\varphi\right)\cos\left(2\pi\frac{j}{m}\widetilde{p}\right)\right. \\
&\left.-\int_0^{2\pi}\left(\int_0^{2\pi} H_0^{(1)}\left(\kappa\left|r\mathrm{e}^{\mathrm{i}\varphi}-R\mathrm{e}^{\mathrm{i}\theta}\right|\right)\cos(\widetilde{l}\varphi)\,\mathrm{d}\varphi\right)\cos(\widetilde{p}\theta)\,\mathrm{d}\theta\right) \\
=&\frac{1}{2\pi^2 H_{\widetilde{p}}^{(1)}(\kappa R)}\left(\frac{2\pi}{m}\sum_{j=1}^{m}\left(2\pi H_{\widetilde{l}}^{(1)}(\kappa R)J_{\widetilde{l}}(\kappa r)\cos\left(\widetilde{l}\theta^{(j/m)}\right)\right)\cos\left(2\pi\frac{j}{m}\widetilde{p}\right)\right. \\
&\left.-\int_0^{2\pi}\left(2\pi H_{\widetilde{l}}^{(1)}(\kappa R)J_{\widetilde{l}}(\kappa r)\cos(\widetilde{l}\theta)\right)\cos(\widetilde{p}\theta)\,\mathrm{d}\theta\right) \\
=&\frac{H_{\widetilde{l}}^{(1)}(\kappa R)J_{\widetilde{l}}(\kappa r)}{\pi H_{\widetilde{p}}^{(1)}(\kappa R)}\left(\frac{2\pi}{m}\sum_{j=1}^{m}\cos\left(2\pi\frac{j}{m}\widetilde{l}\right)\cos\left(2\pi\frac{j}{m}\widetilde{p}\right)-\int_0^{2\pi}\cos(\widetilde{l}\theta)\cos(\widetilde{p}\theta)\,\mathrm{d}\theta\right)
\end{aligned}
$$

and likewise

$$\begin{aligned}
\mathscr{F}_{\sin} e_{a,r}^{(m,\widetilde{p}/\widetilde{m})}(\widetilde{l}) &= \frac{H_{\widetilde{l}}^{(1)}(\kappa R) J_{\widetilde{l}}(\kappa r)}{\pi H_{\widetilde{p}}^{(1)}(\kappa R)} \left(\frac{2\pi}{m} \sum_{j=1}^{m} \sin\left(2\pi \frac{j}{m}\widetilde{l}\right) \cos\left(2\pi \frac{j}{m}\widetilde{p}\right) \right. \\
&\qquad \left. - \int_0^{2\pi} \sin(\widetilde{l}\theta)\cos(\widetilde{p}\theta)\,\mathrm{d}\theta \right), \\
\mathscr{F}_{\cos} e_{b,r}^{(m,\widetilde{p}/\widetilde{m})}(\widetilde{l}) &= \frac{H_{\widetilde{l}}^{(1)}(\kappa R) J_{\widetilde{l}}(\kappa r)}{\pi H_{\widetilde{p}}^{(1)}(\kappa R)} \left(\frac{2\pi}{m} \sum_{j=1}^{m} \cos\left(2\pi \frac{j}{m}\widetilde{l}\right) \sin\left(2\pi \frac{j}{m}\widetilde{p}\right) \right. \\
&\qquad \left. - \int_0^{2\pi} \cos(\widetilde{l}\theta)\sin(\widetilde{p}\theta)\,\mathrm{d}\theta \right), \\
\mathscr{F}_{\sin} e_{b,r}^{(m,\widetilde{p}/\widetilde{m})}(\widetilde{l}) &= \frac{H_{\widetilde{l}}^{(1)}(\kappa R) J_{\widetilde{l}}(\kappa r)}{\pi H_{\widetilde{p}}^{(1)}(\kappa R)} \left(\frac{2\pi}{m} \sum_{j=1}^{m} \sin\left(2\pi \frac{j}{m}\widetilde{l}\right) \sin\left(2\pi \frac{j}{m}\widetilde{p}\right) \right. \\
&\qquad \left. - \int_0^{2\pi} \sin(\widetilde{l}\theta)\sin(\widetilde{p}\theta)\,\mathrm{d}\theta \right).
\end{aligned}$$

The next lemma helps to evaluate the trigonometric integral defects within the Fourier coefficients above.

Lemma 14. *Fixing $m \in \mathbb{N}$, it holds for $0 \le \widetilde{l} < \infty$, $0 \le \widetilde{p} \le \widetilde{m}$ that*

$$\begin{aligned}
&\frac{2\pi}{m} \sum_{j=1}^{m} \sin\left(2\pi \frac{j}{m}\widetilde{l}\right) \sin\left(2\pi \frac{j}{m}\widetilde{p}\right) - \int_0^{2\pi} \sin(\widetilde{l}\theta)\sin(\widetilde{p}\theta)\,\mathrm{d}\theta \\
&= \begin{cases}
-\pi\,, & \text{for } \widetilde{p} = \widetilde{l} \neq 0,\ (\widetilde{l}+\widetilde{p}) \in m\mathbb{Z} \\
\pi\,, & \text{for } \widetilde{p} \neq \widetilde{l},\ (\widetilde{l}-\widetilde{p}) \in m\mathbb{Z},\ (\widetilde{l}+\widetilde{p}) \notin m\mathbb{Z} \\
-\pi\,, & \text{for } (\widetilde{l}-\widetilde{p}) \notin m\mathbb{Z},\ (\widetilde{l}+\widetilde{p}) \in m\mathbb{Z} \\
0\,, & \text{else}\,,
\end{cases}
\end{aligned}$$

$$\frac{2\pi}{m}\sum_{j=1}^{m}\cos\left(2\pi\frac{j}{m}\widetilde{l}\right)\cos\left(2\pi\frac{j}{m}\widetilde{p}\right)-\int_0^{2\pi}\cos(\widetilde{l}\theta)\cos(\widetilde{p}\theta)\,\mathrm{d}\theta$$
$$=\begin{cases}\pi\,, & \text{for } \widetilde{p}=\widetilde{l}\neq 0,\ (\widetilde{l}+\widetilde{p})\in m\mathbb{Z}\\ \pi\,, & \text{for } \widetilde{p}\neq\widetilde{l},\ (\widetilde{l}-\widetilde{p})\in m\mathbb{Z},\ (\widetilde{l}+\widetilde{p})\notin m\mathbb{Z}\\ 2\pi\,, & \text{for } \widetilde{p}\neq\widetilde{l},\ (\widetilde{l}-\widetilde{p})\in m\mathbb{Z},\ (\widetilde{l}+\widetilde{p})\in m\mathbb{Z}\\ \pi\,, & \text{for } (\widetilde{l}-\widetilde{p})\notin m\mathbb{Z},\ (\widetilde{l}+\widetilde{p})\in m\mathbb{Z}\\ 0\,, & \text{else}\,,\end{cases}$$

and

$$\frac{2\pi}{m}\sum_{j=1}^{m}\sin\left(2\pi\frac{j}{m}\widetilde{l}\right)\cos\left(2\pi\frac{j}{m}\widetilde{p}\right)-\int_0^{2\pi}\sin(\widetilde{l}\theta)\cos(\widetilde{p}\theta)\,\mathrm{d}\theta=0\,.$$

Proof. We recall for $q\neq 1$ the identity $\sum_{j=0}^{m-1}q=(1-q^m)/(1-q)$ which implies

$$\sum_{j=0}^{m-1}\mathrm{e}^{2\pi\mathrm{i}\frac{j}{m}r}=\sum_{j=1}^{m}\mathrm{e}^{2\pi\mathrm{i}\frac{j}{m}r}=\sum_{j=1}^{m}\left(\mathrm{e}^{2\pi\mathrm{i}\frac{r}{m}}\right)^j=\begin{cases}m\,, & \text{for } r\in m\mathbb{Z}\\ 0\,, & \text{else}\end{cases}$$

and we may infer

$$\sum_{j=1}^{m}\sin\left(2\pi\frac{j}{m}r\right)=\sum_{j=1}^{m}\frac{\mathrm{e}^{2\pi\mathrm{i}\frac{j}{m}r}-\mathrm{e}^{-2\pi\mathrm{i}\frac{j}{m}r}}{2\mathrm{i}}=0\,,\qquad\forall r\in\mathbb{Z}$$
$$\sum_{j=1}^{m}\cos\left(2\pi\frac{j}{m}r\right)=\sum_{j=1}^{m}\frac{\mathrm{e}^{2\pi\mathrm{i}\frac{j}{m}r}+\mathrm{e}^{-2\pi i\frac{j}{m}r}}{2}=\begin{cases}m\,, & \text{for } r\in m\mathbb{Z}\\ 0\,, & \text{else}\,.\end{cases}$$

Since $\sin(\alpha)-\sin(\beta)=2\cos\left((\alpha+\beta)/2\right)\sin\left((\alpha-\beta)/2\right)$, we obtain with Lemma 12 for the mixed integral assertion independent of $\widetilde{p}$ and $\widetilde{l}$

$$\frac{2\pi}{m}\sum_{j=1}^{m}\sin\left(2\pi\frac{j}{m}\widetilde{l}\right)\cos\left(2\pi\frac{j}{m}\widetilde{p}\right)-\int_0^{2\pi}\sin(\widetilde{l}\theta)\cos(\widetilde{p}\theta)\,\mathrm{d}\theta=0\,.$$

For the other identities we use $\cos(\alpha)-\cos(\beta)=-2\sin\left((\alpha+\beta)/2\right)\sin\left((\alpha-\beta)/2\right)$ and $\cos(\alpha)+\cos(\beta)=2\cos\left((\alpha+\beta)/2\right)\cos\left((\alpha-\beta)/2\right)$, respectively, as well as orthogonality

again to conclude

$$\begin{aligned}
&\frac{2\pi}{m}\sum_{j=1}^{m}\sin\left(2\pi\frac{j}{m}\widetilde{l}\right)\sin\left(2\pi\frac{j}{m}\widetilde{p}\right)-\int_0^{2\pi}\sin(\widetilde{l}\theta)\sin(\widetilde{p}\theta)\,\mathrm{d}\theta\\
&=\frac{\pi}{m}\sum_{j=1}^{m}\left(\cos\left(2\pi\frac{j}{m}(\widetilde{l}-\widetilde{p})\right)-\cos\left(2\pi\frac{j}{m}(\widetilde{l}+\widetilde{p})\right)\right)-\int_0^{2\pi}\cos(\widetilde{l}\theta)\cos(\widetilde{p}\theta)\,\mathrm{d}\theta\\
&=\begin{cases}
0\,, & \text{for } \widetilde{p}=\widetilde{l}=0\\
-\pi\,, & \text{for } \widetilde{p}=\widetilde{l}\neq 0,\ (\widetilde{l}+\widetilde{p})\in m\mathbb{Z}\\
0\,, & \text{for } \widetilde{p}=\widetilde{l}\neq 0,\ (\widetilde{l}+\widetilde{p})\notin m\mathbb{Z}\\
\pi\,, & \text{for } \widetilde{p}\neq\widetilde{l},\ (\widetilde{l}-\widetilde{p})\in m\mathbb{Z},\ (\widetilde{l}+\widetilde{p})\notin m\mathbb{Z}\\
0\,, & \text{for } \widetilde{p}\neq\widetilde{l},\ (\widetilde{l}-\widetilde{p})\in m\mathbb{Z},\ (\widetilde{l}+\widetilde{p})\in m\mathbb{Z}\\
-\pi\,, & \text{for } (\widetilde{l}-\widetilde{p})\notin m\mathbb{Z},\ (\widetilde{l}+\widetilde{p})\in m\mathbb{Z}\\
0\,, & \text{else}
\end{cases}
\end{aligned}$$

and

$$\begin{aligned}
&\frac{2\pi}{m}\sum_{j=1}^{m}\cos\left(2\pi\frac{j}{m}\widetilde{l}\right)\cos\left(2\pi\frac{j}{m}\widetilde{p}\right)-\int_0^{2\pi}\cos(\widetilde{l}\theta)\cos(\widetilde{p}\theta)\,\mathrm{d}\theta\\
&=\frac{\pi}{m}\sum_{j=1}^{m}\left(\cos\left(2\pi\frac{j}{m}(\widetilde{l}-\widetilde{p})\right)+\cos\left(2\pi\frac{j}{m}(\widetilde{l}+\widetilde{p})\right)\right)-\int_0^{2\pi}\cos(\widetilde{l}\theta)\cos(\widetilde{p}\theta)\,\mathrm{d}\theta\\
&=\begin{cases}
0\,, & \text{for } \widetilde{p}=\widetilde{l}=0\\
\pi\,, & \text{for } \widetilde{p}=\widetilde{l}\neq 0,\ (\widetilde{l}+\widetilde{p})\in m\mathbb{Z}\\
0\,, & \text{for } \widetilde{p}=\widetilde{l}\neq 0,\ (\widetilde{l}+\widetilde{p})\notin m\mathbb{Z}\\
\pi\,, & \text{for } \widetilde{p}\neq\widetilde{l},\ (\widetilde{l}-\widetilde{p})\in m\mathbb{Z},\ (\widetilde{l}+\widetilde{p})\notin m\mathbb{Z}\\
2\pi\,, & \text{for } \widetilde{p}\neq\widetilde{l},\ (\widetilde{l}-\widetilde{p})\in m\mathbb{Z},\ (\widetilde{l}+\widetilde{p})\in m\mathbb{Z}\\
\pi\,, & \text{for } (\widetilde{l}-\widetilde{p})\notin m\mathbb{Z},\ (\widetilde{l}+\widetilde{p})\in m\mathbb{Z}\\
0\,, & \text{else}\,.
\end{cases}
\end{aligned}$$

□

We can deduce the first spectral decay estimate for MFS approximations of Fourier-Bessel functions on spheres.

Lemma 15. *Let $0<r<R$, $\kappa\in\mathbb{R}$ and choose $r_-\leq r$ such that κ is no Dirichlet Laplace eigenvalue of the disc $B_{r_-}(0)$. Then for arbitrary approximation orders $l\geq 0$ and fixed Fourier-Bessel degree $\widetilde{m}\in\mathbb{N}$ the MFS error $u^{(m,\widetilde{m})}-\widetilde{u}^{(\widetilde{m})}$ from* (4.24) *with m equiangular*

source points on $\partial B_R(0)$ can be bounded in the regime $2\widetilde{m} < m$ by

$$\left\|u^{(m,\widetilde{m})} - \widetilde{u}^{(\widetilde{m})}\right\|_{H^l(\partial B_r(0))} \leq C m^l \left(\frac{r}{R}\right)^{m-2\widetilde{m}} \left(\frac{r}{r_-}\right)^{\widetilde{m}} \left\|\widetilde{u}^{(\widetilde{m})}\right\|_{L^2(\partial B_{r_-}(0))},$$

where the constant C depends only on l, κ and the radii r_-, r, R.

Proof. For a given wave number $\kappa \in \mathbb{R}$ and radii $r < R$, we fix some admissible $r_- \leq r$ and observe that $J_p(\kappa r_-) \neq 0$ according to (3.9) for every $p \in \mathbb{N}$. Therefore, we may compute for $l \geq 0$

$$\begin{aligned}
&\left\|u^{(m,\widetilde{m})} - \widetilde{u}^{(\widetilde{m})}\right\|_{H^l(\partial B_r(0))} \\
&= \left\| a^{(0/\widetilde{m})} e_{a,r}^{(m,0/\widetilde{m})} + \sum_{\widetilde{p}=1}^{\widetilde{m}} a^{(\widetilde{p}/\widetilde{m})} e_{a,r}^{(m,\widetilde{p}/\widetilde{m})} + b^{(\widetilde{p}/\widetilde{m})} e_{b,r}^{(m,\widetilde{p}/\widetilde{m})} \right\|_{H^l(\partial B_r(0))} \\
&\leq \left\| a^{(0/\widetilde{m})} J_0(\kappa r_-) \frac{e_{a,r}^{(m,0/\widetilde{m})}}{J_0(\kappa r_-)} \right\|_{H^l(\partial B_r(0))} \\
&\quad + \left\| \sum_{\widetilde{p}=1}^{\widetilde{m}} a^{(\widetilde{p}/\widetilde{m})} J_{\widetilde{p}}(\kappa r_-) \frac{e_{a,r}^{(m,\widetilde{p}/\widetilde{m})}}{J_{\widetilde{p}}(\kappa r_-)} + b^{(\widetilde{p}/\widetilde{m})} J_{\widetilde{p}}(\kappa r_-) \frac{e_{b,r}^{(m,\widetilde{p}/\widetilde{m})}}{J_{\widetilde{p}}(\kappa r_-)} \right\|_{H^l(\partial B_r(0))} \\
&\leq \left| a^{(0/\widetilde{m})} J_0(\kappa r_-) \right| \left\| \frac{e_{a,r}^{(m,0/\widetilde{m})}}{J_0(\kappa r_-)} \right\|_{H^l(\partial B_r(0))} \\
&\quad + \sum_{\widetilde{p}=1}^{\widetilde{m}} \left| a^{(\widetilde{p}/\widetilde{m})} J_{\widetilde{p}}(\kappa r_-) \right| \left\| \frac{e_{a,r}^{(m,\widetilde{p}/\widetilde{m})}}{J_{\widetilde{p}}(\kappa r_-)} \right\|_{H^l(\partial B_r(0))} + \left| b^{(\widetilde{p}/\widetilde{m})} J_{\widetilde{p}}(\kappa r_-) \right| \left\| \frac{e_{b,r}^{(m,\widetilde{p}/\widetilde{m})}}{J_{\widetilde{p}}(\kappa r_-)} \right\|_{H^l(\partial B_r(0))} \\
&\leq \frac{1}{\pi} \left\| \widetilde{u}^{(\widetilde{m})} \right\|_{L^2(\partial B_{r_-}(0))} \varepsilon_r^{(m,\widetilde{m})}
\end{aligned}$$

with

$$\varepsilon_r^{(m,\widetilde{m})} := \sqrt{\left\| \frac{e_a^{(m,0/\widetilde{m})}}{J_0(\kappa r_-)} \right\|_{H^l(\partial B_r(0))}^2 + \sum_{\widetilde{p}=1}^{\widetilde{m}} \left\| \frac{e_a^{(m,\widetilde{p}/\widetilde{m})}}{J_{\widetilde{p}}(\kappa r_-)} \right\|_{H^l(\partial B_r(0))}^2 + \left\| \frac{e_b^{(m,\widetilde{p}/\widetilde{m})}}{J_{\widetilde{p}}(\kappa r_-)} \right\|_{H^l(\partial B_r(0))}^2}. \tag{4.26}$$

In the last step we applied (2.9) according to the Fourier coefficient relations

$$\mathscr{F}\widetilde{u}^{(\widetilde{m})}(0) = a^{(0/\widetilde{m})} J_0(\kappa r_-)$$

and

$$\begin{aligned}\left|\mathscr{F}\widetilde{u}^{(\widetilde{m})}(\widetilde{p})\right|^2+\left|\mathscr{F}\widetilde{u}^{(\widetilde{m})}(-\widetilde{p})\right|^2 &= \left(\left|\frac{a^{(\widetilde{p}/\widetilde{m})}-\mathrm{i}b^{(\widetilde{p}/\widetilde{m})}}{2}\right|^2+\left|\frac{a^{(\widetilde{p}/\widetilde{m})}+\mathrm{i}b^{(\widetilde{p}/\widetilde{m})}}{2}\right|^2\right)J_{\widetilde{p}}^2(\kappa r_-)\\ &= \frac{\left|a^{(\widetilde{p}/\widetilde{m})}\right|^2+\left|b^{(\widetilde{p}/\widetilde{m})}\right|^2}{2}J_{\widetilde{p}}^2(\kappa r_-)\end{aligned} \tag{4.27}$$

for all $1\le\widetilde{p}\le\widetilde{m}$ and fixed $r=r_-$. The remainder of this proof aims at controlling $\varepsilon_r^{(m,\widetilde{m})}$ in terms of m which we will consider summand-wise. Combining (4.25) with Lemma 14, exploiting especially $2\widetilde{m}<m$ and $\mathscr{F}_{\sin}e_{a,r}^{(m,\widetilde{p}/\widetilde{m})}(\widetilde{l})=\mathscr{F}_{\cos}e_{b,r}^{(m,\widetilde{p}/\widetilde{m})}(\widetilde{l})=0$ for all frequencies $\widetilde{l}\ge 0$, we obtain

$$\begin{aligned}e_{b,r}^{(m,\widetilde{p}/\widetilde{m})}(\varphi) &= \sum_{\widetilde{l}=1}^{\infty}\mathscr{F}_{\sin}e_{b,r}^{(m,\widetilde{p}/\widetilde{m})}(\widetilde{l})\sin(\widetilde{l}\varphi)\\ &= \sum_{\widetilde{l}=1}^{\infty}\frac{H_{\widetilde{l}}^{(1)}(\kappa R)J_{\widetilde{l}}(\kappa r)}{\pi H_{\widetilde{p}}^{(1)}(\kappa R)}\left(\frac{2\pi}{m}\sum_{j=1}^{m}\sin\left(2\pi\frac{j}{m}\widetilde{l}\right)\sin\left(2\pi\frac{j}{m}\widetilde{p}\right)\sin(\widetilde{l}\varphi)\right.\\ &\qquad\left.-\int_0^{2\pi}\sin(\widetilde{l}\theta)\sin(\widetilde{p}\theta)\,\mathrm{d}\theta\right)\\ &= \sum_{t=1}^{\infty}\frac{H_{tm+\widetilde{p}}^{(1)}(\kappa R)J_{tm+\widetilde{p}}(\kappa r)}{H_{\widetilde{p}}^{(1)}(\kappa R)}\sin((tm+\widetilde{p})\varphi)\\ &\quad+\sum_{t=1}^{\infty}\frac{H_{tm-\widetilde{p}}^{(1)}(\kappa R)J_{tm-\widetilde{p}}(\kappa r)}{H_{\widetilde{p}}^{(1)}(\kappa R)}\sin((tm-\widetilde{p})\varphi)\end{aligned}$$

for $1\le\widetilde{p}\le\widetilde{m}$ and likewise

$$\begin{aligned}e_{a,r}^{(m,\widetilde{p}/\widetilde{m})}(\varphi) &= \sum_{\widetilde{l}=1}^{\infty}\mathscr{F}_{\cos}e_{a,r}^{(m,\widetilde{p}/\widetilde{m})}(\widetilde{l})\cos(\widetilde{l}\varphi)\\ &= \sum_{t=1}^{\infty}\frac{H_{tm+\widetilde{p}}^{(1)}(\kappa R)J_{tm+\widetilde{p}}(\kappa r)}{H_{\widetilde{p}}^{(1)}(\kappa R)}\cos((tm+\widetilde{p})\varphi)\\ &\quad+\sum_{t=1}^{\infty}\frac{H_{tm-\widetilde{p}}^{(1)}(\kappa R)J_{tm-\widetilde{p}}(\kappa r)}{H_{\widetilde{p}}^{(1)}(\kappa R)}\cos((tm-\widetilde{p})\varphi)\,.\end{aligned}$$

In order to dominate all the resulting series, we use the following large-order asymptotics for Bessel functions with fixed argument $z \neq 0$, cf. Equation 9.3.1 in [1],

$$J_p(z) \sim \frac{1}{\sqrt{2\pi p}} \left(\frac{\mathrm{e}z}{2p}\right)^p, \quad p \to \infty,$$
$$Y_p(z) \sim \sqrt{\frac{2}{\pi p}} \left(\frac{\mathrm{e}z}{2p}\right)^{-p}, \quad p \to \infty.$$

Since $H_p^{(1)}(z) = J_p(z) + \mathrm{i}Y_p(z)$, there is a uniform constant $C > 0$ such that

$$\frac{H_{\widetilde{l}}^{(1)}(\kappa R) J_{\widetilde{l}}(\kappa r)}{H_{\widetilde{p}}^{(1)}(\kappa R)} \leq C \sqrt{\frac{2\widetilde{p}}{\widetilde{l}^2 \pi}} \left(\frac{r}{R}\right)^{\widetilde{l}} \left(\frac{\mathrm{e}\kappa R}{2\widetilde{p}}\right)^{\widetilde{p}}$$

for all $\widetilde{p}, \widetilde{l} > 0$ but fixed κ, r, R. We then obtain with (4.27) and (2.10)

$$\begin{aligned}
\left\| e_{a,r}^{(m,\widetilde{p}/\widetilde{m})} \right\|_{H^l(\partial B_r(0))}^2 &= \frac{1}{2\pi} \sum_{\widetilde{l} \in \mathbb{Z}} \left| \mathscr{F} e_{a,r}^{(m,\widetilde{p}/\widetilde{m})}(\widetilde{l}) \right|^2 (1 + |\widetilde{l}|^2)^l \\
&= \frac{1}{4\pi} \sum_{t=1}^{\infty} \left| \frac{H_{tm+\widetilde{p}}^{(1)}(\kappa R) J_{tm+\widetilde{p}}(\kappa r)}{H_{\widetilde{p}}^{(1)}(\kappa R)} \right|^2 (1 + |tm + \widetilde{p}|^2)^l \\
&\quad + \frac{1}{4\pi} \sum_{t=1}^{\infty} \left| \frac{H_{tm-\widetilde{p}}^{(1)}(\kappa R) J_{tm-\widetilde{p}}(\kappa r)}{H_{\widetilde{p}}^{(1)}(\kappa R)} \right|^2 (1 + |tm - \widetilde{p}|^2)^l \\
&\leq \frac{C^2}{4\pi} \sum_{t=1}^{\infty} \left(\frac{2\widetilde{p}}{(tm+\widetilde{p})^2 \pi} \left(\frac{r}{R}\right)^{2tm+2\widetilde{p}} \left(\frac{\mathrm{e}\kappa R}{2\widetilde{p}}\right)^{2\widetilde{p}} \right) 2^l |tm + \widetilde{p}|^{2l} \\
&\quad + \frac{C^2}{4\pi} \sum_{t=1}^{\infty} \left(\frac{2\widetilde{p}}{(tm-\widetilde{p})^2 \pi} \left(\frac{r}{R}\right)^{2tm-2\widetilde{p}} \left(\frac{\mathrm{e}\kappa R}{2\widetilde{p}}\right)^{2\widetilde{p}} \right) 2^l |tm - \widetilde{p}|^{2l} \\
&\leq C\widetilde{p} \left(\frac{\mathrm{e}\kappa R}{2\widetilde{p}}\right)^{2\widetilde{p}} \left(\frac{r}{R}\right)^{2m-2\widetilde{p}} \sum_{t=0}^{\infty} \left(\frac{r}{R}\right)^{2tm} (tm)^{2l-2} \\
&\leq C\widetilde{p} m^{2l-2} \left(\frac{\mathrm{e}\kappa R}{2\widetilde{p}}\right)^{2\widetilde{p}} \left(\frac{r}{R}\right)^{2m-2\widetilde{p}}
\end{aligned}$$

where we successively absorbed several numeracy or l-dependent constants into C without explicit relabeling. Hence we can bound for $0 < \widetilde{p} \leq \widetilde{m} < m$

$$\begin{aligned}\left\|\frac{e_a^{(m,\widetilde{p}/\widetilde{m})}}{J_{\widetilde{p}}(\kappa r_-)}\right\|^2_{H^l(\partial B_r(0))} &\le C\widetilde{p}m^{2l-2}\left(\frac{\mathrm{e}\kappa R}{2\widetilde{p}}\right)^{2\widetilde{p}}\left(\frac{r}{R}\right)^{2m-2\widetilde{p}}\widetilde{p}\left(\frac{\mathrm{e}\kappa r_-}{2\widetilde{p}}\right)^{-2\widetilde{p}}\\ &\le Cm^{2l}\left(\frac{r}{R}\right)^{2m-4\widetilde{p}}\left(\frac{r}{r_-}\right)^{2\widetilde{p}}.\end{aligned}$$

Similarly, we obtain

$$\left\|\frac{e_b^{(m,\widetilde{p}/\widetilde{m})}}{J_{\widetilde{p}}(\kappa r_-)}\right\|^2_{H^l(\partial B_r(0))} \le Cm^{2l}\left(\frac{r}{R}\right)^{2m-4\widetilde{p}}\left(\frac{r}{r_-}\right)^{2\widetilde{p}}.$$

If $\widetilde{p}=0$, it suffices to consider

$$\begin{aligned}\left\|e_{a,r}^{(m,0/\widetilde{m})}\right\|^2_{H^l(\partial B_r(0))} &= \frac{1}{2\pi}\sum_{\widetilde{l}\in\mathbb{Z}}\left|\mathscr{F}e_{a,r}^{(m,0/\widetilde{m})}(\widetilde{l})\right|^2(1+|\widetilde{l}|^2)^l\\ &= \frac{1}{4\pi}\sum_{t=1}^{\infty}\left|\frac{H_{tm}^{(1)}(\kappa R)J_{tm}(\kappa r)}{H_0^{(1)}(\kappa R)}\right|^2(1+|tm|^2)^l\\ &\le \frac{C}{\left|H_0^{(1)}(\kappa R)\right|^2}\sum_{t=1}^{\infty}\left(\frac{r}{R}\right)^{2tm}(tm)^{2l-2}\\ &\le \frac{C}{\left|H_0^{(1)}(\kappa R)\right|^2}m^{2l-2}\left(\frac{r}{R}\right)^{2m}\end{aligned}$$

and

$$\left\|\frac{e_a^{(m,0/\widetilde{m})}}{J_0(\kappa r_-)}\right\|^2_{H^l(\partial B_r(0))} \le \frac{C}{\left|H_0^{(1)}(\kappa R)J_0(\kappa r_-)\right|^2}m^{2l}\left(\frac{r}{R}\right)^{2m}.$$

Therefore, we can bound (4.26) in total by

$$\begin{aligned}\left(\varepsilon_r^{(m,\widetilde{m})}\right)^2 &\le Cm^{2l}\sum_{\widetilde{p}=0}^{\widetilde{m}}\left(\frac{r}{R}\right)^{2m-4\widetilde{p}}\left(\frac{r}{r_-}\right)^{2\widetilde{p}}\\ &\le Cm^{2l}\left(\frac{r}{r_-}\right)^{2\widetilde{m}}\left(\frac{r}{R}\right)^{2m-4\widetilde{m}}\sum_{\widetilde{p}=0}^{\widetilde{m}}\left(\frac{r}{R}\right)^{4\widetilde{m}-4\widetilde{p}}\\ &\le Cm^{2l}\left(\frac{r}{r_-}\right)^{2\widetilde{m}}\left(\frac{r}{R}\right)^{2m-4\widetilde{m}}\end{aligned}$$

which proves the lemma. □

We can finally put all estimates from this section together to specify the error decay (4.20) for MFS approximations of Helmholtz solutions in terms of the collocation number and domain regularity. For clarity, we absorb former dependencies on the source radius R into control constants C in the following.

Theorem 16. *Let all the conditions from Theorem 11 be true and choose $D \subset B_R(0)$. Then any solution $u \in H^l(D)$ of the Helmholtz equation with wave number $\kappa > 0$ can be approximated by functions $u^{(m)}$ of the form* (3.3) *with identical κ and m equiangular source points distributed on $\partial B_R(0)$ such that*

$$\left\|u - u^{(m)}\right\|_{H^j(D)} \leq C \left(\frac{\ln(m)}{m}\right)^{\lambda(l-j)} \|u\|_{H^l(D)} \tag{4.28}$$

for $1 \leq j \leq l$. The constant C is independent of u and m.

Proof. We recall observation (4.20) which decomposes the desired decay estimate (4.28) into

$$\left\|u - u^{(m,\widetilde{m})}\right\|_{H^j(D)} \leq \left\|u - \widetilde{u}^{(\widetilde{m})}\right\|_{H^j(D)} + \left\|\widetilde{u}^{(\widetilde{m})} - u^{(m,\widetilde{m})}\right\|_{H^j(D)} . \tag{4.29}$$

Here, $u^{(m)} := u^{(m,\widetilde{m})}$ and $\widetilde{u}^{(\widetilde{m})}$ are as in Theorem 15 with $\widetilde{m}$ to be specified next. For this we choose $r_- < r < R$ such that $B_{r_-}(0) \subset D \subset B_r(0)$ and κ is no Dirichlet Laplace eigenvalue of both $B_{r_-}(0)$ and $B_r(0)$. Fixing some exponent $p > 1$, we pick for any $m > 1$ the unique $\widetilde{m} \in \mathbb{N}$ determined by

$$\begin{aligned} \left(\frac{r}{R}\right)^{m-2\widetilde{m}} \left(\frac{r}{r_-}\right)^{\widetilde{m}} &\leq \frac{1}{\widetilde{m}^p} , \\ \left(\frac{r}{R}\right)^{m-2(\widetilde{m}+1)} \left(\frac{r}{r_-}\right)^{\widetilde{m}+1} &\geq \frac{1}{(\widetilde{m}+1)^p} , \end{aligned} \tag{4.30}$$

which exists since the left-hand side is increasing while the right-hand side is decreasing in $\widetilde{m}$. Exploiting monotonicity of the logarithm then, we obtain

$$\begin{aligned} \widetilde{m}\left(2 + \frac{\ln\left(\frac{r}{r_-}\right)}{\ln\left(\frac{R}{r}\right)}\right) + \ln(\widetilde{m}) \frac{p}{\ln\left(\frac{R}{r}\right)} &\leq m , \\ (\widetilde{m}+1)\left(2 + \frac{\ln\left(\frac{r}{r_-}\right)}{\ln\left(\frac{R}{r}\right)}\right) + \ln(\widetilde{m}+1) \frac{p}{\ln\left(\frac{R}{r}\right)} &\geq m . \end{aligned}$$

In particular, we deduce $2\widetilde{m} < m < \widetilde{C}\widetilde{m}$ for some constant $\widetilde{C} > 0$ which depends only on p and $r_- < r < R$. Thus, the first summand on the right-hand side of (4.29) can be bounded with Theorem 11 by

$$\left\|u - \widetilde{u}^{(\widetilde{m})}\right\|_{H^j(D)} \leq C\left(\frac{\ln(\widetilde{m})}{\widetilde{m}}\right)^{\lambda(l-j)} \|u\|_{H^l(D)} \leq C\left(\frac{\ln(m)}{m}\right)^{\lambda(l-j)} \|u\|_{H^l(D)} \tag{4.31}$$

for some adapted constant $C > 0$. For the other term in (4.29) we employ the previous lemma with $2\widetilde{m} < m < \widetilde{C}\widetilde{m}$ and (4.30) to obtain

$$\begin{aligned}
\left\|\widetilde{u}^{(\widetilde{m})} - u^{(m,\widetilde{m})}\right\|_{H^j(D)} &\leq \left\|\widetilde{u}^{(\widetilde{m})} - u^{(m,\widetilde{m})}\right\|_{H^j(B_r(0))} \\
&\leq C\left\|\widetilde{u}^{(\widetilde{m})} - u^{(m,\widetilde{m})}\right\|_{H^{j-\frac{1}{2}}(\partial B_r(0))} \\
&\leq C\frac{m^j}{\widetilde{m}^p}\left\|\widetilde{u}^{(\widetilde{m})}\right\|_{L^2(\partial B_{r_-}(0))} \\
&\leq C\frac{1}{m^{p-j}}\left\|\widetilde{u}^{(\widetilde{m})}\right\|_{H^{\frac{1}{2}}(B_{r_-}(0))} \\
&\leq C\frac{1}{m^{p-j}}\left\|\widetilde{u}^{(\widetilde{m})}\right\|_{H^j(D)} .
\end{aligned}$$

Here, we also used our assumptions on the radii r_-, r in combination with (2.19) and the trace theorem. By (4.31), $\left\|\widetilde{u}^{(\widetilde{m})}\right\|_{H^j(D)} \leq \left\|u - \widetilde{u}^{(\widetilde{m})}\right\|_{H^j(D)} + \|u\|_{H^j(D)}$ can be uniformly bounded in terms of $\|u\|_{H^l(D)}$. Since p was chosen arbitrary, the decay within (4.29) is dominated by the first summand and thus by the right-hand side of (4.31). □

We see that our derived MFS convergence rates established in the theorem above are inherited from those of Fourier-Bessel trial functions. This is not very surprising since the proof takes the latter as successive target functions which usually admit better convergence results than domain-restricted approximations, cf. [10, 77]. Altogether, we can use the new findings to further quantify theoretical ITE errors when approximating boundary data of eigenfunctions with MFS trial functions for real-valued k and sufficiently smooth domains D, cf. Corollary 3. It also gives an idea about which convergence rate one might expect when the conditions of Theorem 1 are met by certain optimal $\left\{\left(v_{min}^{(m)}, w_{min}^{(m)}, \kappa_{min}^{(m)}\right)\right\}_{m\in\mathbb{N}} \subset U_{MFS} \times \mathbb{R}$.

Theorem 17. *Let D be of class C^l with $l \geq 4$ fulfilling additionally the domain assumptions of Theorem 11 and let $k > 0$ be an ITE such that all pairs (v,w) of its eigenspace fulfill $\|v\|^2_{L^2(D)} - n\|w\|^2_{L^2(D)} \neq 0$. For every $m \in \mathbb{N}$ distribute a corresponding number of source points equiangularly on $\Gamma = \partial B_R(0)$ with $D \subset B_R(0)$. Then a subsequence of*

$\left\{\left(v_{min}^{(m)}, w_{min}^{(m)}, \kappa_{min}^{(m)}\right)\right\}_{m\in\mathbb{N}} \subset U_{MFS}\times\mathbb{R}$, *defined for each* m *as functional minimizers of*

$$\kappa \mapsto f_{MFS}^{(m)}(\kappa) := \min_{(\widetilde{v},\widetilde{w})\in U_{MFS}^{(m)}(\kappa)} \frac{\sqrt{\|\widetilde{v}-\widetilde{w}\|^2_{H^{\frac{3}{2}}(\partial D)} + \|\partial_\nu(\widetilde{v}-\widetilde{w})\|^2_{H^{\frac{1}{2}}(\partial D)}}}{\|\widetilde{v}\|_{L^2(D)} + \|\widetilde{w}\|_{L^2(D)}}$$

at corresponding local $f_{MFS}^{(m)}$*-minima* $\kappa = \kappa_{min}^{(m)}$ *such that* $\kappa_{min}^{(m)} \to k$*, satisfies*

$$\left|k^2 - \left(\kappa_{min}^{(m)}\right)^2\right| \leq C\left(\frac{\ln(m)}{m}\right)^{\lambda(l-4)} .$$

Here, the constant C *is independent of* m*.*

Proof. Dominated by Corollary 9, we infer that $f_{MFS}^{(m)}\left(\kappa_{min}^{(m)}\right) \leq f_{MFS}^{(m)}(k) \to 0$ which implies that $\left\{\left(v_{min}^{(m)}, w_{min}^{(m)}, \kappa_{min}^{(m)}\right)\right\}_{m\in\mathbb{N}}$ fulfills the assumptions of Theorem 1. In particular, a subsequence of the functional minimizers converges weakly in $L^2(D)\times L^2(D)$ to some eigenfunction pair $(v,w) \in H^{l-2}(D)\times H^{l-2}(D)$ according to Lemma 10. With the help of the previous theorem then, we can find $\left(v^{(m)}, w^{(m)}\right) \in U_{MFS}^{(m)}(k)$ such that

$$\begin{aligned}\left\|v - v^{(m)}\right\|_{H^2(D)} &\leq C\left(\frac{\ln(m)}{m}\right)^{\lambda(l-4)} \|v\|_{H^{l-2}(D)} ,\\ \left\|w - w^{(m)}\right\|_{H^2(D)} &\leq C\left(\frac{\ln(m)}{m}\right)^{\lambda(l-4)} \|w\|_{H^{l-2}(D)}\end{aligned}$$

for all $m\in\mathbb{N}$. Since $(v-w)_{|\partial D} = \partial_\nu(v-w)_{|\partial D} = 0$, the trace theorem ensures

$$\begin{aligned}\left\|v^{(m)} - w^{(m)}\right\|_{H^{\frac{3}{2}}(\partial D)} &\leq \left\|v - v^{(m)}\right\|_{H^{\frac{3}{2}}(\partial D)} + \left\|w - w^{(m)}\right\|_{H^{\frac{3}{2}}(\partial D)}\\ &\leq C\left(\left\|v - v^{(m)}\right\|_{H^2(D)} + \left\|w - w^{(m)}\right\|_{H^2(D)}\right)\end{aligned}$$

and likewise

$$\left\|\partial_\nu\left(v^{(m)} - w^{(m)}\right)\right\|_{H^{\frac{1}{2}}(\partial D)} \leq C\left(\left\|v - v^{(m)}\right\|_{H^2(D)} + \left\|w - w^{(m)}\right\|_{H^2(D)}\right) .$$

Corollary 3 finally yields

$$\begin{aligned}\left|k^2-\left(\kappa_{min}^{(m)}\right)^2\right| &\leq C\frac{\sqrt{\left\|v_{min}^{(m)}-w_{min}^{(m)}\right\|^2_{H^{\frac{3}{2}}(\partial D)}+\left\|\partial_\nu\left(v_{min}^{(m)}-w_{min}^{(m)}\right)\right\|^2_{H^{\frac{1}{2}}(\partial D)}}}{\left\|v_{min}^{(m)}\right\|_{L^2(D)}+\left\|w_{min}^{(m)}\right\|_{L^2(D)}}\\ &\leq C\frac{\sqrt{\left\|v^{(m)}-w^{(m)}\right\|^2_{H^{\frac{3}{2}}(\partial D)}+\left\|\partial_\nu\left(v^{(m)}-w^{(m)}\right)\right\|^2_{H^{\frac{1}{2}}(\partial D)}}}{\left\|v^{(m)}\right\|_{L^2(D)}+\left\|w^{(m)}\right\|_{L^2(D)}}\\ &\leq C\left(\frac{\ln(m)}{m}\right)^{\lambda(l-4)},\end{aligned}$$

where all dependencies on (v,w) have been absorbed successively into $C>0$. □

Note for infinitely smooth domains D we would obtain spectral decay, at least in theory. Therefore, we will finally focus on numerical aspects of the modified MFS algorithm for ITE computations and study if the conclusions from this section are reflected by the discrete setting, too.

4.4 The modified method of fundamental solutions from a numerical perspective

So far we have established an abstract framework for ITE approximations of homogeneous and isotropic media in exact arithmetics and Sobolev norms. In practice, however, the effects of round-off errors and discretized norms are unavoidable and need to be taken into account. In the following we apply the modified MFS algorithm for ITE calculations and present numerical results to explore the practical competition between ill-conditioning, as intrinsic to radial-basis-function-schemes, and theoretical convergence rates stated by Theorem 17.

4.4.1 Implementation details

In Section 3.4 we introduced the modified MFS which was specifically designed there for the computation of Laplace eigenvalues. Recall that the main ingredient was an a posteriori estimate like (3.10) which directly relates boundary errors from approximate eigenfunction candidates of Trefftz-kind to corresponding eigenvalue misfits. In the non-self-adjoint ITP case, approximation of ITEs and accompanying error bounds in terms of trial function defects could also be derived yet in a more modular fashion, cf. Theorem 1 and Lemma 2. Hence our concrete numerical implementation of the modified MFS for the ITP will emerge as a

combination of both as indicated by Theorem 17. In order to explore the full computational potential then, we relax some material conditions made in the theoretical section since they served to simplify technical difficulties so far. In the following we also include Lipschitz domains D since practical collocation is actually invisible with respect to local regularity properties of boundaries. Regarding the various computational points required, we adopt the notation from Chapter 3 and select for each m again $\{s^{(1/m)},\dots,s^{(m/m)}\} \subset \Gamma$ as sources to generate $U^{(m)}_{MFS}(\kappa)$ as well as $\{x^{(1/m)},\dots,x^{(m/m)}\} \subset \partial D$ for the boundary collocation procedure. Further, we fix $\widehat{m}$ random indicator points $\{\widehat{x}^{(1/\widehat{m})},\dots,x^{(\widehat{m}/\widehat{m})}\} \in D$ which are to free the MFS as auxiliary parameters from spurious eigenvalues also in the ITP case, cf. Section 3.3.

Given some ITE k, a reasonable collocation version of Theorem 1 (setting $C = 1$ by disregarding discretization errors for the sake of derivation) would seek for approximate eigenfunction pairs $\big(v^{(m)}, w^{(m)}\big) \in U^{(m)}_{MFS}\big(\kappa^{(m)}\big)$ such that

$$\frac{1}{\widehat{m}} \sum_{j=1}^{\widehat{m}} \big|v^{(m)}\big(\widehat{x}^{(j,\widehat{m})}\big)\big|^2 + \big|w^{(m)}\big(\widehat{x}^{(j,\widehat{m})}\big)\big|^2 \approx 1 \tag{4.32}$$

while

$$\sum_{j=1}^{m} \big|v^{(m)}\big(x^{(j/m)}\big) - w^{(m)}\big(x^{(j/m)}\big)\big|^2 + \big|\partial_\nu v^{(m)}\big(x^{(j/m)}\big) - \partial_\nu w^{(m)}\big(x^{(j/m)}\big)\big|^2 \to 0 \tag{4.33}$$

for $m \to \infty$. In this way, the control assumptions (ii) and (iii) are directly addressed numerically, and (i) should be checked by inspecting the successive $\kappa^{(m)}$-output. However, note that a consistent discretization with respect to the actually prescribed, fractional Sobolev norms in (iii) requires more advanced techniques due to their rather collocation-incompatible nature (2.10), so the boundary collocation above can alternatively be modified. Returning to our compromise, trial function dependencies of $\big(v^{(m)}, w^{(m)}\big)$ will be captured by the coefficient matrices $B(\kappa)$, $\nabla B(\kappa)\nu$, $\widehat{I}(\kappa)$ and $B(\sqrt{n}\kappa)$, $\nabla B(\sqrt{n}\kappa)\nu$, $\widehat{I}(\sqrt{n}\kappa)$ from Chapter 3, respectively. In analogy to (3.12) now, the modified MFS matrix for the ITP characterized by (4.32) and (4.33) would read, after absorbing appearing minus signs into trial function coefficients,

$$M(\kappa) = \begin{pmatrix} B(\kappa) & B(\sqrt{n}\kappa) \\ \nabla B(\kappa)\nu & \nabla B(\sqrt{n}\kappa)\nu \\ \widehat{I}(\kappa) & 0 \\ 0 & \widehat{I}(\sqrt{n}\kappa) \end{pmatrix}. \tag{4.34}$$

Having thus derived $M(\kappa)$, we can proceed as in Section 3.4, Figure 3.5, to get rid of spurious ITEs and decompose

$$M(\kappa) = Q(\kappa)R(\kappa) = \begin{pmatrix} Q_B(\kappa) \\ Q_I(\kappa) \end{pmatrix} R(\kappa) \,, \tag{4.35}$$

with $Q_I(\kappa) \in \mathbb{C}^{2\widehat{m}\times 2m}$ and $Q_B(\kappa) \in \mathbb{C}^{2m\times 2m}$ now. Recall that the ranges of $M(\kappa)$ and $Q(\kappa)$ are equal but it is only the unitary factor which, similar to (3.13), fulfills (4.33) implicitly as soon as (4.32) holds. Therefore, it again amounts to make the latter vanish for which we extract the smallest singular value from $Q_B(\kappa)$ at each collocation step m as a function of $\kappa \in \mathbb{C}\backslash\{0\}$, i.e.

$$\kappa \mapsto \sigma_{min}(\kappa) = \min_{\eta\in\mathbb{C}^{2m},|\eta|=1} |Q_B(\kappa)\eta| \tag{4.36}$$

and call sufficiently small local minima $\kappa^{(m)}$ approximate ITEs. We will also write $\kappa^{(\ell,m)}$ or $\kappa_{\mathbb{R}}^{(\ell,m)}$ when linking to the ℓ-th ITE $k^{(\ell,m)}$ or $k_{\mathbb{R}}^{(\ell,m)}$, respectively. Likewise, the underlying routine will be referred to as modified MFS.

Note that the modified MFS generally executes without the need of explicitly establishing underlying approximate eigenfunctions. Still they are recoverable by taking the singular vector $\eta_{min} \in \mathbb{C}^{2m}$ associated with $\sigma_{min}(\kappa^{(m)})$, i.e. the corresponding columns of $\overline{V}^T$ in (2.1), and computing the coefficient vector

$$\begin{pmatrix} \alpha \\ \beta \end{pmatrix} = R^{-1}\big(\kappa^{(m)}\big)\eta_{min} \tag{4.37}$$

from (4.15). However, since unitary factors are perfectly conditioned, $M(\kappa)$ and $R(\kappa)$ should both suffer from the same MFS ill-conditioning for all $\kappa \in \mathbb{C}$ which makes the inversion prone to errors. Numerical linear algebra still ensures that the residual, i.e. the collocation misfit of the associated approximate eigenfunction pair from (4.15), is small. A more accurate eigenfunction reconstruction scheme is proposed in [12].

At last, we want to remark that the minimization (4.36) cannot be performed for the smallest singular value only, but also for higher ones. Hence, if $\sigma_{min}(\kappa)$ vanishes numerically and coincides at that approximate eigenvalue κ with two or more singular values from $Q_B(\kappa)$, the corresponding intersection number indicates the geometric multiplicity of κ, see Figure 4.2. This comes from the fact that singular vectors are linear independent for each fixed κ and thus determine the kernel dimension of $Q_B(\kappa)$, too. However, note that a rigorous conclusion for the multiplicity of exact ITEs k in the limit would require deeper investigation.

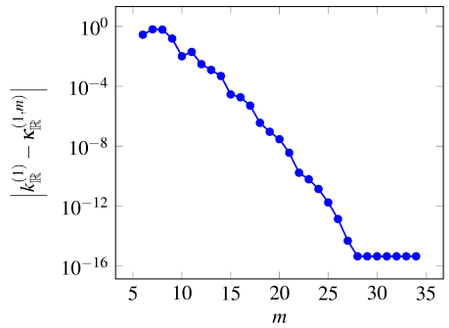

Fig. 4.1 Geometric error decay reaching machine precision for $\kappa_{\mathbb{R}}^{(1,m)}$ approximating the smallest real-valued ITE $k_{\mathbb{R}}^{(1)}$ of the unit disc.

For now we focus on the computational aspects of the modified MFS and calculate concrete ITEs of several test scatterers D in the following.

4.4.2 Numerical results

We complete this chapter with numerical benchmarks for the modified MFS applied to the ITP and investigate its practical competitiveness for ITE computations. Because of

$$\begin{aligned} \Delta w + nk^2 w &= 0 \quad \text{in } D \\ \Delta v + k^2 v &= 0 \quad \text{in } D \\ v &= w \quad \text{on } \partial D \\ \partial_\nu v &= \partial_\nu w \quad \text{on } \partial D \end{aligned} \qquad \Longleftrightarrow \qquad \begin{aligned} \Delta v + \tfrac{1}{n}(\sqrt{n}k)^2 v &= 0 \quad \text{in } D \\ \Delta w + (\sqrt{n}k)^2 w &= 0 \quad \text{in } D \\ w &= v \quad \text{on } \partial D \\ \partial_\nu w &= \partial_\nu v \quad \text{on } \partial D \end{aligned}$$

it suffices to restrict to the representative case $n > 1$. We start with the unit disc as in Chapter 3 and $k_{\mathbb{R}}^{(1)} = 2.902608055212766\ldots$ for $n = 4$ which we could compute independently via (4.14) to have a numerically precise reference value. Concerning the location of collocation and source points, we select m of them equidistantly on a circle with radii 1 and $R > 1$, respectively, and employ a random distribution for $\widehat{m} = 10$ interior samples. Our first observation is that the more R increases, the faster the modified MFS output $\kappa_{\mathbb{R}}^{(1,m)}$ converges. Figure 4.1 shows the convergence history for $R = 5$ which exhibits geometric decay for ITE approximation reaching easily machine precision, cf. Lemma 15 and Theorem 17. Repeating this procedure for higher singular values as announced at the end of the last subsection, Figure 4.2 additionally reveals the multiplicities 2,1,2 for the first three approximate ITEs on the real axis, respectively.

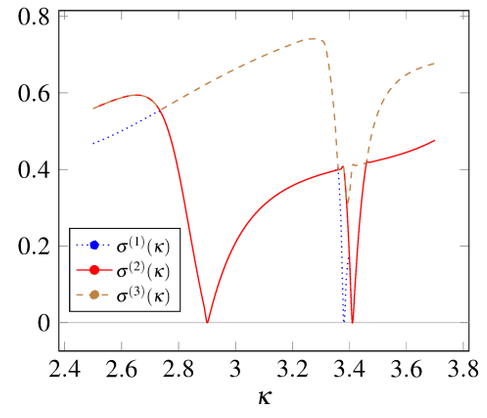

Fig. 4.2 Three smallest singular values of $Q_B(\kappa)$ for the unit disc with $m = 30$ collocation points. For example, the local minimum around $k_{\mathbb{R}}^{(1)}$ clearly disappears for the third singular value which indicates that its multiplicity as approximate eigenvalue is two.

Next we compare a family of consecutive shape deformations to explore sensitivity effects of the modified MFS. More precisely, we want to first focus on the transition from a disc to a compressed ellipse where we fix the major semi-axis as unity and shrink the minor semi-axis b successively. While keeping $\widehat{m} = 10$ throughout our ITE calculations, we select now m equiangular collocation points along the scattering boundary ∂D whose complementing sources are placed likewise on Γ. The latter is again chosen as a concentric circle but with radius 3 now. Unlike for the disc, the distance from sources to collocation points influences the parametric performance more strongly for the ellipses and is even limited by individual thresholds which then spoil the computational outcome when exceeded. Our ITE results in this case are displayed in Figure 4.3. The determined values emerge as unchanged digits from accumulating $\kappa^{(m)}$ for large m whose minimal singular values in (4.36) are sufficiently small, e.g. $m = 25,\ldots,50$ and $\sigma_{min}\left(\kappa^{(m)}\right) < 10^{-10}$. We put tail-digits within the tabular in parenthesis to indicate the existence of minor outliers for increasing m which we still expect to be correct though. Obviously, the different number of recoverable digits suggests that the

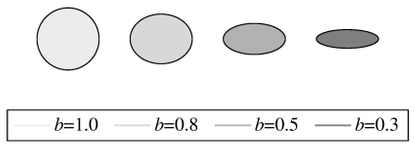

Semi axis b	$k_{\mathbb{R}}^{(1)}$	$k_{\mathbb{R}}^{(2)}$	$k_{\mathbb{R}}^{(3)}$	$k_{\mathbb{R}}^{(4)}$
1	2.90260805521276	3.38419483954017	3.41205395159979	3.97647211159188
0.8	3.13534121519068	3.48518298654316	3.54733071042719	3.88430612796681
0.5	4.33068623074(1)	4.36895654200(3)	5.40918291160(8)	5.60124857917
0.3	6.552756364(5)	6.56055364(1)	8.0949566	8.1574357

Fig. 4.3 First four approximate real-valued ITEs for ellipses with unitary major semi-axis based on the modified MFS without counting multiplicity for $n = 4$. Digits added in parenthesis underlay computational fluctuations but are expected to be correct as well.

more the domain deviates from the disc, the worse the achievable accuracy of our calculation becomes. The intuition here is that the growing ill-conditioning of the modified MFS matrix deteriorates the decomposition (4.35) and thus spoils the theoretical error decay. For instance, the condition number of $M(\kappa)$ for the unit disc D with $m = 30$ at $\kappa = 3.2$, i.e. between $k_{\mathbb{R}}^{(1)}$ and $k_{\mathbb{R}}^{(2)}$, is already of order 10^{10}. In particular, the more collocation points are needed to reasonably reflect ∂D, the more fluctuating results and thus less recoverable ITE digits are expected from the modified MFS. All the observations hold likewise when computing complex-valued ITEs, cf. Figure 4.4. We merely observe that the upper half-space of the complex plane is less affected than the lower one by ill-conditioning artifacts of the modified MFS based on radiating fundamental solutions. However, this seems not restrictive at all since ITEs arise symmetrically in complex-conjugated pairs for real-valued refractive indices n.

Subsequently, an ellipse with a semi-axes ratio of 0.75 is successively deformed to kite shape whose transformation is parametrized for $0 \leq t < 2\pi$ by

$$t \mapsto \begin{pmatrix} 0.75\cos(t) + \varepsilon\cos(2t) \\ \sin(t) \end{pmatrix}. \tag{4.38}$$

This family of scatterers was introduced in [29] for ITE computations via different boundary integral methods which we may therefore use as further references. In terms of the perturbation parameter ε, the modified MFS with equiangular boundary points responds to those domains according to Figure 4.5 and incorporates around 30 to 70 collocation and source

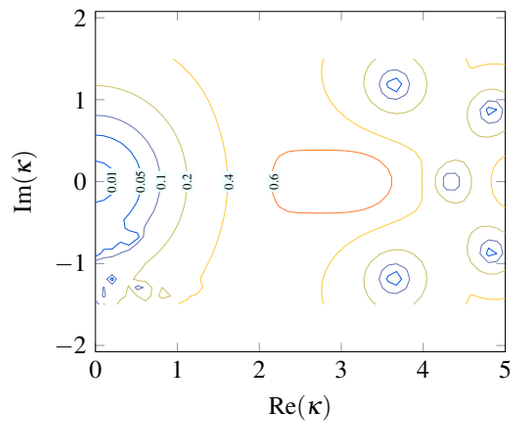

Fig. 4.4 Exemplary output of $\kappa \mapsto \sigma_{min}(\kappa)$ in the complex plane for an ellipse-shaped scatterer with major and minor semi-axis of length 1 and 0.5, respectively. The contour plot is generated for $m = 25$ and $n = 4$. Centers of concentric level sets appearing in conjugated pairs indicate ITEs. Because of too coarse resolution, the first two real-valued ITEs listed in Figure 4.3 are indistinguishable here.

points each. Despite its smoothness, we observe especially for $\varepsilon = 0.3$ that the modified MFS runs into computational challenges with the formation of concave fractions. By trial and error, a radius of $R = 2$ seems optimal when restricting Γ again to concentric circles around the deformed ellipses. Still, we are able to refine the results given in [29]. In agreement with [10], we conclude that the more irregular the scattering boundary becomes, the tighter the sources should be chosen. However, for fixed D, the convergence rates decrease the more Γ approaches ∂D.

We lastly consider non-smooth domains with corners such as regular polygons although being not covered by our developed approximation theory. Here we are only able to extract around 4 ITE digits each with occasional individual improvements. Our final results are listed in Figure 4.6 for polygonal edges of unit length each. They are obtained by equidistant computational points without covering any corners and with Γ as the circumference scaled with a factor of 1.5 away from the scattering boundary. Effective convergence of $\kappa^{(m)}$ starts for $m > 40$. The clear loss of accuracy also underlines the quintessence of [16] that eigenfunctions cannot be locally extended around corners of D at all: While we already choose the sources as truncating singularities for MFS trial functions relatively close to the polygons, Γ is on the other hand constrained to lie disjoint around ∂D by the discretized MFS formulation to simultaneously avoid poles along the scattering boundary. In particular, we conclude that the modified MFS is not well-suited for non-smooth domains.

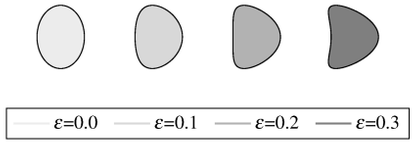

Perturbation ε	$k_{\mathbb{R}}^{(1)}$	$k_{\mathbb{R}}^{(2)}$	$k_{\mathbb{R}}^{(3)}$	$k_{\mathbb{R}}^{(4)}$
0	3.235703038847477	3.611128205541419	3.691028926072422	4.058250609789813
0.1	3.2763480279118	3.5945609393239	3.73942279460228	4.07208521966683
0.2	3.38239714(4)	3.61769602(6)	3.807719411(8)	4.127129460(5)
0.3	3.51642(2)	3.69403(2)	3.87530(5)	4.21836(6)

Fig. 4.5 First four approximate real-valued ITEs for the deformed ellipses from (4.38) based on the modified MFS without counting multiplicity with $n = 4$. Digits added in parenthesis underlay computational fluctuations but are expected to be correct as well.

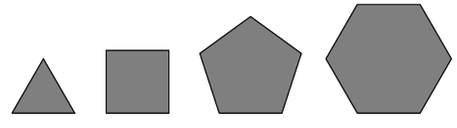

p-gon	$k_{\mathbb{R}}^{(1)}$	$k_{\mathbb{R}}^{(2)}$	$k_{\mathbb{R}}^{(3)}$	$k_{\mathbb{R}}^{(4)}$
triangle	8.9666(38)	9.40511(3)	10.54934(3)	12.43355(8)
square	5.47610(8)	6.10028(3)	6.18437(4)	6.65095(0)
pentagon	4.0556(0)	4.6715(5)	4.7198	5.5188(4)
hexagon	3.2562(0)	3.7745(4)	3.8132(2)	4.3429(6)

Fig. 4.6 First four approximate real-valued ITEs for regular polygons based on the modified MFS without counting multiplicity with $n = 4$. Digits added in parenthesis underlay computational fluctuations but are expected to be correct as well.

Summing up, the modified MFS is a powerful method to compute ITEs for sufficiently regular and convex domains D which then often yields better results than current meshing methods, see for example [29, 47, 54, 62, 92, 99]. Due to calculations in finite arithmetics though, the intrinsic ill-conditioning of MFS matrices practically limits the theoretical potential of the modified MFS for larger collocation points and thus the achievable number of recoverable ITE digits in total.

Chapter 5

Computing interior transmission eigenvalues of anisotropic and homogeneous media

In the following we consider the anisotropic version of the ITP from the last chapter which requires an adapted modified MFS variant due to intrinsically different regularity assumptions on the eigenfunctions. We revisit many aspects from ITEs of isotropic media, but discover also fundamentally new phenomena. Our analysis is based on the results of [66] and is as such partially adopted verbatim without further reference.

5.1 Mathematical framework

From a mathematical point of view, the anisotropic ITP emerges from the PDE setup of Section 4.1 if the diffusive term $\Delta\widetilde{w} = \operatorname{div}(\nabla\widetilde{w})$ in (4.1) is to undergo directional dependencies on the wave (gradient) due to small-scale orientations in the material. However, since acoustic waves are only associated with isotropic media, see [4], a physically correct model suits time-harmonic electromagnetic scattering of infinitely-long cylinders in 3D. Indeed, polarizations perpendicular to the cylinder axis will reduce the setup to our upcoming scalar Helmholtz-type case in two dimensions, see [26, 22].

Anisotropy can formally be expressed by intertwining a corresponding symmetric positive definite matrix $\widetilde{A} \in \mathbb{R}^{2\times 2}$ into the otherwise rotation-invariant PDE whose eigenvalues we

assume to either fulfill

$$1 < A_* := \min_{\substack{\xi \in \mathbb{C}^2 \\ |\xi|=1}} (\xi \cdot \widetilde{A}\xi)$$

or

$$1 > A^* := \max_{\substack{\xi \in \mathbb{C}^2 \\ |\xi|=1}} (\xi \cdot \widetilde{A}\xi) \, .$$

These restrictions on $\widetilde{A} \neq I$ remind of the two admissible cases for the refractive index $0 < n = \text{const} \neq 1$ from the isotropic case which can now be weakened by also allowing for $n = 1$. In order to keep consistent with the PDE notation from Section 2.4, cf. (2.16), we associate a tensorial map $A : \mathbb{C}^{1\times 2} \to \mathbb{C}^{1\times 2}$ with $\widetilde{A}$ determined by

$$A(\widetilde{w}) = \left(\widetilde{A}_{1,1}\partial_1 \widetilde{w} + \widetilde{A}_{1,2}\partial_2 \widetilde{w} \qquad \widetilde{A}_{1,2}\partial_1 \widetilde{w} + \widetilde{A}_{2,2}\partial_2 \widetilde{w} \right) \, .$$

Accordingly, the ITP for anisotropic media reads

$$\begin{aligned} \Delta v + k^2 v = 0 \quad & \text{in } D \\ \Delta_A w + nk^2 w = 0 \quad & \text{in } D \\ v = w \quad & \text{on } \partial D \\ \partial_\nu v = A(\nabla w)\nu \quad & \text{on } \partial D \end{aligned} \tag{5.1}$$

and we call wave numbers $k \in \mathbb{C}\backslash\{0\}$ with non-trivial solutions $v, w \in H^1(D)$ ITEs. Note the improved Sobolev regularity assumptions on v, w in comparison with the ITP for isotropic media from Section 4.1. Since the resulting PDE system for $\widetilde{A} \neq I$ prevents a transformation into a fourth order elliptic equation like (4.5) as the highest order operators for v and w differ now, the eigenproblem analysis requires a different, variational approach. $H^1(D)$ turns then out to provide a feasible Fredholm framework again subject to our initial distinction of A_* and A^*, see [25, 28, 71]. In particular, we may consider the weak form of (5.1) given by

$$\int_D -A(\nabla w) \cdot \nabla \varphi + \nabla v \cdot \nabla \psi + k^2 n w \varphi - k^2 v \psi \, \mathrm{d}x = 0 \, , \tag{5.2}$$

where $\varphi, \psi \in H^1(D)$ are such that $(\varphi - \psi) \in H_0^1(D)$. Our numerical realization of the modified MFS in the anisotropic case and underlying approximation theory to be developed should somehow make use of these several subtleties in comparison with isotropic media.

While the next sections aim at resolving some technical differences, we want to point out that many ITE facts from Section 4.2 still hold with additional restrictions on A, see [25, 28].

5.2 Boundary approximation theory for computing interior transmission eigenvalues

As for ITEs in the isotropic case, we want to provide theory for MFS-based boundary approximation methods subject to anisotropic media which can then be used to update the modified MFS consistently. We follow the approved structural guidelines from the previous chapter and start again from a very general trial function perspective.

5.2.1 A general trial function ansatz

Let the constant material parameters n, A be as in the previous section and assume that D has Lipschitz boundary. On the basis of (2.12), the relaxed regularity assumption on the scattering domain still allows us to define a well-defined negative trace norm for the (co-)normal derivative of ITP eigenfunctions $v, w \in H^1(D)$ via the duality product

$$\langle \partial_\nu v, \varphi \rangle_{H^{-\frac{1}{2}}(\partial D), H^{\frac{1}{2}}(\partial D)} := \int_D \Delta v \varphi - \nabla v \cdot \nabla \varphi \, \mathrm{d}x = -\int_D k^2 v \varphi + \nabla v \cdot \nabla \varphi \, \mathrm{d}x \tag{5.3}$$

(and similarly for the treatment of $A(\nabla w)\nu$). Here, $\varphi \in H^{\frac{1}{2}}(\partial D)$ is arbitrary and extendible to some $\varphi \in H^1(D)$ thanks to right-invertibility of the trace operator which then induces

$$\|\partial_\nu v\|_{H^{-\frac{1}{2}}(\partial D)} := \sup_{\|\varphi\|_{H^{\frac{1}{2}}(\partial D)}=1} \langle \partial_\nu v, \varphi \rangle_{H^{-\frac{1}{2}}(\partial D), H^{\frac{1}{2}}(\partial D)} \leq C \|v\|_{H^1(D)}$$

as refinement of (2.13). Having thus set in which sense approximations of boundary data are to be understood, we define the admissible set of Trefftz-like trial functions for anisotropic media by

$$U_A := \bigcup_{0 \leq \arg(\kappa) \leq \frac{\pi}{2}} U_A(\kappa) \, ,$$

where for $\kappa \in \mathbb{C} \setminus \{0\}$ and fixed $n > 0$ we set

$$U_A(\kappa) := \left\{ (\widetilde{v}, \widetilde{w}) \in C^\infty(\overline{D}) \times C^\infty(\overline{D}) : \, \Delta \widetilde{v} + \kappa^2 \widetilde{v} = 0 \, , \, \Delta_A \widetilde{w} + n\kappa^2 \widetilde{w} = 0 \right\} .$$

Note that unlike U, the index set of U_A is now larger since we do not have concrete locality results for ITEs as in the isotropic case any more except for the symmetry relations with respect to quadrants in the complex plane. The next theorem is then the analogue of Theorem 1 but requires an independent proof due to necessarily different assumptions on ITE approximation sequences in U_A.

Theorem 18. *Assume that the sequence* $\{(v^{(m)}, w^{(m)}, \kappa^{(m)})\}_{m\in\mathbb{N}} \subset U_A \times \mathbb{C}$ *with the initial restrictions on A fulfills for some constant* $1 \leq C < \infty$ *the following conditions:*

1. *eigenvalue convergence:* $\kappa^{(m)} \to k \neq 0$,
2. *uniform interior bound:* $\frac{1}{C} < \left(\|v^{(m)}\|^2_{H^1(D)} + \|w^{(m)}\|^2_{H^1(D)} \right) < C$ *for m large enough,*
3. *vanishing boundary misfit:*
   $\left(\|v^{(m)} - w^{(m)}\|_{H^{\frac{1}{2}}(\partial D)} + \|\partial_\nu v^{(m)} - A(w^{(m)})\nu\|_{H^{-\frac{1}{2}}(\partial D)} \right) \to 0$ *for* $m \to \infty$.

Then, the limit k from (i) *is an ITE and a subsequence of* $(v^{(m)}, w^{(m)})$ *converges weakly in* $H^1(D) \times H^1(D)$ *to some eigenfunction pair* (v, w).

Proof. Because of the uniform interior bounds with respect to $H^1(D)$ we can apply weak compactness again to show that the limit is indeed a non-trivial eigenfunction with ITE k. Without relabeling a possibly extracted subsequence, we assume that $v^{(m)} \rightharpoonup v$ and $w^{(m)} \rightharpoonup w$ in $H^1(D)$. Since $(v^{(m)}, w^{(m)}) \in U_A(\kappa^{(m)})$, they are in particular weak solutions of the following variational equation when testing against $\varphi, \psi \in H^1(D)$ such that $(\varphi - \psi) \in H^1_0(D)$

$$\begin{aligned} &\int_D -A(\nabla w^{(m)}) \cdot \nabla\varphi + \nabla v^{(m)} \cdot \nabla\psi + (\kappa^{(m)})^2 n w^{(m)} \varphi - (\kappa^{(m)})^2 v^{(m)} \psi \, \mathrm{d}x \\ &= \int_{\partial D} \left(A(\nabla w^{(m)})\nu - \partial_\nu v^{(m)} \right) \varphi \, \mathrm{d}s \, . \end{aligned}$$

Thanks to our asymptotically vanishing boundary data we obtain with (5.3)

$$\int_{\partial D} \left(A(\nabla w^{(m)})\nu - \partial_\nu v^{(m)} \right) \varphi \, \mathrm{d}s \leq \|\varphi\|_{H^{\frac{1}{2}}(\partial D)} \|A(\nabla w^{(m)})\nu - \partial_\nu v^{(m)}\|_{H^{-\frac{1}{2}}(\partial D)} \, .$$

As the right-hand side tends to zero for $m \to \infty$, we see with (i) that the pair (v, w) indeed solves (5.2), i.e.

$$\int_D -A(\nabla w) \cdot \nabla\varphi + \nabla v \cdot \nabla\psi + k^2 n w \varphi - k^2 v \psi \, \mathrm{d}x = 0 \, .$$

In particular, $A(\nabla w)\nu = \partial_\nu v$ holds in the sense of $H^{-\frac{1}{2}}$ traces. The fact that $(v - w) \in H^1_0(D)$ follows from the continuity of the trace operator $\tau : H^1(D) \to H^{\frac{1}{2}}(\partial D)$ and the evanescent

Dirichlet data for $\left\{\left(v^{(m)}-w^{(m)}\right)\right\}_{m\in\mathbb{N}}\subset H^1(D)$ when $m\to\infty$. Thus we are left to prove that (v,w) is non-trivial.

For this purpose we observe that if we had an estimate like (ii) for the weaker $L^2(D)$ norm, i.e.

$$\liminf_{m\to\infty}\left(\left\|v^{(m)}\right\|^2_{L^2(D)}+\left\|w^{(m)}\right\|^2_{L^2(D)}\right)>0\,,$$

our eigenfunction candidate (v,w) would immediately be non-trivial by its definition as weak $H^1(D)$-limit which is compactly embedded in $L^2(D)$. Therefore, we assume contrarily that there exists a subsequence, not relabeled, such that

$$\lim_{m\to\infty}\left(\left\|v^{(m)}\right\|^2_{L^2(D)}+\left\|w^{(m)}\right\|^2_{L^2(D)}\right)=0\,, \tag{5.4}$$

which implies that our uniform lower bound from (ii) is now completely concentrated on the gradients, i.e.

$$\liminf_{m\to\infty}\left(\left\|\nabla v^{(m)}\right\|^2_{L^2(D)}+\left\|\nabla w^{(m)}\right\|^2_{L^2(D)}\right)\geq C>0\,. \tag{5.5}$$

Since $v^{(m)}$ is a strong solution of the Helmholtz equation with wave number $\kappa^{(m)}$, we may use integration by parts with $\psi\in H^1(D)$ to obtain

$$\int_D\nabla v^{(m)}\cdot\nabla\psi\,\mathrm{d}x=\int_D\left(\kappa^{(m)}\right)^2v^{(m)}\psi\,\mathrm{d}x+\int_{\partial D}\partial_\nu v^{(m)}\psi\,\mathrm{d}s\,.$$

By duality and $\sup_m\left\|v^{(m)}\right\|^2_{H^1(D)}<C$ we conclude that also $\sup_m\left\|\partial_\nu v^{(m)}\right\|_{H^{-\frac{1}{2}}(\partial D)}<\infty$. With $\psi=\overline{u}^{(m)}$, where $u^{(m)}:=v^{(m)}-w^{(m)}$, the above right-hand side then vanishes for $m\to\infty$ due to (5.4) and (iii), so we obtain the relation

$$\lim_{m\to\infty}\int_D\nabla v^{(m)}\cdot\nabla\overline{u}^{(m)}\,\mathrm{d}x=0\,. \tag{5.6}$$

For the remainder of the proof we try to find a contradiction to (5.6) by incorporating our explicit assumptions on the eigenvalues of A. First note that $u^{(m)}$ can also be characterized as a weak solution of the system

$$\begin{aligned}
\Delta_A u^{(m)}+n\left(\kappa^{(m)}\right)^2u^{(m)}=\Delta_{A-I}v^{(m)}+(n-1)\left(\kappa^{(m)}\right)^2v^{(m)} &\quad\text{in } D\\
u^{(m)}=v^{(m)}-w^{(m)} &\quad\text{on } \partial D\\
A\left(\nabla u^{(m)}\right)\nu=A\left(\nabla v^{(m)}-\nabla w^{(m)}\right)\nu &\quad\text{on } \partial D
\end{aligned}$$

with identity tensor $I : \mathbb{C}^{1\times 2} \to \mathbb{C}^{1\times 2}$. Its variational form reads for $\psi \in H^1(D)$

$$\begin{aligned} &\int_D \left(-A\left(\nabla u^{(m)}\right) + (A-I)\left(\nabla v^{(m)}\right)\right) \cdot \nabla \psi \, \mathrm{d}x \\ &= \int_D \left(\kappa^{(m)}\right)^2 \left((n-1)v^{(m)} - nu^{(m)}\right) \psi \, \mathrm{d}x + \int_{\partial_D} \left(\partial_\nu v^{(m)} - A\left(w^{(m)}\right)\nu\right) \psi \, \mathrm{d}s \, . \end{aligned} \tag{5.7}$$

Assume first that $A_* > 1$. Choosing $\psi = \overline{w}^{(m)}$ in (5.7) and taking the limit $m \to \infty$, (5.6), (5.4) and some uniform upper bound on $\left\|\overline{w}^{(m)}\right\|_{H^{\frac{1}{2}}(\partial D)}$ yield

$$\begin{aligned} 0 &= \lim_{m\to\infty} \int_D \left(-A\left(\nabla u^{(m)}\right) + (A-I)\left(\nabla v^{(m)}\right)\right) \cdot \nabla \overline{w}^{(m)} \, \mathrm{d}x \\ &= \lim_{m\to\infty} \int_D \left(-A\left(\nabla u^{(m)}\right) + (A-I)\left(\nabla u^{(m)} + \nabla w^{(m)}\right)\right) \cdot \nabla \overline{w}^{(m)} \, \mathrm{d}x \\ &= \lim_{m\to\infty} \int_D \left((A-I)\left(\nabla w^{(m)}\right) - \nabla u^{(m)}\right) \cdot \nabla \overline{w}^{(m)} \, \mathrm{d}x \\ &= \lim_{m\to\infty} \int_D (A-I)\left(\nabla w^{(m)}\right) \cdot \nabla \overline{w}^{(m)} - \nabla u^{(m)} \cdot \nabla\left(\overline{v}^{(m)} - \overline{u}^{(m)}\right) \mathrm{d}x \\ &= \lim_{m\to\infty} \int_D (A-I)\left(\nabla w^{(m)}\right) \cdot \nabla \overline{w}^{(m)} + \left|\nabla u^{(m)}\right|^2 \mathrm{d}x - \lim_{m\to\infty} \int_D \nabla \overline{v}^{(m)} \cdot \nabla u^{(m)} \, \mathrm{d}x \\ &= \lim_{m\to\infty} \int_D (A-I)\left(\nabla w^{(m)}\right) \cdot \nabla \overline{w}^{(m)} + \left|\nabla u^{(m)}\right|^2 \mathrm{d}x \\ &\geq \lim_{m\to\infty} \left((A_*-1)\left\|\nabla w^{(m)}\right\|^2_{L^2(D)} + \left\|\nabla u^{(m)}\right\|^2_{L^2(D)}\right) . \end{aligned}$$

Therefore $\nabla w^{(m)} \to 0$ in $L^2(D)$ and since $\nabla u^{(m)} \to 0$ in $L^2(D)$ as well, we may conclude

$$\lim_{m\to\infty} \left(\left\|\nabla v^{(m)}\right\|^2_{L^2(D)} + \left\|\nabla w^{(m)}\right\|^2_{L^2(D)} \right) = 0 \, ,$$

which is a contradiction to (5.5) in the case $A_* > 1$. If $A^* < 1$, we first rewrite (5.6), using symmetry of $\widetilde{A}$, in the following way

$$\begin{aligned} 0 &= \lim_{m\to\infty} -\int_D \nabla v^{(m)} \cdot \nabla \overline{u}^{(m)} \, \mathrm{d}x \\ &= \lim_{m\to\infty} \int_D (-A + A - I)\left(\nabla v^{(m)}\right) \cdot \nabla \overline{u}^{(m)} \, \mathrm{d}x \\ &= \lim_{m\to\infty} \int_D -A\left(\nabla v^{(m)}\right) \cdot \nabla \overline{u}^{(m)} + (A-I)\left(\nabla v^{(m)}\right) \cdot \nabla \overline{u}^{(m)} \, \mathrm{d}x \\ &= \lim_{m\to\infty} \int_D -A\left(\nabla \overline{u}^{(m)}\right) \cdot \nabla v^{(m)} + (A-I)\left(\nabla v^{(m)}\right) \cdot \nabla \overline{u}^{(m)} \, \mathrm{d}x \end{aligned}$$

and observe that a combination of (5.7) with $\psi = \overline{v}^{(m)}$ and $\psi = u^{(m)}$, respectively, yields thanks to (5.4) and the vanishing boundary data

$$\begin{aligned}&\lim_{m\to\infty}\int_D -A\big(\nabla\overline{u}^{(m)}\big)\cdot\nabla v^{(m)} + (A-I)\big(\nabla v^{(m)}\big)\cdot\nabla\overline{u}^{(m)}\,\mathrm{d}x\\ =&\lim_{m\to\infty}\int_D (I-A)\big(\nabla v^{(m)}\big)\cdot\nabla\overline{v}^{(m)} + A\big(\nabla u^{(m)}\big)\cdot\nabla\overline{u}^{(m)}\,\mathrm{d}x\,.\end{aligned}$$

Putting both equations together gives

$$\begin{aligned}0 &= \lim_{m\to\infty}\int_D (I-A)\big(\nabla\overline{v}^{(m)}\big)\cdot\nabla v^{(m)} + A\big(\nabla u^{(m)}\big)\cdot\nabla\overline{u}^{(m)}\,\mathrm{d}x\\ &\geq \lim_{m\to\infty}\left((1-A^*)\big\|\nabla v^{(m)}\big\|^2_{L^2(D)} + A_*\big\|\nabla u^{(m)}\big\|^2_{L^2(D)}\right)\,.\end{aligned}$$

This again implies that

$$\lim_{m\to\infty}\left(\big\|\nabla v^{(m)}\big\|^2_{L^2(D)} + \big\|\nabla w^{(m)}\big\|^2_{L^2(D)}\right) = 0\,,$$

which also contradicts (5.5) in the case $A^* < 1$. □

The updated error estimate for ITE defects in terms of approximate eigenfunctions in the anisotropic case reads:

Lemma 19. *Let k be an ITE with eigenfunction pair $(v,w) \in H^1(D)\times H^1(D)$ and assume that $(\widetilde{v},\widetilde{w}) \in U_A(\kappa)$. If*

$$\frac{\left|\int_D v\widetilde{v} - nw\widetilde{w}\,\mathrm{d}x\right|}{\|\widetilde{v}\|_{L^2(D)} + \|\widetilde{w}\|_{L^2(D)}} \geq \widetilde{\varepsilon} > 0\,, \tag{5.8}$$

then there exists a constant $\widetilde{C} > 0$ which depends only on the boundary data of (v,w) such that for admissible $(\widetilde{v},\widetilde{w})$ it holds that

$$|k^2 - \kappa^2| \leq \frac{\widetilde{C}}{\widetilde{\varepsilon}}\frac{\sqrt{\|\widetilde{v}-\widetilde{w}\|^2_{H^{\frac{1}{2}}(\partial D)} + \|\partial_\nu\widetilde{v} - A(\widetilde{w})\nu\|^2_{H^{-\frac{1}{2}}(\partial D)}}}{\|\widetilde{v}\|_{L^2(D)} + \|\widetilde{w}\|_{L^2(D)}}\,. \tag{5.9}$$

Proof. We compute with (5.3), using symmetry of $\widetilde{A}$,

$$\begin{aligned}
&k^2 \int_D \widetilde{v}v - n\widetilde{w}w \,\mathrm{d}x \\
=&\int_D -\widetilde{v}\Delta v + \widetilde{w}\Delta_A w \,\mathrm{d}x \\
=&\int_D \nabla\widetilde{v}\cdot\nabla v \,\mathrm{d}x - \int_D \nabla\widetilde{w}\cdot A(\nabla w)\,\mathrm{d}x \\
&- \langle \partial_\nu v, \widetilde{v}\rangle_{H^{-\frac{1}{2}}(\partial D),H^{\frac{1}{2}}(\partial D)} + \langle A(\nabla w)\nu, \widetilde{w}\rangle_{H^{-\frac{1}{2}}(\partial D),H^{\frac{1}{2}}(\partial D)} \\
=&\int_D \nabla\widetilde{v}\cdot\nabla v \,\mathrm{d}x - \int_D A(\nabla\widetilde{w})\cdot\nabla w \,\mathrm{d}x - \langle \partial_\nu v, \widetilde{v}-\widetilde{w}\rangle_{H^{-\frac{1}{2}}(\partial D),H^{\frac{1}{2}}(\partial D)} \\
=&\int_D -v\Delta\widetilde{v} + w\Delta_A\widetilde{w}\,\mathrm{d}x + \langle \partial_\nu\widetilde{v}, v\rangle_{H^{-\frac{1}{2}}(\partial D),H^{\frac{1}{2}}(\partial D)} - \langle A(\nabla\widetilde{w})\nu, w\rangle_{H^{-\frac{1}{2}}(\partial D),H^{\frac{1}{2}}(\partial D)} \\
&- \langle \partial_\nu v, \widetilde{v}-\widetilde{w}\rangle_{H^{-\frac{1}{2}}(\partial D),H^{\frac{1}{2}}(\partial D)} \\
=&\,\kappa^2 \int_D \widetilde{v}v - n\widetilde{w}w\,\mathrm{d}x + \langle \partial_\nu\widetilde{v} - A(\nabla\widetilde{w})\nu, v\rangle_{H^{-\frac{1}{2}}(\partial D),H^{\frac{1}{2}}(\partial D)} \\
&- \langle \partial_\nu v, \widetilde{v}-\widetilde{w}\rangle_{H^{-\frac{1}{2}}(\partial D),H^{\frac{1}{2}}(\partial D)}\,.
\end{aligned}$$

Rearranging, we obtain

$$\begin{aligned}
&(k^2-\kappa^2)\int_D \widetilde{v}v - n\widetilde{w}w\,\mathrm{d}x \\
=&\langle \partial_\nu\widetilde{v} - A(\nabla\widetilde{w})\nu, v\rangle_{H^{-\frac{1}{2}}(\partial D),H^{\frac{1}{2}}(\partial D)} - \langle \partial_\nu v, \widetilde{v}-\widetilde{w}\rangle_{H^{-\frac{1}{2}}(\partial D),H^{\frac{1}{2}}(\partial D)}
\end{aligned}$$

and taking absolute values yields

$$\begin{aligned}
&\left|\langle \partial_\nu\widetilde{v} - A(\nabla\widetilde{w})\nu, v\rangle_{H^{-\frac{1}{2}}(\partial D),H^{\frac{1}{2}}(\partial D)}\right| + \left|\langle \partial_\nu v, \widetilde{v}-\widetilde{w}\rangle_{H^{-\frac{1}{2}}(\partial D),H^{\frac{1}{2}}(\partial D)}\right| \\
\le&\, \|\partial_\nu\widetilde{v} - A(\nabla\widetilde{w})\nu\|_{H^{-\frac{1}{2}}(\partial D)}\|v\|_{H^{\frac{1}{2}}(\partial D)} + \|\partial_\nu v\|_{H^{-\frac{1}{2}}(\partial D)}\|\widetilde{v}-\widetilde{w}\|_{H^{\frac{1}{2}}(\partial D)} \\
\le&\sqrt{\|v\|^2_{H^{\frac{1}{2}}(\partial D)} + \|\partial_\nu v\|^2_{H^{-\frac{1}{2}}(\partial D)}}\sqrt{\|\widetilde{v}-\widetilde{w}\|^2_{H^{\frac{1}{2}}(\partial D)} + \|\partial_\nu\widetilde{v} - A(\nabla\widetilde{w})\nu\|^2_{H^{-\frac{1}{2}}(\partial D)}} \\
=&\,\widetilde{C}\sqrt{\|\widetilde{v}-\widetilde{w}\|^2_{H^{\frac{1}{2}}(\partial D)} + \|\partial_\nu\widetilde{v} - A(\nabla\widetilde{w})\nu\|^2_{H^{-\frac{1}{2}}(\partial D)}}\,,
\end{aligned}$$

where

$$\widetilde{C} := \sqrt{\|v\|^2_{H^{\frac{1}{2}}(\partial D)} + \|\partial_\nu v\|^2_{H^{-\frac{1}{2}}(\partial D)}}\,.$$

□

Corollary 3 can also be restated in the following way.

Corollary 20. *Let conditions (i)–(iii) of Theorem 18 hold for* $\left\{\left(v^{(m)}, w^{(m)}, \kappa^{(m)}\right)\right\}_{m\in\mathbb{N}} \subset U_A \times \mathbb{C}$ *which detects some ITE k. Assume that each eigenfunction pair* (v,w) *from the eigenspace of k fulfills*

$$\int_D v^2 - nw^2 \,\mathrm{d}x \neq 0 \tag{5.10}$$

(or alternatively $\|v\|^2_{L^2(D)} - n\|w\|^2_{L^2(D)} \neq 0$ *if* $k = k_{\mathbb{R}}$*). Then there is a constant* $C > 0$ *which depends only on the data of corresponding* (v,w) *such that*

$$\left|k^2 - \left(\kappa^{(m)}\right)^2\right| \leq C \frac{\sqrt{\left\|v^{(m)} - w^{(m)}\right\|^2_{H^{\frac{1}{2}}(\partial D)} + \left\|\partial_\nu v^{(m)} - A\left(\nabla w^{(m)}\right)\nu\right\|^2_{H^{-\frac{1}{2}}(\partial D)}}}{\|v^{(m)}\|_{L^2(D)} + \|w^{(m)}\|_{L^2(D)}} \,. \tag{5.11}$$

It would be helpful to derive concrete conditions under which the integral constraint (5.10) does not vanish similar to Theorem 4. However, since the ITP eigenfunctions v and w are not representable via their difference in a closed fashion like in (4.4) any more, the derived proof does not apply in the anisotropic case and a corresponding result remains open. However, Corollary 5 keeps valid as a consequence of (5.2) choosing $\varphi = \overline{w}$ and $\psi = \overline{v}$ and taking imaginary parts.

5.2.2 Approaching the method of fundamental solutions' framework

Again, the abstract results presented so far hold for general boundary approximation methods of Trefftz-kind to compute ITEs of anisotropic media. Getting more concrete, we want to refocus on the MFS setting which requires to find the fundamental solution $\Phi_{A,\kappa}$ of the operator $\Delta_A + n\kappa^2 I$ first. Recall that the associated matrix $\widetilde{A} \in \mathbb{R}^{2\times 2}$ for the tensor A is symmetric positive definite so there also exists a unique symmetric positive definite root $\widetilde{A}^{\frac{1}{2}} \in \mathbb{R}^{2\times 2}$ such that $\widetilde{A}^{\frac{1}{2}}\widetilde{A}^{\frac{1}{2}} = \widetilde{A}$. Therefore we may define the pulled-back scatterer

$$D_A := \widetilde{A}^{-\frac{1}{2}} D \in \mathbb{R}^2 \,.$$

The following lemma shows that the anisotropic PDE for w solved within the ITP on D is equivalent to a pure Helmholtz equation on D_A.

Lemma 21. *The function* $w \in H^1(D)$ *is a solution of* $\Delta_A w + n\kappa^2 w = 0$ *in D if and only if its pull-back* $w_A \in H^1(D_A)$ *defined by* $w_A(\cdot) := w\left(\widetilde{A}^{\frac{1}{2}}\,\cdot\right)$ *solves* $\Delta w_A + n\kappa^2 w_A = 0$ *on* D_A*. Likewise, if* $\Phi_{\sqrt{n}\kappa}$ *is the fundamental solution of the Helmholtz equation with wave number*

$\kappa\sqrt{n}$, *then*

$$\Phi_{A,\sqrt{n}\kappa} := \det\big(\widetilde{A}^{-\frac{1}{2}}\big)\Phi_{\sqrt{n}\kappa}\big(\widetilde{A}^{-\frac{1}{2}}\bullet\big) \tag{5.12}$$

solves $(\Delta_A + n\kappa^2)\Phi_{A,\sqrt{n}\kappa} = \delta_0(\cdot)$ *in the sense of distributions.*

Proof. We associate for any $\varphi \in H_0^1(D)$ a representative $\varphi_A := \varphi\big(\widetilde{A}^{\frac{1}{2}}\bullet\big) \in H_0^1(D_A)$. Then the two PDEs under consideration are connected via

$$\begin{aligned}
&\int_{D_A} \nabla w_A(x_A)\cdot\nabla\varphi_A(x_A) - n\kappa^2 w_A(x_A)\varphi_A(x_A)\,\mathrm{d}x_A \\
&= \int_{D_A} \big(\nabla w\big(\widetilde{A}^{\frac{1}{2}}x_A\big)\widetilde{A}^{\frac{1}{2}}\big)\cdot\big(\nabla\varphi\big(\widetilde{A}^{\frac{1}{2}}x_A\big)\widetilde{A}^{\frac{1}{2}}\big) - n\kappa^2 w\big(\widetilde{A}^{\frac{1}{2}}x_A\big)\varphi\big(\widetilde{A}^{\frac{1}{2}}x_A\big)\,\mathrm{d}x_A \\
&= \det\big(\widetilde{A}^{-\frac{1}{2}}\big)\int_D \big(\nabla w(x)\widetilde{A}^{\frac{1}{2}}\big)\cdot\big(\nabla\varphi(x)\widetilde{A}^{\frac{1}{2}}\big) - n\kappa^2 w(x)\varphi(x)\,\mathrm{d}x \\
&= \det\big(\widetilde{A}^{-\frac{1}{2}}\big)\int_D \big(\nabla w(x)\widetilde{A}\big)\cdot\nabla\varphi(x) - n\kappa^2 w(x)\varphi(x)\,\mathrm{d}x \\
&= \det\big(\widetilde{A}^{-\frac{1}{2}}\big)\int_D A(\nabla w)\cdot\nabla\varphi - n\kappa^2 w\varphi\,\mathrm{d}x\,.
\end{aligned}$$

□

As in Section 4.3.2, having fixed some source contour Γ of class C^2 with $|\Gamma| < \infty$, the admissible trial function set U_A can now be updated for the MFS by

$$U_{A,MFS} := \bigcup_{0\le\arg(\kappa)\le\frac{\pi}{2}} U_{A,MFS}(\kappa)\,,$$

where we set for $\kappa \in \mathbb{C}\backslash\{0\}$

$$U_{A,MFS}(\kappa) := \Big\{\big(\widetilde{v},\widetilde{w}\big) :\ \widetilde{v} = \Phi_\kappa *_{|\Gamma} a,\ \widetilde{w} = \Phi_{A,\sqrt{n}\kappa} *_{|\Gamma} b,\ (a,b)\in L^2(\Gamma)\times L^2(\Gamma)\Big\}$$

and

$$\Phi_{A,\sqrt{n}\kappa} = \det\big(\widetilde{A}^{-\frac{1}{2}}\big)H_0^{(1)}\big(\sqrt{n}\kappa\big|\widetilde{A}^{-\frac{1}{2}}\bullet\big|\big)$$

according to (5.12). Analogue to Lemma 6, $U_{A,MFS}(\kappa)$ can be discretized with respect to increasing sets of source points. Hence we directly proceed with $U_{A,MFS}$ to prove density with respect to ITP eigenfunctions in $H^1(D)$. Note that the difference $v-w$ is by definition as good as v and w each which thus separates the approximation problem without loss of regularity unlike in the isotropic case. We start with the analysis for v:

Theorem 22. *Let $v \in H^1(D)$ be a solution to the Helmholtz equation with wave number $0 \leq \arg(\kappa) \leq \frac{\pi}{2}$. Then there exists a sequence of elements $v^{(m)} = \Phi_\kappa *_{|\Gamma} a^{(m)}$ with $a^{(m)} \in L^2(\Gamma)$ such that $v^{(m)} \to v$ in $H^1(D)$.*

Proof. The following proof is inspired by Lemma 2.1 from [25]. Hence we also aim to show that, for fixed κ, the adjoint

$$h \mapsto \int_D \overline{\Phi_\kappa(\bullet - x)} h(x) + \nabla_x \overline{\Phi_\kappa(\bullet - x)} \cdot \nabla h(x) \, \mathrm{d}x \ \in L^2(\Gamma) \tag{5.13}$$

(we use $\nabla_\bullet$ to relate differentiation to its underlying variables) of the boundary convolution operator $a \mapsto \Phi_\kappa *_{|\Gamma} a \in \{v \in H^1(D) : \ \Delta v + \kappa^2 v = 0\}$ is injective which would then give the desired density result. For this we assume that $h \in \{v \in H^1(D) : \ \Delta v + \kappa^2 v = 0\}$ is chosen such that the entire function v defined by the complex-conjugated right-hand side of (5.13) vanishes along Γ while inheriting the Sommerfeld radiation condition from Φ_κ and $\nabla_x \Phi_\kappa$. By analyticity and uniqueness of radiating exterior Helmholtz solutions for $\mathrm{Im}(\kappa) \geq 0$, see [72, 32], we conclude that $v_{|D^c} = 0$ and by regularity properties of the underlying potential $v \in H_0^1(D)$. Since h solves the Helmholtz equation in a weak sense with respect to κ by assumption, this implies on the one hand

$$\int_D -\nabla h \cdot \nabla v + \kappa^2 h v \, \mathrm{d}x = 0 \, .$$

On the other hand, we can find a sequence $\left\{h^{(m)}\right\}_{m \in \mathbb{N}} \subset \mathscr{D}(\mathbb{R}^2)$ such that $h^{(m)} \to h$ in $H^1(D)$. Now we compute, using integration by parts without boundary contributions as well as the fundamental solution property of the kernel Φ_κ

$$\begin{aligned}
&\int_D -\nabla h \cdot \nabla v + \kappa^2 h v \, \mathrm{d}x \\
&= \lim_{m \to \infty} \int_{\mathbb{R}^2} -\nabla h^{(m)} \cdot \nabla v + \kappa^2 h^{(m)} v \, \mathrm{d}x \\
&= \lim_{m \to \infty} \int_{\mathbb{R}^2} v(\Delta + \kappa^2) h^{(m)} \, \mathrm{d}x \\
&= \lim_{m \to \infty} \int_{\mathbb{R}^2} \left(\int_D \Phi_\kappa(x-y) \overline{h}(y) + \nabla_y \Phi_\kappa(x-y) \cdot \nabla \overline{h}(y) \, \mathrm{d}y \right) (\Delta + \kappa^2) h^{(m)}(x) \, \mathrm{d}x \\
&= \lim_{m \to \infty} \Bigg(\int_{\mathbb{R}^2} \int_D \Phi_\kappa(x-y) \overline{h}(y) \, \mathrm{d}y \, (\Delta + \kappa^2) h^{(m)}(x) \, \mathrm{d}x \\
&\quad - \int_{\mathbb{R}^2} \int_D \nabla_x \Phi_\kappa(x-y) \cdot \nabla \overline{h}(y) \, \mathrm{d}y \, (\Delta + \kappa^2) h^{(m)}(x) \, \mathrm{d}x \Bigg)
\end{aligned}$$

$$
\begin{aligned}
&= \lim_{m\to\infty} \left(\int_{\mathbb{R}^2} \int_D \Phi_\kappa(x-y)\overline{h}(y)\,\mathrm{d}y\,(\Delta+\kappa^2)\overline{h}^{(m)}(x)\,\mathrm{d}x \right. \\
&\quad \left. + \int_{\mathbb{R}^2} \int_D \Phi_\kappa(x-y)\nabla\overline{h}(y)\,\mathrm{d}y\cdot(\Delta+\kappa^2)\nabla h^{(m)}(x)\,\mathrm{d}x \right) \\
&= \lim_{m\to\infty} \int_{\mathbb{R}^2} (\Delta_x+\kappa^2) \int_D \Phi_\kappa(x-y)\overline{h}(y)\,\mathrm{d}y\, h^{(m)}(x)\,\mathrm{d}x \\
&\quad + \int_{\mathbb{R}^2} (\Delta_x+\kappa^2) \int_D \Phi_\kappa(x-y)\nabla\overline{h}(y)\,\mathrm{d}y\cdot\nabla h^{(m)}(x)\,\mathrm{d}x \\
&= \lim_{m\to\infty} \int_{\mathbb{R}^2} (\mathbb{1}_D\overline{h})h^{(m)} + (\mathbb{1}_D\nabla\overline{h})\cdot\nabla h^{(m)}\,\mathrm{d}x \\
&= \|h\|_{H^1(D)}\,.
\end{aligned}
$$

Hence $\|h\|_{H^1(D)} = 0$ which in turn implies injectivity of (5.13). □

The complementing density proof for the approximation of w with corresponding trial functions in $U_{A,MFS}$ can be inherited from the results of v by a pull-back argument.

Corollary 23. *Let $w \in H^1(D)$ be a solution to $\Delta_A w + \kappa^2 w = 0$ with wave number $0 \leq \arg(\kappa) \leq \frac{\pi}{2}$. Then for there exists $w^{(m)} = \Phi_{A,\kappa} *_{|\Gamma} b^{(m)}$ with $b^{(m)} \in L^2(\Gamma)$ such that $w^{(m)} \to w$ in $H^1(D)$.*

Proof. For any solution $w \in H^1(D)$ of $\Delta_A w + k^2 w = 0$ we know by Lemma 21 that $w_A := w\big(\widetilde{A}^{\frac{1}{2}}\bullet\big) \in H^1(D_A)$ solves $\Delta w_A + \kappa^2 w_A = 0$ on D_A. We also associate a surrounding source boundary with the pulled-back scatterer D_A by $\Gamma_A := \widetilde{A}^{-\frac{1}{2}}\Gamma$. Then Theorem 22 guarantees existence of a sequence $\big\{g_A^{(m)}\big\}_{m\in\mathbb{N}} \in L^2(\Gamma_A)$ such that the functions

$$
w_A^{(m)} := \int_{\Gamma_A} \Phi_\kappa(\bullet - s_A) g_A^{(m)}(s_A)\,\mathrm{d}s_A
$$

fulfill $w_A^{(m)} \to w_A$ in $H^1(D_A)$. Using the transformation formula for curvilinear coordinates, e.g. [46], $w_A^{(m)}$ can also be expressed in terms of $\Phi_{A,\kappa}$ according to

$$
\begin{aligned}
&w_A^{(m)}(x_A) \\
&= \int_{\Gamma_A} \Phi_\kappa(x_A - s_A) g_A^{(m)}(s_A)\,\mathrm{d}s_A \\
&= \int_{\Gamma} \Phi_\kappa\big(x_A - \widetilde{A}^{-\frac{1}{2}}s\big) g_A^{(m)}(\widetilde{A}^{-\frac{1}{2}}s)\big|\widetilde{A}^{-\frac{1}{2}}\nu\big|\det\big(\widetilde{A}^{-\frac{1}{2}}\big)\,\mathrm{d}s \\
&= \int_{\Gamma} \Big(\det\big(\widetilde{A}^{-\frac{1}{2}}\big)\Phi_\kappa\big(x_A - \widetilde{A}^{-\frac{1}{2}}s\big)\Big)\Big(g_A^{(m)}\big(\widetilde{A}^{-\frac{1}{2}}s\big)\big|\widetilde{A}^{-\frac{1}{2}}\nu\big|\Big)\,\mathrm{d}s \\
&= \int_{\Gamma} \Phi_{A,\kappa}\big(\widetilde{A}^{\frac{1}{2}}x_A - s\big) g^{(m)}(s)\,\mathrm{d}s\,,
\end{aligned}
$$

for every $x_A \in D_A$, where we set $g^{(m)}(s) := g_A^{(m)}\big(\widetilde{A}^{-\frac{1}{2}}s\big)\big|\widetilde{A}^{-\frac{1}{2}}\nu\big|$ for the transformed coefficient functions. Therefore, $w^{(m)} := w_A^{(m)}\big(\widetilde{A}^{\frac{1}{2}}\bullet\big)$ satisfies

$$
\begin{aligned}
&\big\|w_A^{(m)} - w_A\big\|^2_{H^1(D_A)}\\
&= \int_{D_A} \big|w_A^{(m)} - w_A\big|^2 \,\mathrm{d}x_A + \int_{D_A} \big|\nabla w_A^{(m)} - \nabla w_A\big|^2 \,\mathrm{d}x_A\\
&= \int_D \det\big(\widetilde{A}^{-\frac{1}{2}}\big)\big|\big(w_A^{(m)} - w_A\big)\big(\widetilde{A}^{-\frac{1}{2}}x\big)\big|^2 \,\mathrm{d}x + \int_D \det\big(\widetilde{A}^{-\frac{1}{2}}\big)\big|\big(\nabla w_A^{(m)} - \nabla w_A\big)\big(\widetilde{A}^{-\frac{1}{2}}x\big)\big|^2 \,\mathrm{d}x\\
&= \det\big(\widetilde{A}^{-\frac{1}{2}}\big)\left(\int_D \big|w^{(m)} - w\big|^2 \,\mathrm{d}x + \int_D \big|\big(\nabla w^{(m)} - \nabla w\big)\widetilde{A}^{\frac{1}{2}}\big|^2 \,\mathrm{d}x\right)\\
&\geq \det\big(\widetilde{A}^{-\frac{1}{2}}\big)\min\big\{1, \sqrt{A_*}\big\}\left(\int_D \big|w^{(m)} - w\big|^2 \,\mathrm{d}x + \int_D \big|\big(\nabla w^{(m)} - \nabla w\big)\big|^2 \,\mathrm{d}x\right)\\
&= \det\big(\widetilde{A}^{-\frac{1}{2}}\big)\min\big\{1, \sqrt{A_*}\big\}\big\|w^{(m)} - w\big\|^2_{H^1(D)}\,.
\end{aligned}
$$

□

With the same pull-back argument as in the proof above, the convergence rate analysis from Section 4.3.3, especially Theorem 16, takes over to the anisotropic case yet with different source contours $\Gamma_v = \partial B_R(0)$ and $\Gamma_w = \widetilde{A}^{-\frac{1}{2}}\Gamma_v$ for v and w, respectively, provided the eigenfunction pair (v,w) is known to be more regular than in $H^1(D)\times H^1(D)$. The original case when $\Gamma = \Gamma_v = \Gamma_w$ will only be investigated numerically in the sequel for which we state the next corollary as a summary of this subsection.

Corollary 24. *Let k be any ITE with $0 \leq \arg(k) \leq \frac{\pi}{2}$. Then there exist MFS trial functions $\big\{\big(v^{(m)}, w^{(m)}, \kappa^{(m)}\big)\big\}_{m\in\mathbb{N}} \in U_{A,MFS}\times\mathbb{C}$ such that (i)–(iii) from Theorem 18 are satisfied.*

Proof. The assertion follows by setting $\kappa^{(m)} = k$ and $\kappa^{(m)} = \sqrt{n}k$ in Theorem 22 and Corollary 23, respectively. □

5.3 The modified method of fundamental solutions from a numerical perspective

In virtue of the different assumptions on ITP eigenfunctions for isotropic and anisotropic media, we have provided individual approximation setups each that remain to be implemented numerically for the latter. After establishing corresponding modified MFS version, we will use it to compute exemplary ITEs and particularly focus on new phenomena arising in comparison with the isotropic case.

5.3.1 Implementation details

We aim to adapt the modified MFS algorithm as presented in Subsection 4.4.1 to anisotropic media. Our numerical guidelines should likewise reflect a synthesis of Theorem 18 and Lemma 19 to have a reliable basis for the proposed computation routine. Hence, recall that the purpose of the introduced modified MFS matrix $M(\kappa)$ is to store both boundary collocation and interior data from admissible ITP trial functions which need to be optimized in a further step to give a sufficiently small ratio. However, the actual norms required in conditions (ii) and (iii) of Theorem 18 are different from those in Theorem 8. In practice, we take as usual a variable number of collocation points $\{x^{(1,m)},\dots,x^{(m,m)}\} \subset \partial D$, sources $\{s^{(1,m)},\dots,s^{(m,m)}\} \subset \Gamma$ along some admissible contour Γ surrounding $\overline{D}$ and fixed random indicator points $\{\widehat{x}^{(1,\widehat{m})},\dots,x^{(\widehat{m},\widehat{m})}\} \in D$. Then we set

$$M(\kappa) = \begin{pmatrix} B(\kappa) & B_A(\sqrt{n}\kappa) \\ \nabla B(\kappa)\nu & A(\nabla B_A(\sqrt{n}\kappa))\nu \\ \widehat{I}(\kappa) & 0 \\ \partial_1\widehat{I}(\kappa) & 0 \\ \partial_2\widehat{I}(\kappa) & 0 \\ 0 & \widehat{I}_A(\sqrt{n}\kappa) \\ 0 & \partial_1\widehat{I}_A(\sqrt{n}\kappa) \\ 0 & \partial_2\widehat{I}_A(\sqrt{n}\kappa) \end{pmatrix}, \tag{5.14}$$

where the boundary matrices in the first two block lines are given by (3.4) and (3.5), respectively. Recall that in this form, they still circumvent the abstract fractional Sobolev norms from (iii) of Theorem 18 similar to (4.34), so the characteristically higher regularity of eigenfunctions in the anisotropic case should at least be numerically reflected now by some consistent implementation of the refined interior bounds (ii). Therefore, we have added to $\widehat{I}(\kappa)$ and $\widehat{I}_A(\kappa)$ in (5.14) also gradient contributions of corresponding MFS trial functions, i.e.

$$\partial_i\widehat{I}_T(\kappa) := \begin{pmatrix} \partial_i\Phi_{T,\kappa}\big(x^{(1/\widehat{m})} - s^{(1/m)}\big) & \dots & \partial_i\Phi_{T,\kappa}\big(x^{(1/\widehat{m})} - s^{(m/m)}\big) \\ \vdots & \ddots & \vdots \\ \partial_i\Phi_{T,\kappa}\big(x^{(\widehat{m}/\widehat{m})} - s^{(1/m)}\big) & \dots & \partial_i\Phi_{T,\kappa}\big(x^{(\widehat{m}/\widehat{m})} - s^{(m/m)}\big) \end{pmatrix} \in \mathbb{C}^{\widehat{m}\times m},$$

for $i = 1,2$. Our proposed modified MFS for anisotropic media is then obtained as in Figure 3.5 by performing a QR factorization of $M(\kappa)$

$$M(\kappa) = Q(\kappa)R(\kappa) = \begin{pmatrix} Q_B(\kappa) \\ Q_I(\kappa) \end{pmatrix} R(\kappa) \ , \quad R(\kappa), Q_B(\kappa) \in \mathbb{C}^{2m\times 2m}$$

and extracting local minimizers $\kappa^{(m)} \in \mathbb{C}\backslash\{0\}$ of

$$\kappa \mapsto \sigma_{min}(\kappa) = \min_{\eta\in\mathbb{C}^{2m},|\eta|=1} |Q_B(\kappa)\eta| \ .$$

5.3.2 Numerical results

Since there are only few other works addressing the numerics of ITEs for anisotropic media so far, see [26], we want to apply the modified MFS in that context, too. We would like to go a bit further and focus more closely on the two cases $A_* > 1$ and $A^* < 1$ which turn out to be significantly different instead of only disjoint auxiliary situations for technical reasons. To see this, let us confine to the real-valued ITE spectrum for simplicity, fix $n = 4$ and assume first that $\widetilde{A} = aI$ with $a \in \{0.99, 1.0, 1.01\}$ is pseudo-anisotropic, i.e. we perturb the homogeneous isotropic case (4.3), where $a = 1$, slightly from below and above by a scalar factor. Figure 5.1 was generated for D being the unit disc with $m = 20$ sources and collocation points each lying equidistantly on concentric circles of radius 5 and 1, respectively. Supplementarily, we take $\widetilde{m} = 10$ indicator points randomly in the interior. As evanescent valleys of the smallest-singular-value-function shall indicate existence of nearby ITEs, the plot already shows that while the trivial ITE $k = 0$ keeps uniformly isolated for $a < 1$, there seems to be an accumulation of eigenvalues around zero if $a > 1$, consisting of 9 ones so far. Since the ITP is rotationally symmetric for any $a > 0$, we may again compute eigenvalues analytically using a Fourier-Bessel expansion, see [20]. Accordingly, we need to solve

$$\det \begin{pmatrix} J_p(\kappa) & J_p\left(\sqrt{\frac{\pi}{a}}\kappa\right) \\ \kappa J_p'(\kappa) & \sqrt{na}\kappa J_p'\left(\sqrt{\frac{\pi}{a}}\kappa\right) \end{pmatrix} = 0 \ ,$$

whose roots in κ coincide with those of

$$g_p(\kappa, a) = f_p(\kappa) - \frac{f_p\left(\sqrt{\frac{\pi}{a}}\kappa\right)}{a} \ , \tag{5.15}$$

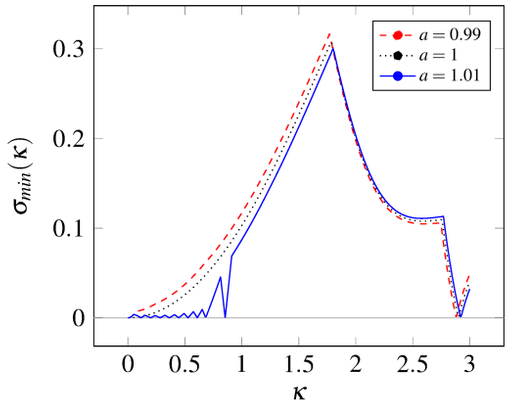

Fig. 5.1 Different ITE behavior for the unit disc D near $\kappa = 0$ with parameters $m = 20$, $n = 4$ and $A^* = A_* = a$ being slightly larger or smaller than 1, respectively.

where

$$f_p(y) = \frac{pJ_p(y)}{J'_p(y)y} .$$

Numerical calculations then confirm for $a = 1.01$ the existence of at least 24 ITEs, almost equidistantly distributed, within the interval $(0,2)$ as the consecutive smallest positive roots k_p of g_p for $p = 1,\ldots,24$:

0.115311585535849, 0.199588421652397, 0.282144281238904, 0.364146487789215,
0.445898824589272, 0.527516720334738, 0.609053860429526, 0.690538657514437,
0.771987575480684, 0.853410820048637, 0.934815057189782, 1.016204826695360,
1.097583327960807, 1.178952881037817, 1.260315209516204, 1.341671620743993,
1.423023124392495, 1.504370512663545, 1.585714415871614, 1.667055341806005,
1.748393704134480, 1.829729843252073, 1.911064041822514, 1.992396536525989.

We now compare these values with each positive root $\widetilde{k}_p$ of the second order Taylor polynomial $\widetilde{g}_p(\bullet,a)$ of $g_p(\bullet,a)$ around zero

$$\widetilde{g}_p(\kappa,a) = \frac{a-1}{a} - \frac{n-a^2}{2a^2p(p+1)}\kappa^2 . \tag{5.16}$$

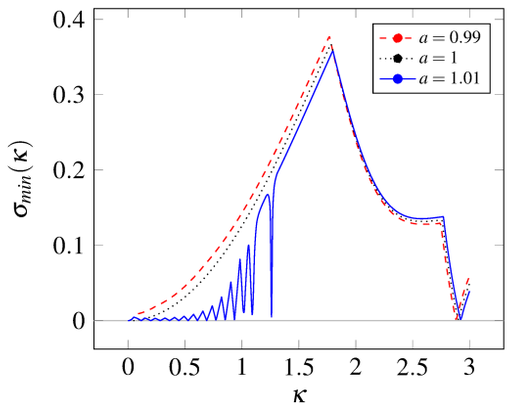

Fig. 5.2 With identical input data as in Figure 5.1 except for a larger number of collocation points ($m = 30$) additional minima appear for $a = 1.01$, while the two exemplary graphs for $a \leq 1$ keep rather unchanged.

The latter was derived via standard recursive differentiation formulas as well as low-argument asymptotics for Bessel functions, see [1]. Since $\widetilde{g}_p(\bullet, a)$ is strictly decreasing for $a^2 < n$, but $\widetilde{g}_p(0,a) < 0$ for $a < 1$, we get a first idea about why we do not observe ITEs close to zero for $a = 0.99$. However, for $a > 1$ the parabola intersects the κ-axis at

$$\widetilde{k}_p = \sqrt{\frac{2(a^2-a)}{n-a^2} p(p+1)}\,, \tag{5.17}$$

for different p and yields 0.116436686356126, 0.201674256633773, 0.285210468912994 and 1.852038873292762, 1.934391514809814, 2.016742566337728 for our marginal test samples $p = 1,2,3$ and $p = 22,23,24$, respectively. We recognize the almost equidistant structure of the exact k_p consistent with the approximation formula (5.17) which gives rise to believe that this pattern even continues for larger p. Obviously, the modified MFS does not point to all of these existent eigenvalues with a local valley for $m = 20$ yet. Increasing the number of collocation points to $m = 30$, we see in Figure 5.2 that successively further, but still not all minima, especially not those which are more distant from zero, appear within an acceptable number of collocation points. In fact, for larger m the output deteriorates by ill-conditioning effects and finally results in noisy artifacts within the graph. We conclude that the regime $a > 1$ with $n > 1$ (or equivalently $a < 1$ with $n < 1$) seems to be not well suited for eigenvalue approximations on the basis of the modified MFS as long as minima of the smallest-singular-value-function are forced to oscillate strongly. The following lemma

shows that the situation is even worse for $a \searrow 1$ since an accumulation of ITEs around zero is induced. Our interpretation of this observation is that the eigenspace of $k = 0$ for $a = 1$, which consists of all harmonic functions $v = w$, emerges from the collection of eigenstates that are absorbed by the trivial ITE in the right-hand-side limit of a.

Lemma 25. *Fix $n > 1$. Then for any $p \in \mathbb{N}$ and any upper threshold $\kappa > 0$ there exists $a_p > 1$ such that for all $a_p > a > 1$ there exists a positive root $k_{p,a}$ of $g_p(\cdot, a)$ from* (5.15) *with $\kappa > k_{p,a}$. The same holds true for the sign relations $n < 1$ and $a_p < a < 1$ correspondingly.*

Proof. We will work with $n, a > 1$ since the proof for the converse case can be performed in a similar fashion. We will make use of the intermediate value theorem to prove that the continuous function $g_p(\cdot, a)$ switches its sign in the interval $(0, \kappa)$ for sufficiently close $1 < a < a_p$. For this we first note that by (5.16) we have that

$$g_p(0, a) = \frac{a-1}{a} > 0 \tag{5.18}$$

for all $a > 1$. We want to show next that $g_p(\kappa_p, a) < 0$ for some $0 < \kappa_p < \kappa$ and for every $1 < a < a_p$. Since $f_p(y) = 1 + y^2/(2p(p+1)) + \mathcal{O}(y^{p+4})$ for $y \to 0$, we can always find an open interval $I_p = (0, i_p)$, $i_p > 0$ on which f_p is strictly monotonically increasing. For now we fix $0 < \kappa_p < \kappa$ such that $\kappa_p \sqrt{n} < i_p$ as well as some $1 < \widetilde{a} < n$. Then we set

$$a_p := \min \left\{ \widetilde{a}, \frac{f_p(\sqrt{\frac{n}{\widetilde{a}}}\kappa_p)}{f_p(\kappa_p)} \right\} > 1 \ .$$

Hence, for any $1 < a < a_p$ we get by monotonicity of f_p on I_p that

$$0 > f_p(\kappa_p) - \frac{f_p(\sqrt{\frac{n}{\widetilde{a}}}\kappa_p)}{a} > f_p(\kappa_p) - \frac{f_p(\sqrt{\frac{n}{a}}\kappa_p)}{a} = g_p(a, \kappa_p) \ .$$

Since κ_p is independent of a, the intermediate value theorem applies in combination with (5.18) for all $1 < a < a_p$ and thereby ensures the existence of roots $k_{p,a} > 0$. □

However, despite the different behavior of the eigenvalues for $a \nearrow 1$ and $a \searrow 1$ including their retarded numerical appearance in the latter case with $n > 1$, it should be noted that Figures 5.1 and 5.2 also indicate that for any approximate ITE k_- with $a < 1$ we can find early, with respect to the number of collocation points, a neighboring ITE k_+ for $a > 1$ with the same limit point when both a approach 1: Our exemplary reference pair from the right corner of the plot is computed by the modified MFS with machine precision and detects the smallest real-valued ITEs 2.882728798537896 and 2.922641535098038 of the unit disc for $a = 0.99$ and $a = 1.01$, respectively, thus surrounding closely $k_{\mathbb{R}}^{(1)} \approx 2.902608055212766$

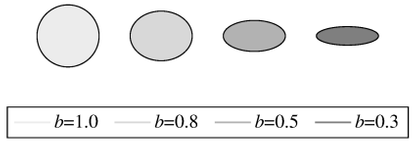

b	(A_{11},A_{22},n)	$k_{\mathbb{R}}^{(1)}$	$k_{\mathbb{R}}^{(2)}$	$k_{\mathbb{R}}^{(3)}$	$k_{\mathbb{R}}^{(4)}$
1.0	(1/8, 1/2, 1)	2.432342816525	2.630469896016	3.59558793161	3.67772382000
	(2, 8, 1)	5.422742998449	6.104903895458	6.701155193070	6.807186612188
	(1/8, 1/2, 4)	1.102569011198	1.54251886201	1.59628152267	1.60949290139
	(2, 8, 4)	1.0943753002121	2.6607655055967	3.2850748911309	4.741801624682
0.8	(1/8, 1/2, 1)	2.8165335886620	2.9285919681719	4.07689045702	4.29727034976
	(2, 8, 1)	6.533520997906	7.416596066665	7.518127550666	7.698364095496
	(1/8, 1/2, 4)	1.2746345105108	1.2937710253833	1.708033787158	1.764558638514
	(2, 8, 4)	1.0949963906964	3.295035558059	3.883765024644	4.66548759617
0.5	(1/8, 1/2, 1)	4.04671357026	4.0805282756	5.2097578799	5.2372873746
	(2, 8, 1)	10.014688061884	10.43413680087	10.67428849705	11.00440368778
	(1/8, 1/2, 4)	1.86432077115	1.86788372558	2.2749471210	2.2899879956
	(2, 8, 4)	1.094252956180	2.153141477577	3.263881703236	3.587938159800
0.3	(1/8, 1/2, 1)	6.3010969	6.3020803	7.352124	7.361319
	(2, 8, 1)	16.1836653485	16.2620312417	16.317697464	16.50554137
	(1/8, 1/2, 4)	2.94403372897	2.94412360374	3.338511006	3.338761987
	(2, 8, 4)	1.092202884187	2.070214109320	3.091592773591	4.147922758215

Fig. 5.3 First four approximate real-valued ITEs without counting multiplicity for ellipses with major semi-axis of length 1 and varied minor semi axis b.

for $a = 1$, see Chapter 4. In particular, the modified MFS is here far more accurate than the boundary element method from [65] where apparently only 2 digits of their given ITE approximations are correct.

Due to symmetry of ITEs inherited from

$$\begin{aligned} a\Delta w + nk^2 w &= 0 \quad \text{in } D \\ \Delta v + k^2 v &= 0 \quad \text{in } D \\ v &= w \quad \text{on } \partial D \\ \partial_\nu v &= a\partial_\nu w \quad \text{on } \partial D \end{aligned} \iff \begin{aligned} \tfrac{1}{a}\Delta v + \tfrac{1}{n}\left(\tfrac{\sqrt{n}k}{\sqrt{a}}\right)^2 v &= 0 \quad \text{in } D \\ \Delta w + \left(\tfrac{\sqrt{n}k}{\sqrt{a}}\right)^2 w &= 0 \quad \text{in } D \\ w &= v \quad \text{on } \partial D \\ \partial_\nu w &= \tfrac{1}{a}\partial_\nu v \quad \text{on } \partial D \end{aligned}$$

it suffices to restrict to $n \geq 1$ in the sequel but we assume that either $A^* < 1$ or $A_* > 1$ is sufficiently distant from unity to avoid for the latter the aforementioned eigenvalue accumulation consequences in practice. Allowing also for $A^* \neq A_*$ now, we basically obtain four different test cases for $\widetilde{A}$ in diagonal form. Accordingly, we chose the exemplary 3-tuples

(A_{11}, A_{22}, n) from

Material class	(A_{11}, A_{22}, n)
$(A_* < 1, n = 1)$	$\left(\frac{1}{8}, \frac{1}{2}, 1\right)$
$(A^* > 1, n = 1)$	(2,8,1)
$(A_* < 1, n > 1)$	$\left(\frac{1}{8}, \frac{1}{2}, 4\right)$
$(A^* > 1, n > 1)$	(2,8,4)

(5.19)

as representative parameters for our ITE computations and employ again the successively-deformed test scatterers from Chapter 4 to better retrace the numerical behavior of the modified MFS. We pick $\widehat{m} = 10$ random interior points each whose precise distribution keeps numerically irrelevant as before. To compensate the more complex anisotropic structure of corresponding fundamental solutions, the source points are now either manually fixed equiangularly on $\Gamma = \partial D(S)$, coinciding with the boundary of a slightly scaled-up scatterer by a factor $S > 1$ (i.e. $\partial D(1) = \partial D$), or on outer circles $\Gamma = \partial B_R(0)$ with proper radii R. Our scatterer determine then quite individually if and how to choose S or R, respectively. As derived from the isotropic case, the larger S or R is, the faster the MFS output is expected to converge with respect to m up to a certain threshold, but simultaneously ill-conditioning effects are likely to impede the detection. With these conventions, m in combination with S or R and modeling parameters given by (5.19) fully describes our modified MFS setup. We start again with the unit disc interpreted as an ellipse with equal axes and shrink the minor axis b in y-direction step by step to 0.8, 0.5 and 0.3. Respective results are shown in Figure 5.3 with $m = 30, \ldots, 60$ and are obtained for $R = 5b$. We observe that not only the scattering shape itself influences the numerical accuracy, but also the material parameters. An explanation for the latter is that the anisotropic parameters enter in our MFS ansatz as inner variations of the underlying fundamental solution, see (5.12), which, in terms of a pull-back, resembles spatial evaluations of isotropic radial basis functions along more or less deformed collocation boundaries.

Next, we focus on the transition from an ellipse to a kite shape parametrized by (4.38) whose deformation parameter ε passes from 0 to 0.3. Figure 5.4 then displays our modified MFS results for these samples and shows that more complex scattering shapes or concave parts reduce the accuracy of the output as in the isotropic case. It is therefore necessary to choose a compensating tighter scaling factor for Γ with respect to ∂D again which turns out to work well for $S = 2 - \varepsilon$. Likewise, the number of collocation points required for accumulating approximate ITEs increases in comparison with the ellipses and ranges from about 35 to 80 here. In comparison with Figure 5.3, material parameters do not show significant effects on the computational output.

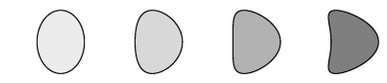

ε	(A_{11},A_{22},n)	$k_{\mathbb{R}}^{(1)}$	$k_{\mathbb{R}}^{(2)}$	$k_{\mathbb{R}}^{(3)}$	$k_{\mathbb{R}}^{(4)}$
0.0	(1/8, 1/2, 1)	2.8471025260348	3.1600761111251	3.8992194907200	4.0633832879825
	(2, 8, 1)	5.813165368996797	6.483618475707658	7.70907468441514	8.0359270276980
	(1/8, 1/2, 4)	1.25548301224033	1.25437465935063	1.69500812538264	1.75549467161328
	(2, 8, 4)	1.45615282653635	2.7053687255745	3.5755403402386	5.3469141120703
0.1	(1/8, 1/2, 1)	2.844832741265	3.175258583036	3.894779056630	4.09507454531
	(2, 8, 1)	5.849387560813	6.477010844996	7.728576868915	7.99190658583
	(1/8, 1/2, 4)	1.234632318588	1.257786433541	1.699972423624	1.762508594273
	(2, 8, 4)	1.438716788003	2.694965222759	3.55348405570	5.395815566
0.2	(1/8, 1/2, 1)	2.868977355	3.19024736	3.929439900	4.14548893
	(2, 8, 1)	5.96482555	6.48350477	7.805845131	7.91285541
	(1/8, 1/2, 4)	1.255163101	1.273766679	1.714003852	1.788830942
	(2, 8, 4)	1.392899663	2.643884081	3.493341629	5.62747817
0.3	(1/8, 1/2, 1)	2.93627	3.2048	4.03421	4.1863
	(2, 8, 1)	6.1597	6.5494	7.8795	7.9617
	(1/8, 1/2, 4)	1.27293	1.31188	1.73880	1.83879
	(2, 8, 4)	1.32210	2.49773	3.42292	4.28398

Fig. 5.4 First four approximate real-valued ITEs without counting multiplicity for the shape transition ellipse-kite with deformation parameter ε.

Finally, in order to see how the method responds to shapes with corners, especially since Lipschitz boundaries are now included by our theoretical framework unlike for the isotropic case, we examplarily examine the unit square $D = [-0.5,0.5]^2$. However, it is clear at first sight at Figure 5.5 that the modified MFS also lacks accuracy here. Choosing $S = 1.2$, we are still able to improve the unit square results from [26] for the smallest ITE induced by the material parameters $(A_{11},A_{22},n) = (1/8,1/2,1)$. It should be noted that m needs to exceed 100 collocation points here until minimal dips for $\sigma_{min}\big(\kappa^{(m)}\big)$ in the graph become effectively apparent. Evidently, while approximation theory for the ITP of isotropic and anisotropic media is technically different, we obtain consistent numerical results when including additional computational points for the latter to account for the supplementary degrees of freedom by A.

(A_{11}, A_{22}, n)	$k_{\mathbb{R}}^{(1)}$	$k_{\mathbb{R}}^{(2)}$	$k_{\mathbb{R}}^{(3)}$	$k_{\mathbb{R}}^{(4)}$
(1/8, 1/2, 1)	4.386	4.845	6.615	6.646
(2, 8, 1)	10.036	11.14	11.60	12.32
(1/8, 1/2, 4)	1.998	2.021	2.798	2.853
(2, 8, 4)	1.85	4.92	5.14	6.11

Fig. 5.5 First four approximate real-valued ITEs without counting multiplicity for the unit square.

Chapter 6

More applications for the modified method of fundamental solutions

We extend the modified MFS introduced for the two-dimensional isotropic case in Chapter 4 to the elastic ITP, to piecewise homogeneous media and lastly to three dimensional scatterers, respectively. Since most of our developed theory can be inherited after solving minor technical obstacles, we only sketch how to pass from one setup to another. The main focus will be on numerical implementations and concrete examples to prove broader applicability of the method as well as revealing model-specific effects.

6.1 The elastic interior transmission problem

The scalar acoustic model from Chapter 4 does not apply any more when vibrations within isotropic solids $D \subset \mathbb{R}^2$ need to be described since they respond to any kind of material displacements $u : D \to \mathbb{C}^2$ with shear couplings, see [39]. Assuming therefore Hooke's law from linear elasticity

$$\sigma(\nabla u) = 2\mu\varepsilon + \lambda \mathrm{tr}(\varepsilon)\mathrm{I} \tag{6.1}$$

which relates strain $\varepsilon = \left(\nabla u + (\nabla u)^{\mathrm{T}}\right)/2$ and stress σ in a tensorial way, corresponding waves are called elastic and propagate for time-harmonic states according to the Navier equations

$$\Delta_\sigma u + \rho\omega^2 u = 0\,. \tag{6.2}$$

Therein, ρ is a homogeneous material density ratio, ω is the vibration frequency and λ, μ are constitutive Lamé parameters which are constrained in 2D to fulfill $\mu > 0$ and $2\mu + \lambda > 0$ in order to guarantee strong ellipticity of the Navier operator Δ_σ, see [76]. The elastic ITP then becomes

$$\begin{aligned} \Delta_\sigma v + \omega^2 v &= 0 \quad \text{in } D \\ \Delta_\sigma w + \rho\omega^2 w &= 0 \quad \text{in } D \\ v &= w \quad \text{on } \partial D \\ \sigma(\nabla v)\nu &= \sigma(\nabla w)\nu \quad \text{on } \partial D \end{aligned} \tag{6.3}$$

and imposes, as before in the isotropic context, the eigenfunction conditions $v, w \in L^2(D, \mathbb{C}^2)$ and $(v-w) \in H_0^2(D, \mathbb{C}^2)$. However, ITEs $\omega \in \mathbb{C}\backslash\{0\}$ represent particular frequencies instead of wave numbers now whose physical unit is formally converted through μ, λ.

Mathematically, the acoustic and elastic ITP distinguish by the differential operators involved as well as the range dimensions of their eigenfunctions. Still, they share general PDE structures and thus enable a common analytical approach for main ITE studies, cf. [11] and [28]. Numerically, the elastic ITP is less explored, see [52, 84, 100, 101], which is why we want to present the modified MFS and provide results in that case, too. Our survey is reproduced from [68] where also underlying approximation theory for $C^{1,1}$-domains D analogue to Section 4.3 is detailed to justify upcoming calculations.

First of all, we need a proper fundamental solution system for (6.2) whose non-unique choice should be made carefully. For instance, in Theorem 8 we have seen that radiation conditions which yield uniqueness of exterior Helmholtz solutions guarantee dense MFS trial functions independent of the source contour Γ. In order to obtain a corresponding result for the Navier system, we note that by the Helmholtz decomposition, see [73], any entire solution $\widetilde{u} = \widetilde{u}_p + \widetilde{u}_s$ can be divided into a longitudinal compressional part $\widetilde{u}_p$ and a transversal shear contribution $\widetilde{u}_s$ which then solve

$$\Delta\widetilde{u}_p + \kappa_p^2 \widetilde{u}_p = 0 \qquad \text{and} \qquad \Delta\widetilde{u}_s + \kappa_s^2 \widetilde{u}_s = 0$$

with wave numbers

$$\kappa_p^2 := \frac{\rho\omega^2}{\lambda + 2\mu} \qquad \text{and} \qquad \kappa_s^2 := \frac{\rho\omega^2}{\mu}\,. \tag{6.4}$$

The vector field u is then said to fulfill the 2D Kupradze's radiation condition if

$$\lim_{r\to\infty}\sqrt{r}(\partial_r\widetilde{u}_p-\mathrm{i}\kappa_p\widetilde{u}_p)=0 \qquad \text{and} \qquad \lim_{r\to\infty}\sqrt{r}(\partial_r\widetilde{u}_s-\mathrm{i}\kappa_s\widetilde{u}_s)=0$$

uniformly in all angular directions. The radiating fundamental solution system for (6.2) in the above sense is given by

$$\Phi_{\sigma,\omega^2}=\frac{\mathrm{i}}{4\mu}H_0^{(1)}(k_s|\bullet|)\cdot\mathrm{I}+\frac{\mathrm{i}}{4\omega^2}\nabla^\top\nabla\left(H_0^{(1)}(k_p|\bullet|)-H_0^{(1)}(k_s|\bullet|)\right)\,,$$

where $I\in\mathbb{C}^{2\times 2}$ is the identity matrix, see [9]. Recalling that Φ_{σ,ω^2} adopts all the relevant scalar operations despite its multidimensional range, see Section 2.4, the modified MFS for the elastic ITP can be derived as in (4.34) – (4.36) but in terms of block matrices for each Φ_{σ,ω^2}-evaluation: Selecting for any scatterer D and some accompanying source contour Γ the usual m-dependent points $\left\{x^{(1/m)},\dots,x^{(m/m)}\right\}\subset\partial D$ and $\left\{s^{(1/m)},\dots,s^{(m/m)}\right\}\subset\Gamma$, respectively, as well as $\left\{\widehat{x}^{(1/\widehat{m})},\dots,\widehat{x}^{(\widehat{m}/\widehat{m})}\right\}\subset D$ randomly, the modified MFS matrix reads

$$M(\omega)=\begin{pmatrix} B_\sigma(\omega) & B_\sigma(\sqrt{\rho}\omega)\\ \sigma(\nabla B_\sigma(\omega))\nu & \sigma(\nabla B_\sigma(\sqrt{\rho}\omega))\nu\\ \widehat{I}_\sigma(\omega) & 0\\ 0 & \widehat{I}_\sigma(\sqrt{\rho}\omega)\end{pmatrix}\,.$$

Approximate ITEs $\omega=\omega^{(m)}$ are then again characterized by making the squared boundary-restricted unitary part $Q_B(\omega)$ of $M(\omega)$ sufficiently singular, cf. Figure 3.5.

Based on this, we exemplarily compute ITEs for a disc D_d of radius 0.5, for an ellipse D_e with a minor and major semi-axis of length 0.5 and 1, respectively, for a kite-shaped scatterer D_k defined by setting $\varepsilon=0.3$ in (4.38) and for the unit square D_s. We fix the material parameters

$$\mu=\frac{1}{16}\,,\quad \lambda=\frac{1}{4}\,,\quad \rho=4$$

which were also used in the context of [52]. In particular, we aim at improving the numerical results from there via the modified MFS in the following. Supplementarily, we take the source boundaries $\Gamma_d=2\cdot\partial D_d$,$\Gamma_e=1.9\cdot\partial D_e$,$\Gamma_k=1.6\cdot\partial D_k$,$\Gamma_s=1.3\cdot\partial D_s$ where the multiplication is understood as scaling with respect to the origin. Both collocation and source points are distributed equiangularly on corresponding boundaries while the remaining $\widehat{m}=10$ interior samples are fixed randomly inside of the domains. With these input arrangements, Figure 6.1 lists our successfully-refined ITE results in the elastic case and confirms that,

Shape	$\omega_{\mathbb{R}}^{(1)}$	$\omega_{\mathbb{R}}^{(2)}$	$\omega_{\mathbb{R}}^{(3)}$	$\omega_{\mathbb{R}}^{(4)}$
disc	1.451304027606383	1.704638247023373	1.984530256321993	2.269112085458542
ellipse	1.296728136516	1.302785814026	1.540896035208	1.565151107263
kite	0.947	1.047	1.111	1.235
square	1.3938	1.6182	1.8020	1.9362

Fig. 6.1 First four approximate real-valued ITEs without counting multiplicity for several scatterers with material parameters $\mu = 1/16,\ \lambda = 1/4,\ \rho = 4$.

despite the larger matrix size compared to (4.34) for each m due to vector-valued trial functions, the modified MFS is barely affected by additional range dimensions. It actually substantiates our numerical observations from Subsection 4.4.2.

6.2 The interior transmission problem for piecewise homogeneous media

In many real-world scenarios the scatterer of interest is macroscopically a composition of different material components, either due to inner pollutions or manufactured structures. Depending on the modeling resolution required, the constitutive parameters need to be adapted. In order to make still use of the modified MFS for corresponding ITE computations which has only been established for constant-coefficient ITPs so far, we investigate the relaxed isotropic case when either $n > 1$ or $0 < n < 1$ is piecewise constant on D, i.e. the medium consists of finitely many, say $d \in \mathbb{N}$, homogeneous components. Accordingly, we also partition $\bigcup_{h=1}^{d} D^{(h/d)} \subset D \subset \overline{D} = \bigcup_{h=1}^{d} \overline{D}^{(h/d)}$ such that $n^{(h/d)} := n_{|D^{(h/d)}} = \text{const}$ where all $D^{(h/d)}$ are disjoint, open and connected. We can then apply the modified MFS on each $D^{(h/d)}$ in the sense that trial functions need to match as smooth as possible across transitional component boundaries. We will sketch the accompanying mathematical framework for the 2D acoustic ITP from (4.3) with the above restrictions on n in the following. For a more detailed analysis, we refer to the underlying studies in [86] from which we also copy the numerical results.

First, we point out that material inhomogeneities will be restricted to inner components which are compactly contained in another one completely, see Figure 6.2. Otherwise, the global domain regularity necessary for using the trace theorem as in Chapter 4, e.g. Theorem 1, would not be transferable any more to each component due to arising cusps. We thus assume the existence of a surrounding bulk material given by $D^{(1/d)}$ and which encompasses $\partial D \subset \partial D^{(1/d)}$ while $\partial D \cap \partial D^{(h/d)} = \emptyset$ for $2 \leq h \leq d$. We also demand for $i \neq j$ that either $\partial D^{(i/d)} \cap \partial D^{(j/d)} = \emptyset$ or $\partial D^{(i/d)} \cap \partial D^{(j/d)}$ is a closed $C^{1,1}$-curve. In particular, meshing of

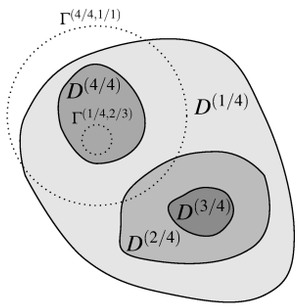

Fig. 6.2 Exemplary piecewise homogeneous scatterer D with bulk $D^{(1/4)}$ that contains three inner components $D^{(2/4)}, D^{(3/4)}, D^{(4/4)}$. Some compatible pair of source boundaries necessary for collocation across $\partial D^{(4/4)}$ are added as dotted circles.

general inhomogeneous scatterers is not possible with our proposed modified MFS scheme in theory. But since admissible components might henceforth contain voids when separated from each other, we need to discuss feasible source contour setups in such a case.

As a rule of thumb, MFS trial functions can be obtained by selecting sources in each connected part of the component's complement. Note that v still solves an n-independent and constant-coefficient PDE on D such that approximate eigenfunctions $v^{(m)}$ can be expanded as before given exterior source points along some $\Gamma^v = \Gamma = \overline{D}^{\mathsf{c}}$, see (4.15). Concerning w, we assign for each $D^{(h/d)}$ component-wise-supported trial functions by

$$\varphi^{(l/m,h/d,r/h^{\mathsf{c}})}_{\sqrt{n^{(h/d)}}\kappa} := \frac{\mathrm{i}}{4} H_0^{(1)}\left(\sqrt{n^{(h/d)}}\kappa \left| \bullet - s^{(l/m,h/d,r/h^{\mathsf{c}})} \right|\right) \mathbb{1}_{\overline{D}^{(h/d)}} \,,$$

where $s^{(l/m,h/d,r/h^{\mathsf{c}})} \in \Gamma^{(h/d,r/h^{\mathsf{c}})}$ for $1 \leq l \leq m$. The latter is a closed non-intersecting source contour located in the r-th connected component of $\left(D^{(h/d)}\right)^{\mathsf{c}}$ whose total number we denote by h^{c} for $1 \leq h \leq d$. By convenience, $r = 1$ is to label the respective unbounded exterior for every $1 \leq h \leq d$ so we may in particular set for the bulk $\Gamma^{(1/d,1/1^{\mathsf{c}})} = \Gamma^v$. If $h^{\mathsf{c}} > 1$ for some $1 \leq h \leq d$, voids exist in $D^{(h/d)}$. Accompanying inner source contours need to be selected then carefully to make the density proof from Theorem 8 with fixed wave numbers κ also work for multiply connected homogeneous components each, i.e. we downsize $\Gamma^{(h/d,r/h^{\mathsf{c}})}$ with $r > 1$ whenever it is a resonant interior Dirichlet boundary for κ to avoid new kind of spurious ITEs in the end, cf. [96]. Note that the product of Dirichlet eigenvalue times domain area is scaling-invariant in 2D so sufficiently small inner source contours can always be found.

We can now formulate the modified MFS for piecewise homogeneous media: Having found for some environment of κ proper $\Gamma^{(h/d,r/h^c)}$ with m source points each, we also choose m collocation points $\left\{x^{(i<j/d,1/m)},\ldots,x^{(i<j/d,m/m)}\right\}$ if $\partial D^{(i/d)} \cap \partial D^{(j/d)} \neq \emptyset$ for the ordered indices $0 \leq i < j \leq d$. Here, we have set $D^{(0/d)} := \overline{D}^c$ to include the overall domain boundary, too. In particular, $x^{(0<j/d,l/m)}$ does not exist as such for any $2 \leq j$ and $1 \leq l \leq m$ due to our bulk assumption on $D^{(1/d)}$, for example. Finally, we choose as usual random interior points $\left\{\widehat{x}^{(1/\widehat{m})},\ldots,\widehat{x}^{(\widehat{m}/\widehat{m})}\right\} \subset D$ independent of the component decomposition. The modified MFS matrix then reads

$$M(\kappa) := \begin{pmatrix} B^{(1/1^c,0<1/d)}(\kappa) & B^{(1/1^c,0<1/d)}(\sqrt{n^{(1/d)}}\kappa) & \ldots & B^{(1^c/1^c,0<1/d)}(\sqrt{n^{(1/d)}}\kappa) & 0 & \ldots \\ 0 & B^{(1/1^c,1<2/d)}(\sqrt{n^{(1/d)}}\kappa) & \ldots & B^{(1^c/1^c,1<2/d)}(\sqrt{n^{(1/d)}}\kappa) & B^{(1/2^c,1<2/d)}(\sqrt{n^{(2/d)}}\kappa) & \ldots \\ \vdots & \vdots & & \vdots & \vdots & \\ \nabla B^{(1/1^c0<1/d)}(\kappa)\nu & \nabla B^{(1/1^c,0<1/d)}(\sqrt{n^{(1/d)}}\kappa)\nu & \ldots & \nabla B^{(1^c/1^c,0<1/d)}(\sqrt{n^{(1/d)}}\kappa)\nu & 0 & \ldots \\ 0 & \nabla B^{(1/1^c,1<2/d)}(\sqrt{n^{(1/d)}}\kappa)\nu & \ldots & \nabla B^{(1^c/1^c,1<2/d)}(\sqrt{n^{(1/d)}}\kappa)\nu & \nabla B^{(1/2^c,1<2/d)}(\sqrt{n^{(2/d)}}\kappa)\nu & \ldots \\ \vdots & \vdots & & \vdots & \vdots & \\ \widetilde{I}^{(1/1^c)}(\kappa) & 0 & \ldots & \ldots & \ldots & \ldots \\ 0 & \widetilde{I}^{(1/1^c)}(\sqrt{n^{(1/d)}}\kappa) & \ldots & \widetilde{I}^{(1^c/1^c)}(\sqrt{n^{(1/d)}}\kappa) & \widetilde{I}^{(1/2^c)}(\sqrt{n^{(2/d)}}\kappa) & \ldots \end{pmatrix}, \tag{6.5}$$

where

$$B^{(r/h^c,i<j/d)}(\kappa) := \begin{pmatrix} \varphi_\kappa^{(1/m,h/d,r/h^c)}\left(x^{(i<j/d,1/m)}\right) & \ldots & \varphi_\kappa^{(m/m,h/d,r/h^c)}\left(x^{(i<j/d,1/m)}\right) \\ \vdots & \ddots & \vdots \\ \varphi_\kappa^{(1/m,h/d,r/h^c)}\left(x^{(i<j/d,m/m)}\right) & \ldots & \varphi_\kappa^{(m/m,h/d,r/h^c)}\left(x^{(i<j/d,m/m)}\right) \end{pmatrix}$$

for either $h = i$ or $h = j$, and $B^{(r/h^c,i<j/d)}(\kappa) = 0$ otherwise. Similar definitions apply to $\widetilde{I}^{(r/h^c)}(\kappa)$ with respect to its interior points and $\nabla B^{(r/h^c,i<j/d)}(\kappa)\nu$ so that $M(\kappa)$ contains many zero blocks, compensating its complex block structure in total. As before, collocation points are varied column-wise and sources are listed row-wise within M as guiding arrangement. Also, the first block column is linked to v as in (4.34) whereas the other ones are completely due to w and its different source contour contributions now. Altogether, we are ready to compute ITEs for piecewise homogeneous media by applying again the modified MFS to (6.5) as depictedd in Figure 3.5.

For this purpose, we want to examine the unit disc scatterer D again but with two different inner-component configurations, see [86]. The first one should have completely separated components and is as such indicated by $D_{\circ\circ}$, while the other, $D_{\circledcirc}$, has a corresponding

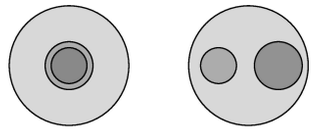

Interior	$k_{\mathbb{R}}^{(1)}$	$k_{\mathbb{R}}^{(2)}$	$k_{\mathbb{R}}^{(3)}$	$k_{\mathbb{R}}^{(4)}$
$D_{\circledcirc}$	3.3472649097009	3.5339744459219	3.8215531039714	4.0276794096285
$D_{\circ\circ}$	2.9695607637622	3.8151728473562	4.2620616635742	4.3612725527356

Fig. 6.3 Visualization of the scatterers $D_{\circledcirc}$ (left) and $D_{\circ\circ}$ (right) and listing of the first four real ITEs without counting multiplicity for $n^{(1/3)} = 4$, $n^{(2/3)} = 3$, $n^{(3/3)} = 2$.

concentric composition, cf. Figure 6.3. More concretely, we analyze for $d = 3$

$$\begin{aligned} D_{\circ\circ}^{(2/3)} &:= B_{0.4}\big((0.5,0)^\top\big)\,, \\ D_{\circ\circ}^{(3/3)} &:= B_{0.3}\big((-0.5,0)^\top\big)\,, \\ D_{\circ\circ}^{(1/3)} &:= B_1\big((0,0)^\top\big)\setminus\big(D_{\circ\circ}^{(2/3)} \cup D_{\circ\circ}^{(3/3)}\big)\,, \end{aligned}$$

and

$$\begin{aligned} D_{\circledcirc}^{(2/3)} &:= B_{0.4}\big((0,0)^\top\big)\,, \\ D_{\circledcirc}^{(3/3)} &:= B_{0.3}\big((0,0)^\top\big)\,, \\ D_{\circledcirc}^{(1/3)} &:= B_1\big((0,0)^\top\big)\setminus\big(D_{\circledcirc}^{(2/3)} \cup D_{\circledcirc}^{(3/3)}\big)\,, \end{aligned}$$

where $B_r(x)$ is centered at $x = (x_1,x_2)^\top \in \mathbb{R}^2$. Note that ITEs for $D_{\circ\circ}$ can even be computed exactly via an adapted Fourier-Bessel ansatz, see [42]. For the modified MFS, we choose for $D^{\circ\circ}$

$$\begin{aligned} \Gamma_{\circ\circ}^{(1/3,1/3)} &:= \partial B_S\big((0,0)^\top\big)\,, \\ \Gamma_{\circ\circ}^{(1/3,2/3)} &:= \partial B_{0.4s}\big((0.5,0)^\top\big)\,, \\ \Gamma_{\circ\circ}^{(1/3,3/3)} &:= \partial B_{0.3s}\big((-0.5,0)^\top\big)\,, \\ \Gamma_{\circ\circ}^{(2/3,1/1)} &:= \partial B_{0.4S}\big((0.5,0)^\top\big)\,, \\ \Gamma_{\circ\circ}^{(3/3,1/1)} &:= \partial B_{0.3S}\big((-0.5,0)^\top\big)\,, \end{aligned}$$

and for $D^{\circledcirc}$

$$\begin{aligned}
\Gamma_{\circledcirc}^{(1/3,1/2)} &:= \partial B_S\big((0,0)^\top\big)\,,\\
\Gamma_{\circledcirc}^{(1/3,2/2)} &:= \partial B_{0.4s}\big((0,0)^\top\big)\,,\\
\Gamma_{\circledcirc}^{(2/3,1/2)} &:= \partial B_{0.4S}\big((0,0)^\top\big)\,,\\
\Gamma_{\circledcirc}^{(2/3,2/2)} &:= \partial B_{0.3s}\big((0,0)^\top\big)\,,\\
\Gamma_{\circledcirc}^{(3/3,1/1)} &:= \partial B_{0.3S}\big((0,0)^\top\big)\,,
\end{aligned}$$

with $S = 1.5$ and $s = 0.5$. Hence, we can readily distribute both m sources and collocation points each on corresponding circles equidistantly. The complementing interior points are picked randomly throughout D. The final modified MFS results for $n^{(1/3)} = 4$, $n^{(2/3)} = 3$, $n^{(3/3)} = 2$ are then shown in Figure 6.3. Our overall conclusion is that for a moderate number of inner components, i.e. when d is not too large, ITEs for piecewise homogeneous media can still be computed very accurately with our proposed method.

6.3 The interior transmission problem in 3D

Having studied in detail the modified MFS with its several ITP modeling scenarios in 2D, we finally address the problem of computing ITEs for bounded $D \subset \mathbb{R}^3$. For the sake of simplicity we confine to the homogeneous acoustic case (4.3) and convince ourselves that the general approximation-theoretical framework introduced in Section 4.3 applies likewise for 3D scattering configurations after updating dimension-dependent quantities. For instance, the fundamental solution Φ_κ^{3D} for the Helmholtz equation with wave number $\kappa \neq 0$ which is radiating in the sense of

$$\lim_{r\to\infty} r^{\frac{3}{2}}\left(\partial_r \Phi_\kappa^{3D} - \mathrm{i}\kappa\Phi_\kappa^{3D}\right) = 0$$

becomes

$$\Phi_\kappa^{3D} = \frac{1}{4\pi}\frac{\mathrm{e}^{\mathrm{i}\kappa|\bullet|}}{|\bullet|}\,,$$

see [25]. Hence, we can directly move forward to numerical aspects of the modified MFS in 3D and discuss the distribution of computational points first. The latter gets more involved now as ITE approximations proved to be sensitive already in 2D with respect to varying the distance of source contour to collocation boundary via radial scaling. Since even a further angular degree of freedom comes into play in 3D, the situation is expected to become only

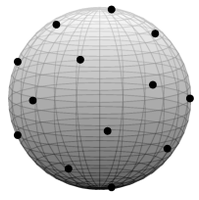

Fig. 6.4 Fibonacci lattice on the sphere with 21 points in total from which only the visible ones in the front side are indicated by black dots.

worse due to the enhanced total number of computational points required. Besides, it is not possible any more to find for each m equally distributed points on a sphere, cf. Platonic solids and [88], which turns the ball more asymmetric from a collocation perspective whereas in 2D the disc could be treated most easily via arc length with optimal results, see Figure 4.1. We will therefore try to examine representatively the smallest real-valued ITE $k_{\mathbb{R}}^{(1)}$ of the unit ball $D = B_1(0) \subset \mathbb{R}^3$ again to get a first feeling for the modified MFS in 3D. We take Γ to be a sphere as well but with a larger radius $R > 1$ so that collocation and source points exhaust the same kind of concentric surface. We can then employ the Fibonacci lattice from [44] to have both $\left\{x^{(1/m)},\ldots,x^{(m/m)}\right\} \subset \partial D$ and $\left\{s^{(1/m)},\ldots,s^{(m/m)}\right\} \subset \Gamma$ selected nearly uniformly for arbitrary odd m. Figure 6.4 shows the resulting point distribution for $m = 21$. We also fix $\left\{\widehat{x}^{(1/\widehat{m})},\ldots,x^{(\widehat{m}/\widehat{m})}\right\} \in D$ randomly and can thus build the modified MFS matrix

$$M(\kappa) = \begin{pmatrix} B^{3D}(\kappa) & B^{3D}(\sqrt{n}\kappa) \\ \nabla B^{3D}(\kappa)\nu & \nabla B^{3D}(\sqrt{n}\kappa)\nu \\ \widehat{I}^{\,3D}(\kappa) & 0 \\ 0 & \widehat{I}^{\,3D}(\sqrt{n}\kappa) \end{pmatrix}$$

with respect to Φ_{κ}^{3D}. We are left to minimize $\kappa \mapsto \sigma_{min}(\kappa)$ according to Figure 3.5 for which the exemplary graph along the real κ-axis based on $m = 301$, $\widehat{m} = 20$, $n = 4$ and $R = 5$ is shown in Figure 6.5 (left). From [63] we know that $k_{\mathbb{R}}^{(1)} = \pi$ which is again indicated in our plot by a neighboring vanishing minimum of the smallest-singular-value function. In the end, it turns out that decay of $\sigma_{min}\left(\kappa_{\mathbb{R}}^{(1,m)}\right)$ is significantly slower than its 2D analogon, cf. Figure 4.1, where $m = 30$ is already sufficient to compute the smallest real-valued ITE with machine precision. In contrast, $m \leq 30^2$ in 3D yields only $k_{\mathbb{R}}^{(1)} \approx 3.14159$ where the squared collocation number is chosen as comparing surface to curve-type boundaries. Simultaneously, ill-conditioning effects hinder further improvements, cf. Figure 6.5 (right).

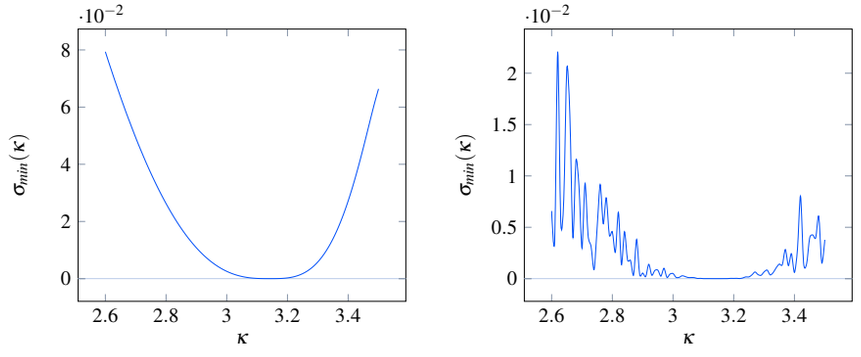

Fig. 6.5 Modified MFS applied to the unit ball in 3D with $n = 4$ for $m = 301$ (left) and $m = 601$ (right) collocation points, respectively. Ill-conditioning artifacts for computing the smallest singular value start early in comparison with the accuracy of approximate ITEs which only reveal 3 correct digits for $k_{\mathbb{R}}^{(1)} = \pi$ in both cases.

We conclude that in higher dimensions the modified MFS lacks accuracy already for very easy test scatterers. Our short excursion is to illustrate the necessity of further research and potential reconsideration of optimization techniques to make the modified MFS more attractive for eigenvalue computations in 3D.

Chapter 7

Summary and Outlook

This thesis has provided novel numerical and theoretical insights into the ITP for different wave type models in two dimensions. The mathematical core is guided by the development, analysis and verification of the modified MFS which is capable of computing complex-valued ITEs for (piecewise) homogeneous scatterers. The method has proven to be best-suited for smooth and convex domains (decomposing into at most few material components) whose boundaries can be reasonably discretized with a moderate number of collocation points. For instance, 8 correct eigenvalue digits and often more can be calculated readily with less than 60 boundary points for standard scatterers such as ellipses or kite-shapes, beating thus many alternative methods with regard to accuracy, complexity and convergence rates in practice. Throughout, tuning parameters and points have been selected manually according to certain approved criteria, but could alternatively be optimized within an independent pre-process to further improve our current results.

Concerning computational challenges, all the issues that we have encountered in the course of establishing the modified MFS were linked to the well-known ill-posedness of the underlying MFS ansatz. On the one hand, spurious eigenvalues, which are typical for discretized compact operator equations, could be easily avoided by our algorithm so that significantly higher accuracy than for the standard MFS is attained as illustrated for the related yet easier Dirichlet Laplace eigenproblem. Our derived convergence theory for approximating ITEs via the modified MFS even shows that the resulting error achieves up to spectral decay depending on the regularity of the scattering boundary. On the other hand, the attainable accuracy for relatively large collocation numbers is in practice still limited due to the growing ill-conditioning of the coefficient matrices and their induced error propagation within the modified MFS algorithm. In particular, 3D applications or complex scattering boundaries, especially corners, cannot be treated efficiently yet. According to the uncertainty principle though, i.e. the incompatible interplay of good convergence rates and blowing-up

condition numbers in the context of interpolation with radial basis functions, only higher precision updates may handle this intrinsic subtlety completely upon additional numerical costs.

From a theoretical point of view, the structure of the ITP is non-standard which is why a novel approximation framework has been set up in terms of general Trefftz-like trial functions. As such it also yields a spurious-free basis for other boundary collocation methods and takes into account the usual distinction on isotropic and anisotropic scattering media. Specific for the modified MFS, we have shown that the whole eigenvalue spectrum can be detected and proved a posteriori error estimates as well as convergence rates. A natural next step would be to extend the introduced method with its theory to absorbing media whose refractive indices then exhibit a dispersive and complex-valued structure. The latter is an important field of current research with many open questions.

References

[1] Abramowitz, M. and Stegun, I. A. (1965). *Handbook of mathematical functions: with formulas, graphs, and mathematical tables*, volume 55. Courier Corporation.

[2] Agmon, S. (2010). *Lectures on elliptic boundary value problems*. American Mathematical Society.

[3] Agranovich, M. S. (2015). *Sobolev spaces, their generalizations and elliptic problems in smooth and Lipschitz domains*. Springer.

[4] Alkhalifah, T. (2000). An acoustic wave equation for anisotropic media. *Geophysics*, 65(4):1239–1250.

[5] Alt, H. W. (1992). *Linear functional analysis*. Springer.

[6] Alves, C. J. (2009). On the choice of source points in the method of fundamental solutions. *Engineering Analysis with Boundary Elements*, 33(12):1348–1361.

[7] Alves, C. J. and Antunes, P. R. (2009). The method of fundamental solutions applied to the calculation of eigensolutions for 2D plates. *International Journal for Numerical Methods in Engineering*, 77(2):177–194.

[8] Antunes, P. R. (2018). Reducing the ill conditioning in the method of fundamental solutions. *Advances in Computational Mathematics*, 44(1):351–365.

[9] Arens, T. (2001). Linear sampling methods for 2D inverse elastic wave scattering. *Inverse Problems*, 17(5):1445.

[10] Barnett, A. H. and Betcke, T. (2008). Stability and convergence of the method of fundamental solutions for Helmholtz problems on analytic domains. *Journal of Computational Physics*, 227(14):7003–7026.

[11] Bellis, C., Cakoni, F., and Guzina, B. B. (2012). Nature of the transmission eigenvalue spectrum for elastic bodies. *The IMA Journal of Applied Mathematics*, 78(5):895–923.

[12] Betcke, T. (2008). The generalized singular value decomposition and the method of particular solutions. *SIAM Journal on Scientific Computing*, 30(3):1278–1295.

[13] Betcke, T. and Trefethen, L. N. (2005). Reviving the method of particular solutions. *SIAM Review*, 47(3):469–491.

[14] Beyn, W.-J. (2012). An integral method for solving nonlinear eigenvalue problems. *Linear Algebra and its Applications*, 436(10):3839–3863.

[15] Blåsten, E. and Päivärinta, L. (2013). Completeness of generalized transmission eigenstates. *Inverse Problems*, 29(10):104002.

[16] Blåsten, E., Päivärinta, L., and Sylvester, J. (2014). Corners always scatter. *Communications in Mathematical Physics*, 331:725–753.

[17] Bogomolny, A. (1985). Fundamental solutions method for elliptic boundary value problems. *SIAM Journal on Numerical Analysis*, 22(4):644–669.

[18] Bondarenko, O., Harris, I., and Kleefeld, A. (2017). The interior transmission eigenvalue problem for an inhomogeneous media with a conductive boundary. *Applicable Analysis*, 96(1):2–22.

[19] Cakoni, F., Cayoren, M., and Colton, D. (2008). Transmission eigenvalues and the nondestructive testing of dielectrics. *Inverse Problems*, 24(15):065016.

[20] Cakoni, F. and Colton, D. (2013). *A qualitative approach to inverse scattering theory*. Springer.

[21] Cakoni, F., Colton, D., and Gintides, D. (2010a). The interior transmission eigenvalue problem. *SIAM Journal on Mathematical Analysis*, 42(6):2912–2921.

[22] Cakoni, F., Colton, D., and Haddar, H. (2009). The computation of lower bounds for the norm of the index of refraction in an anisotropic media from far field data. *The Journal of Integral Equations and Applications*, 21(2):203–227.

[23] Cakoni, F., Colton, D., and Haddar, H. (2010b). The interior transmission problem for regions with cavities. *SIAM Journal on Mathematical Analysis*, 42(1):145–162.

[24] Cakoni, F., Colton, D., and Haddar, H. (2010c). On the determination of Dirichlet or transmission eigenvalues from far field data. *Comptes Rendus Mathematique*, 348(7–8):379–383.

[25] Cakoni, F., Colton, D., and Haddar, H. (2016). *Inverse scattering theory and transmission eigenvalues*. SIAM.

[26] Cakoni, F., Colton, D., Monk, P., and Sun, J. (2010d). The inverse electromagnetic scattering problem for anisotropic media. *Inverse Problems*, 26(7):074004.

[27] Cakoni, F., Gintides, D., and Haddar, H. (2010e). The existence of an infinite discrete set of transmission eigenvalues. *SIAM Journal on Mathematical Analysis*, 42(1):237–255.

[28] Cakoni, F. and Haddar, H. (2012). Transmission eigenvalues in inverse scattering theory. *Inside Out II*, 60:527–578.

[29] Cakoni, F. and Kress, R. (2017). A boundary integral equation method for the transmission eigenvalue problem. *Applicable Analysis*, 96(1):23–38.

[30] Cheung, Y., Jin, W., and Zienkiewicz, O. (1991). Solution of Helmholtz equation by trefftz method. *International Journal for Numerical Methods in Engineering*, 32(1):63–78.

[31] Colton, D., Kirsch, A., and Päivärinta, L. (1989). Far-field patterns for acoustic waves in an inhomogeneous medium. *SIAM Journal on Mathematical Analysis*, 20(6):1472–1483.

[32] Colton, D. and Kress, R. (2013). *Integral equation methods in scattering theory*. SIAM.

[33] Colton, D. and Kress, R. (2018). Looking back on inverse scattering theory. *SIAM Review*, 60(4):779–807.

[34] Colton, D. and Leung, Y.-J. (2012). Complex transmission eigenvalues for spherically stratified media. *Inverse Problems*, 28(7):075005.

[35] Colton, D. and Monk, P. (1984). The inverse scattering problem for time-harmonic acoustic waves. *SIAM Review*, 26(3):323–350.

[36] Colton, D., Paivarinta, L., and Sylvester, J. (2007). The interior transmission problem. *Inverse Problems and Imaging*, 1(1):13.

[37] Evans, L. C. (2010). *Partial differential equations*, volume 19. American Mathematical Society.

[38] Fairweather, G. and Karageorghis, A. (1998). The method of fundamental solutions for elliptic boundary value problems. *Advances in Computational Mathematics*, 9(1):69–95.

[39] Fichtner, A. (2011). *Full seismic waveform modelling and inversion*. Advances in Geophysical and Environmental Mechanics and Mathematics. Springer.

[40] Fornberg, B. and Piret, C. (2007). A stable algorithm for flat radial basis functions on a sphere. *SIAM Journal on Scientific Computing*, 30(1):60–80.

[41] Fox, L., Henrici, P., and Moler, C. (1967). Approximations and bounds for eigenvalues of elliptic operators. *SIAM Journal on Numerical Analysis*, 4(1):89–102.

[42] Gintides, D. and Pallikarakis, N. (2013). A computational method for the inverse transmission eigenvalue problem. *Inverse Problems*, 29(10):104010.

[43] Gong, B., Sun, J., Turner, T., and Zheng, C. (2020). Finite element approximation of transmission eigenvalues for anisotropic media. *arXiv:2001.05340*.

[44] González, Á. (2010). Measurement of areas on a sphere using Fibonacci and latitude–longitude lattices. *Mathematical Geosciences*, 42(1):49.

[45] Grafakos, L. (2008). *Classical Fourier analysis*, volume 2. Springer.

[46] Gurtin, M. E. (1982). *An introduction to continuum mechanics*, volume 158. Academic Press.

[47] Han, J. and Yang, Y. (2016). An adaptive finite element method for the transmission eigenvalue problem. *Journal of Scientific Computing*, 69(3):1279–1300.

[48] Harris, I., Cakoni, F., and Sun, J. (2014). Transmission eigenvalues and non-destructive testing of anisotropic magnetic materials with voids. *Inverse Problems*, 30(3):035016.

[49] Hörmander, L. (1963). *Linear partial differential operators*. Springer.

[50] Hörmander, L. (2005). *The analysis of linear partial differential operators II: Differential operators with constant coefficients*. Springer.

[51] Hörmander, L. (2015). *The analysis of linear partial differential operators I: Distribution theory and Fourier analysis*. Springer.

[52] Ji, X., Li, P., and Sun, J. (2020). Computation of interior elastic transmission eigenvalues using a conforming finite element and the secant method. *Results in Applied Mathematics*, 5:100083.

[53] Ji, X. and Sun, J. (2013). A multi-level method for transmission eigenvalues of anisotropic media. *Journal of Computational Physics*, 255:422–435.

[54] Ji, X., Sun, J., and Xie, H. (2014). A multigrid method for Helmholtz transmission eigenvalue problems. *Journal of Scientific Computing*, 60(2):276–294.

[55] Jiguang, S. (1991). Perturbation bounds for the Cholesky and QR factorization. *BIT Numerical Mathematics*, 31(2):341–352.

[56] Kac, M. (1966). Can one hear the shape of a drum? *The American Mathematical Monthly*, 73(4):1–23.

[57] Katsurada, M. and Okamoto, H. (1996). The collocation points of the fundamental solution method for the potential problem. *Computers & Mathematics with Applications*, 31(1):123–137.

[58] Kirsch, A. (1986). The denseness of the far field patterns for the transmission problem. *IMA Journal of Applied Mathematics*, 37(3):213–225.

[59] Kirsch, A. (1999). Factorization of the far-field operator for the inhomogeneous medium case and an application in inverse scattering theory. *Inverse Problems*, 15(2):413–429.

[60] Kirsch, A. (2011). *An introduction to the mathematical theory of inverse problems*, volume 120. Springer.

[61] Kirsch, A. and Lechleiter, A. (2013). The inside–outside duality for scattering problems by inhomogeneous media. *Inverse Problems*, 29(10):104011.

[62] Kleefeld, A. (2013). A numerical method to compute interior transmission eigenvalues. *Inverse Problems*, 29(10):104012.

[63] Kleefeld, A. (2015). *Numerical methods for acoustic and electromagnetic scattering: Transmission boundary-value problems, interior transmission eigenvalues, and the factorization method*. Habilitation thesis, Brandenburg University of Technology Cottbus–Senftenberg.

[64] Kleefeld, A. (2019). Shape optimization for interior Neumann and transmission eigenvalues. In Constanda, C. and Harris, P., editors, *Integral Methods in Science and Engineering*, pages 185–196. Springer.

[65] Kleefeld, A. and Colton, D. (2017). Interior transmission eigenvalues for anisotropic media. In Constanda, C., Dalla Riva, M., Lamberti, P., and Musolino, P., editors, *Integral Methods in Science and Engineering, volume 1*, pages 139–147. Springer.

[66] Kleefeld, A. and Pieronek, L. (2018a). Computing interior transmission eigenvalues for homogeneous and anisotropic media. *Inverse Problems*, 34(10):105007.

[67] Kleefeld, A. and Pieronek, L. (2018b). The method of fundamental solutions for computing acoustic interior transmission eigenvalues. *Inverse Problems*, 34(3):035007.

[68] Kleefeld, A. and Pieronek, L. (2020). Elastic interior transmission eigenvalues and their computation via the method of fundamental solutions. *Applicable Analysis*.

[69] Kupradze, V. and Aleksidze, M. A. (1964). The method of functional equations for the approximate solution of certain boundary value problems. *USSR Computational Mathematics and Mathematical Physics*, 4(4):82–126.

[70] Kuttler, J. R. and Sigillito, V. G. (1978). Bounding eigenvalues of elliptic operators. *SIAM Journal on Mathematical Analysis*, 9(4):768–773.

[71] Lakshtanov, E. and Vainberg, B. (2012). Ellipticity in the interior transmission problem in anisotropic media. *SIAM Journal on Mathematical Analysis*, 44(2):1165–1174.

[72] Leis, R. (1967). *Vorlesungen über partielle Differentialgleichungen zweiter Ordnung*, volume 165. Hochschultaschenbücher-Verlag.

[73] Li, P., Wang, Y., Wang, Z., and Zhao, Y. (2016). Inverse obstacle scattering for elastic waves. *Inverse Problems*, 32(11):115018.

[74] Li, Z.-C. (2009). The method of fundamental solutions for annular shaped domains. *Journal of Computational and Applied Mathematics*, 228(1):355–372.

[75] Li, Z.-C., Wei, Y., Chen, Y., and Huang, H.-T. (2019). The method of fundamental solutions for the Helmholtz equation. *Applied Numerical Mathematics*, 135:510–536.

[76] McLean, W. (2000). *Strongly elliptic systems and boundary integral equations*. Cambridge University Press.

[77] Melenk, J. and Babuska, I. (1997). Approximation with harmonic and generalized harmonic polynomials in the partition of unity method. *Computer Assisted Mechanics and Engineering Sciences*, 4:607–632.

[78] Moiola, A., Hiptmair, R., and Perugia, I. (2011). Plane wave approximation of homogeneous Helmholtz solutions. *Zeitschrift für angewandte Mathematik und Physik*, 62(5):809.

[79] Neittaanmaki, P., Sprekels, J., and Tiba, D. (2007). *Optimization of elliptic systems: theory and applications*. Springer.

[80] Oden, J. T. and Reddy, J. N. (2012). *An introduction to the mathematical theory of finite elements*. Courier Corporation.

[81] Ortner, N. and Wagner, P. (2015). *Fundamental solutions of linear partial differential operators*. Springer.

[82] Päivärinta, L. and Sylvester, J. (2008). Transmission eigenvalues. *SIAM journal on Mathematical Analysis*, 40(2):738–753.

[83] Peters, S. (2016). *The inside-outside duality in inverse scattering theory*. PhD thesis, University of Bremen.

[84] Peters, S. (2017). The inside–outside duality for elastic scattering problems. *Applicable Analysis*, 96(1):48–69.

[85] Peters, S. and Kleefeld, A. (2016). Numerical computations of interior transmission eigenvalues for scattering objects with cavities. *Inverse Problems*, 32(4):045001.

[86] Pieronek, L. and Kleefeld, A. (2019). The method of fundamental solutions for computing interior transmission eigenvalues of inhomogeneous media. In Constanda, C. and Harris, P., editors, *Integral Methods in Science and Engineering*, pages 353–365. Springer.

[87] Robbiano, L. (2013). Spectral analysis of the interior transmission eigenvalue problem. *Inverse Problems*, 29(10):104001.

[88] Saff, E. B. and Kuijlaars, A. B. (1997). Distributing many points on a sphere. *The Mathematical Intelligencer*, 19(1):5–11.

[89] Schaback, R. (1995). Error estimates and condition numbers for radial basis function interpolation. *Advances in Computational Mathematics*, 3(3):251–264.

[90] Stewart, G. W. (1990). Perturbation theory for the singular value decomposition. Technical report, University of Maryland Institute for Advanced Computer Studies Report No. UMIACS-TR-90-124.

[91] Stoer, J. and Bulirsch, R. (2013). *Introduction to numerical analysis*, volume 12. Springer.

[92] Sun, J. and Zhou, A. (2017). *Finite element methods for eigenvalue problems*. CRC Press.

[93] Tian, Z., Li, Z.-C., Huang, H.-T., and Chen, C.-S. (2017). Analysis of the method of fundamental solutions for the modified Helmholtz equation. *Applied Mathematics and Computation*, 305:262–281.

[94] Trefethen, L. N. (2000). *Spectral methods in MATLAB*, volume 10. SIAM.

[95] Trefftz, E. (1926). Ein Gegenstück zum Ritzschen Verfahren. *Proceedings 2nd International Congress Applied Mechanichs Zurich*, pages 131–137.

[96] Tsai, C., Young, D., Chen, C., and Fan, C. (2006). The method of fundamental solutions for eigenproblems in domains with and without interior holes. *Proceedings of The Royal Society A: Mathematical, Physical and Engineering Sciences*, 462(2069):1443–1466.

[97] Vodev, G. (2015). Transmission eigenvalue-free regions. *Communications in Mathematical Physics*, 336(3):1141–1166.

[98] Wouk, A. (1987). *New computing environments: microcomputers in large-scale computing*, volume 27. SIAM.

[99] Xi, Y. and Ji, X. (2017). Recursive integral method for the nonlinear non-selfadjoint transmission eigenvalue problem. *Journal of Computational Mathematics*, 35(6):828–838.

[100] Xi, Y. and Ji, X. (2020). A lowest order mixed finite element method for the elastic transmission eigenvalue problem. *Computer Physics Communications*, 28(3):1105–1132.

[101] Xi, Y., Ji, X., and Geng, H. (2018). A C^0IP method of transmission eigenvalues for elastic waves. *Journal of Computational Physics*, 374:237–248.

[102] Yang, Y., Bi, H., Li, H., and Han, J. (2016). Mixed methods for the Helmholtz transmission eigenvalues. *SIAM Journal on Scientific Computing*, 38(3):A1383–A1403.

Schriften des Forschungszentrums Jülich
IAS Series

Band / Volume 32
Methoden für die Bemessung der Leistungsfähigkeit multidirektional genutzter Fußverkehrsanlagen
S. Holl (2016), xii, 170 pp
ISBN: 978-3-95806-191-0
URN: urn:nbn:de:0001-2016120103

Band / Volume 33
JSC Guest Student Programme Proceedings 2016
edited by I. Kabadshow (2017), iii, 191 pp
ISBN: 978-3-95806-225-2
URN: urn:nbn:de:0001-2017032106

Band / Volume 34
Multivariate Methods for Life Safety Analysis in Case of Fire
B. Schröder (2017), x, 222 pp
ISBN: 978-3-95806-254-2
URN: urn:nbn:de:0001-2017081810

Band / Volume 35
Understanding the formation of wait states in one-sided communication
M.-A. Hermanns (2018), xiv, 144 pp
ISBN: 978-3-95806-297-9
URN: urn:nbn:de:0001-2018012504

Band / Volume 36
A multigrid perspective on the parallel full approximation scheme in space and time
D. Moser (2018), vi, 131 pp
ISBN: 978-3-95806-315-0
URN: urn:nbn:de:0001-2018031401

Band / Volume 37
Analysis of I/O Requirements of Scientific Applications
S. El Sayed Mohamed (2018), XV, 199 pp
ISBN: 978-3-95806-344-0
URN: urn:nbn:de:0001-2018071801

Band / Volume 38
Wayfinding and Perception Abilities for Pedestrian Simulations
E. Andresen (2018), 4, x, 162 pp
ISBN: 978-3-95806-375-4
URN: urn:nbn:de:0001-2018121810

Schriften des Forschungszentrums Jülich
IAS Series

Band / Volume 39
Real-Time Simulation and Prognosis of Smoke Propagation in Compartments Using a GPU
A. Küsters (2018), xvii, 162, LIX pp
ISBN: 978-3-95806-379-2
URN: urn:nbn:de:0001-2018121902

Band / Volume 40
Extreme Data Workshop 2018
Forschungszentrum Jülich, 18-19 September 2018
Proceedings
M. Schultz, D. Pleiter, P. Bauer (Eds.) (2019), 64 pp
ISBN: 978-3-95806-392-1
URN: urn:nbn:de:0001-2019032102

Band / Volume 41
A lattice QCD study of nucleon structure with physical quark masses
N. Hasan (2020), xiii, 157 pp
ISBN: 978-3-95806-456-0
URN: urn:nbn:de:0001-2020012307

Band / Volume 42
Mikroskopische Fundamentaldiagramme der Fußgängerdynamik – Empirische Untersuchung von Experimenten eindimensionaler Bewegung sowie quantitative Beschreibung von Stau-Charakteristika
V. Ziemer (2020), XVIII, 155 pp
ISBN: 978-3-95806-470-6
URN: urn:nbn:de:0001-2020051000

Band / Volume 43
Algorithms for massively parallel generic *hp*-adaptive finite element methods
M. Fehling (2020), vii, 78 pp
ISBN: 978-3-95806-486-7
URN: urn:nbn:de:0001-2020071402

Band / Volume 44
The method of fundamental solutions for computing interior transmission eigenvalues
L. Pieronek (2020), 115 pp
ISBN: 978-3-95806-504-8

Weitere ***Schriften des Verlags im Forschungszentrum Jülich*** unter
http://wwwzb1.fz-juelich.de/verlagextern1/index.asp

IAS Series
Band / Volume 44
ISBN 978-3-95806-504-8

Mitglied der Helmholtz-Gemeinschaft

JÜLICH
Forschungszentrum